UNIVERSITY OF CALIFORNIA
RIVERSIDE

# Tris(1,3-dichloro-2-propyl) phosphate: Impacts on Epigenetic Reprogramming and Cellular Metabolism During Embryonic Development

A Dissertation submitted in partial satisfaction
of the requirements for the degree of

Doctor of Philosophy

in

Environmental Toxicology

by

Sarah G. Avila-Barnard

September 2023

Dissertation Committee:
Dr. David Volz, Chairperson
Dr. Daniel Schlenk
Dr. Linlin Zhao

The Dissertation of Sarah G. Avila-Barnard is approved:

_____

_____

_____

Committee Chairperson

University of California, Riverside

## Acknowledgments

This dissertation has been completed with the help and support of many individuals. First, I would like to thank my mentor and advisor, Dr. David Volz, for continuing to truly be an exemplary model and advocate for first-generation students and always pushing to have his lab filled with diverse students and creating a safe working environment where we can learn, thrive, develop, and grow into our research niche. He single-handedly has taught me how to mentor and guide undergraduate students, chaperoned me in the academic world, as well as maintained stability in our department and lab through a pandemic. His commitment to not just my own well-being and succession through the program but to all students in our institution who approach and ask him for help is exceptional. His training and guidance are the reasons I was able to ultimately excel in the program and my own research. I would also like to thank the following members who have served on my committees over the past four years for their advice and guidance: Dr. Daniel Schlenk, Dr. Maria Linlin Zhao, Dr. Maria Ninova, and Dr. Changcheng Zhou.

I would also like to thank the past and present members of my lab and supporting labs who were an extension of my lab. I would like to thank Dr. Subham Dasgupta, Dr. Aalekya Reddam, Dr. Vanessa Cheng, Dr. Jenna Wiegand, Dr. Tori McGruer, Dr. Phil Tanabe, Dr. Win Cowger, and John Hoang, for their constant support and for making the lab feel like home and for always providing me with advice, friendship, guidance, support, and additional mentorship when I needed it. You as well are solemnly the reason I truly believed in myself at times when my mental health or support system was lacking, and I forever am grateful to have met you in this program. I was lucky enough to have not only gained colleagues in my lab but also a family that extended outside of my own.

This research was support by UCR's Graduate Division, the NRSA T32 Training Program (T32ES018827), a National Institute of Health grant (R01ES027576), and a USDA National Institute of Food and Agriculture Hatch Project (1009609).

## Copyright Acknowledgements

The text and figures in Chapter 2, in part or in full, are a reprint of the materials as they appear in “Rapid and Efficient Spatiotemporal Monitoring of Normal and Aberrant Cytosine Methylation within Intact Zebrafish Embryos” published in the Journal of Visualized Experiments, Vol 186, 2022. The co-authors David C. Volz helped with the methodology, and investigation, as well as directed and supervised this research.

The text and figures in Chapter 3, in part or in full, are a reprint of the materials as they appear in “Tris(1,3-dichloro-2-propyl) phosphate disrupts the trajectory of cytosine methylation within developing zebrafish embryos” published in Environmental Research, Vol 211, 2022. The co-authors Subham Dasgupta, Vanessa Cheng, Aalekya Reddam, and Jenna Wiegand helped in the methodology and investigation. The co-author David C. Volz directed and supervised this research.

All supplementary materials reported in this dissertation are available through ProQuest Dissertation & Theses.

## Dedication

To my community for standing by my side and providing unconditional love and support while I self-discovered and found my passion. To everyone who has supported my journey to this point in my career. To Gabriel Telles who has supported, believed in, and cared for me through the highs and lows. To Jenna Wiegand for being truly an amazing friend and inspiring researcher, while helping guide me through learning to care for my mental health and social awareness of others around me. To Dr. Dean Dauger and the Dauger family for their wonderful mentorship and beloved friendship which has also guided me through this process mentally and professionally. Finally, to my family for believing in me and investing the time and energy to curate me holistically into the individual that I am today. Collectively your efforts are the key to my success, and I could not have done this without you. From the bottom of my heart, thank you and I appreciate all of you.

ABSTRACT OF THE DISSERTATION

Tris(1,3-dichloro-2-propyl) phosphate:
Impacts on Epigenetic Reprogramming and Cellular Metabolism During Embryonic Development

by

Sarah G. Avila-Barnard

Doctor of Philosophy, Graduate Program in Environmental Toxicology
University of California, Riverside, September 2023
Dr. David C. Volz, Chairperson

Organophosphate flame retardants (OPFR) are semi-volatile additive flame retardants that are found in a variety of products that contain polyurethane foam, textiles, and plasticizers. As products age, these chemicals can leach from their end-use products into the air and adhere to certain environmental media such as dust. Tris(1,3-dichloro-2-propyl) phosphate (TDCIPP) is an organophosphate ester-based flame retardant widely used within the United States. TDCIPP has been detected in breast milk, hair follicles, and placental tissue in biomonitoring studies, and previous research has found a significant association between TDCIPP exposure and adverse health effects within human populations. Therefore, the global presence of TDCIPP within indoor air and dust poses a potential public health concern, particularly for pregnant mothers who may be exposed to TDCIPP-contaminated dust or air via ingestion or inhalation. However, the potential mechanisms underlying TDCIPP-induced effects on DNA

methylation, epigenome plasticity, and cellular metabolism during early embryonic development has yet to be fully understood. Moreover, little is known about whether 1) TDCIPP alters key developmental timepoints regulated by DNA methylation and 2) TDCIPP-induced impacts on DNA methylation impact viability and metabolism within human embryonic cells. Within Chapter 2, we utilized immunohistochemistry, high-content screening, and *in situ*-based protocols to develop a method that allows us to track 5-mC across multiple stages of development and dose concentrations within early embryogenesis of zebrafish embryos. Within Chapter 3, we utilized bisulfite amplicon sequencing (BSAS), bioinformatics, *in vitro* assays, and *in situ*-based protocols to understand how TDCIPP exposure impacts cytosine methylation and 5-mC formation within developing zebrafish embryos. Within Chapter 4, we relied on human embryonic kidney (HEK293) cells to determine whether TDCIPP affects cell viability, reactive oxygen species (ROS) production, global 5-mC methylation, cell membrane integrity, mitochondria abundance, and intracellular ATP production by utilizing a combination of *in vitro*, *in situ*, and real-time cell analysis methods. Overall, the findings from this dissertation have increased our understanding about how TDCIPP alters early embryonic development, cellular metabolism, and global DNA/RNA methylation within zebrafish and human cells.

# Table of Contents

# List of Figures

## Chapter 2



## Chapter 3



## Chapter 4

# Chapter 1: Introduction and Literature Review

## Section 1.1: Epigenetic Overview, DNA Methylation, and Early Embryonic Development

In 1942, Conrad Waddington introduced epigenetics by describing it as a concept that involved a complex developmental process between genotype and phenotype (Deichmann, 2016). The epigenome refers to “above the genome” and not the DNA nucleotide sequence at the base-pair level. The epigenome is important in providing signals that regulate genes that are expressed or repressed in transcription. Epigenetic data were historically underrepresented and minimally utilized in diagnostic medicine. Consequently, decades of research have focused on understanding how epigenetic marks regulate transcription factor binding and gene expression. However, in addition to understanding the epigenome and how it is regulated, it is important to understand how these conserved processes interact with exogenous chemicals. The current understanding of epigenetics focuses on four main mechanisms: methylation, acetylation, histone modification, and chromatin remodeling (Becker and Workman, 2013; Deichmann, 2016; Inbar-Feigenberg et al., 2013; Izzo et al., 2021). In addition, the heritability of methylation and decision to invite or exclude methylation support the idea that DNA methylation is adapted for a specific cellular memory function in development (Bird, 2002; Inbar-Feigenberg et al., 2013).

In 1975, Robin Holliday and A.D. Riggs proposed that DNA methylation plays a role in the regulation of gene expression (Deichmann, 2016). Today, we know that methylation suppresses transcription factors from accessing a gene’s coding region. In addition, alleviation of a methylated site acts as an “opened door”, thus welcoming accessibility to the coding region. CpG islands are important in epigenetic reprogramming

during development in addition to regulating homeostasis in most organisms. Earlier studies estimated that 60% of human genes are associated with CpG islands, where the majority of genes are unmethylated at all stages of development (Bird, 2002; Inbar-Feigenberg et al., 2013; Shen et al., 2007). During early embryonic development, DNA methylation plays a critical role in epigenetic reprogramming and gene expression. Methylation and acetylation within many mammals are crucial for regulating access to genes in a time-dependent manner that corresponds to stages of embryonic development. Key genes are important in developmental processes (e.g., organogenesis, cell proliferation, and cell migration) and are therefore accessible during sensitive windows of development. Environmental contaminants can enter the body and depending on the dose, exposure route, and sensitive window of development, can cause epigenetic alterations and alter the trajectory of the developing embryo.

DNA methylation during embryonic development can occur in two contexts: active methylation or passive methylation. Active methylation is associated with excision repair and passive methylation is associated with cell division (Inbar-Feigenberg et al., 2013). The maternal-to-zygotic transition (MZT) represents an example of a developmental landmark that is highly conserved among mammalian species and occurs during epigenetic reprogramming. During early embryonic development, the zygotic genome heavily relies on yolk-derived maternal mRNA to generate proteins (Dean et al., 2003). Thus, as the cell mass continues to replicate and divide, nutrients from the yolk are utilized and maternal mRNA transcripts become degraded. In addition, there is a period of demethylation that occurs simultaneously with the MZT (Dean et al., 2003; Deichmann, 2016). However, once the zygote has sufficient transcripts to carry out transcription/translation processes on its own, zygotic genome activation (ZGA)

commences and the embryo is no longer dependent on maternal mRNA. Following the ZGA, the zygotic epigenome undergoes remethylation which is heavily coordinated by developmental timing. During epigenetic reprogramming, the epigenome is highly susceptible to environmental stressors which can cause alterations to the epigenetic landscape. These alterations can then change chromatin organization and structure, resulting in alterations to transcription which can impact the memory of stress exposure to subsequent generations through mechanisms of epigenetic inheritance (Fabrizio et al., 2019). However, understanding the mechanism underlying chemically-induced impairment or impacts on the epigenome is still not well understood.

**Section 1.2: Environmental Epigenetics**

Epigenetic signatures are used to understand how certain diseases leave a lasting mark on the epigenome. Therefore, recent research has focused on linking epigenetic signatures to certain disease pathologies, with the ultimate goal of using epigenetics as diagnostic tools. For instance, global DNA methylation is typically lower in patients with neurodegenerative disorders than in healthy patients (Levy et al., 2022b; Martínez-Iglesias et al., 2021; Rooney and Sadikovic, 2022; Tedder et al., 2022; Tost, 2020). The development of EpiSign now allows clinicians to order a microarray methylation analysis which links methylation status to certain syndromes (“EpiSign Complete,” n.d.; Haghshenas et al., 2021; Levy et al., 2022a; Sadikovic et al., 2021). In addition, epigenetic signatures are becoming increasingly helpful in understanding how environmental exposure impacts human health and disease. By understanding the mechanism underlying how exposure influences a cell state, epigenetics can, in turn, serve as a biomarker for exposure (Ladd-Acosta, 2015). Interestingly, microRNAs (miRNAs) have dual roles as epigenetic machinery, as miRNAs regulate DNA methylation but miRNA

genes are also epigenetically modified by DNA methylation similar to other protein-coding genes (Aure et al., 2021; Piletič and Kunej, 2016; Wang et al., 2017). These miRNAs are critical to the epigenome by serving as epigenetic regulators that, for example, recruit specific protein complexes to their respective promoters. Around 50% of miRNA genes are associated with CpG islands and their expression is thus modulated by DNA methylation. Therefore, hyper- or hypomethylation of miRNA promoters or dysregulation of the epigenome and miRNAome has been linked to disease states such as cancer (Piletič and Kunej, 2016). From a toxicological perspective, exposure of individuals to toxicants has the potential to change miRNA expression.

Environmental exposures can be determined using questionnaires, personal monitoring devices, and biomarkers of exposure. An example of a biomarker of exposure is the chemical concentration measured within an individual's biological fluids (Ladd-Acosta, 2015). Epigenetic signatures have the potential to link exposure to a certain disease phenotype but, alternatively, also serve as biomarkers of exposure. DNA methylation is a widely used biomarker to study epigenetic reprogramming in human population studies due to methylation levels being inherited during cellular division and their relative stability (Nwanaji-Enwerem and Colicino, 2020). In addition, DNA methylation profiles have been demonstrated to be indicators of human health as well as disease diagnosis and progression due to the role of methylation in altering gene expression and impacting phenotypes (Nwanaji-Enwerem and Colicino, 2020). Furthermore, during development, the epigenome can vary with each cell type and 5-methylcytosine (5-mC) methylation serves to maintain the organization of different tissues that are derived from the "cellular memory" (Colaneri et al., 2013). However, exposure to stress during critical

stages of development has the potential to cause subtle alterations to the epigenome and thus impact developmental timing.

Pathoepigenetics investigates the role that alterations to epigenetic machinery caused by the interaction of genomic, epigenetic, and environmental factors induce pathogenic events that lead to a particular phenotype (i.e., human disease) (Cacabelos, 2019). An individual's exposome and epigenetic signature are determinant factors for cancer as common fragile sites may influence the cancer pathogenesis (Cacabelos, 2019). During fetal development, partially methylated domains commence and then increase with age and cell divisions. Risk factors such as maternal obesity can alter the epigenome of the next generation and impact fetal growth, organ development, metabolic disorders, and cardiovascular disease (Agarwal et al., 2018). Alterations in DNA methylation can also be involved in a broad range of developmental disorders such as preeclampsia, preterm birth, neural tube defects, and autoimmune disorders (Cacabelos, 2019). Therefore, there have been more recent advancements in identifying, documenting, diagnosing, and treating these stable yet reversible epigenetic signatures.

**Section 1.3: Linking Aberrant Methylation to Alterations in Cellular Metabolism**

By the 1990s, research being conducted on the relationship between DNA methylation, cellular differentiation, and gene expression became more closely associated with epigenetics within molecular biology. However, it was not until the early 2000s that the dynamics regarding demethylation after fertilization revealed differences in the timing between the maternal and paternal genome (Deichmann, 2016; Shi and Haaf, 2002). Prior to fertilization, the sperm and oocyte DNA is highly methylated. At the start of fertilization, the zygotic DNA methylome is rewritten and replaces the parental genome; however, there are subsets of genes that are imprinted and inherited. These genes have the ability to

drive monoallelic, parent-of-origin gene expression to certain cell types at specific stages of development (Inbar-Feigenberg et al., 2013). In addition, the epigenome has developmental plasticity where the modification state can be altered by environmental stressors via various modulating epigenetic enzymes, transcription/recruitment factors, transporters, and regulators. This sensitivity to exogenous and endogenous stimuli can also cause “epimutations” which lead to human disease (Inbar-Feigenberg et al., 2013).

Progressive differentiation leads to declining 5-hydroxymethylcytosine (5-hmC) due to its oxidation by Ten-Eleven Translocation (TET) oxidases, resulting in the accumulation of 5-methylcytosine (5-mC) which can then silence genes in early development (Inbar-Feigenberg et al., 2013). Post-committed cells have a distinct epigenetic signature which is a direct reflection of their developmental history, phenotype, and environmental influences (Inbar-Feigenberg et al., 2013). Alterations in pathways that alter the availability of metabolites that function as substrates for enzymes can negatively impair epigenetic modification regulation. As a result, this may impact an enzyme's functionality and ability to maintain the integrity of the epigenome. In addition, alterations to metabolic and epigenetic reprogramming are known characteristics of cancer cells (Izzo et al., 2021).

There is a close link between enzymes that regulate the epigenome landscape and cellular metabolism. Alterations to certain cellular metabolites or biosynthetic molecules which are used in metabolism can cause epigenetic changes and vice versa in cancer (Thakur and Chen, 2019). Mutations in metabolic enzymes can 1) generate oncometabolites that influence epigenetic regulation of histones and DNA and 2) subject cells to tumorigenesis (Thakur and Chen, 2019). Environmental exposures have the ability to alter the metabolome of cells by altering the availability and subcellular

compartmentalization of metabolites which can then affect modifiers of the epigenetic landscape (Sassone-Corsi, 2013). Along with DNA methylation heritability, histones also have methylated sites that can carry epigenetic information (Janke et al., 2015). Therefore, aberrant epigenetics can cause dysregulated gene expression that can lead to upregulation of cancer metabolism, which causes a feedback loop that affects the bioavailability of metabolites utilized by epigenetic enzymes (Izzo et al., 2021).

**Section 1.4: TDCIPP as a Ubiquitous Environmental Contaminant**

Tris(1,3-dichloro-2-propyl) phosphate (TDCIPP) is an organophosphate ester-based additive flame retardant and semi-volatile organic compound (SVOC) widely used within the United States (Dishaw et al.,2014; Doherty et al., 2019; Fu et al., 2013; Liu et al., 2016; McGee et al., 2012; Tran et al., 2021). As an SVOC, TDCIPP migrates from end-use products (e.g., polyurethane foam) into the air and partitions into environmental media such as surface water, air, and dust. For example, longer commutes are associated with increased human exposure to TDCIPP (Brandsma et al., 2014; Reddam et al., 2020), a finding that may be due to the migration of TDCIPP from interior parts of vehicles such as car seats. TDCIPP is still persistent in the environment as a result of use as a flame retardant in a variety of children's products, upholstered furniture, automotive products, padding, and textiles ("Chlorinated Tris," n.d.; Dodson et al., 2013). Due to its ubiquitous presence within the built environment, there is a need for research to better understand the molecular mechanisms underlying the potential hazards of TDCIPP within human populations.

Currently, little is known about how TDCIPP affects cellular metabolism and the epigenetic landscape within cells. TDCIPP was listed on California's Proposition 65 list in 2011 based on its potential to cause cancer following ingestion. In addition, TDCIPP is

an endocrine-disrupting chemical, impacts reproductive health, and is associated with neurobehavioral defects (Agarwal et al., 2018; Dodson et al., 2013, 2012; Doherty et al., 2019; Hoffman et al., 2017b). An epidemiological study in Europe that surveyed dust in cars found that TDCIPP had a median concentration of 31.1 μg/g (Chupeau et al., 2020). Within the United States, the presence of the primary urinary metabolite of TDCIPP (bis(1,3-dichloro-2-propyl) phosphate, or BDCIPP) in men was negatively associated with reduced oocyte fertilization in couples undergoing *in vitro* fertilization (Chupeau et al., 2020). In addition, TDCIPP is known to increase risk of preterm birth, decrease semen quality in males, as well as alter hormone levels (Chupeau et al., 2020; Stapleton et al., 2009; van der Veen and de Boer, 2012; World Health Organization and International Programme on Chemical Safety, 1998). In a cross-sectional European human biomonitoring study, TDCIPP and BDCIPP were detected within 93% of hair follicle samples from mother-child pairs (Kucharska et al., 2015).

Within an occupational setting, TDCIPP is known to be persistent, but the exposure duration and magnitude can also vary depending on the occupational setting. For instance, a worker in Canada who is exposed via inhalation and works as a dismantler in an e-waste facility is estimated to have a median exposure between 3.38-3.06 ng/kg $bw^{-1}day^{-1}$ (Nguyen et al., 2019). In comparison, an e-waste dismantling worker in Pakistan is estimated to have a human inhalation exposure with an average daily dose of 118 ng/kg $bw^{-1}day^{-1}$ (Ma et al., 2021). Similar findings were found when comparing nail salon workers within Canada being exposed to three times more than the concentration of TDCIPP than that of a U.S. worker due to lack of risk management measures (Craig et al., 2019). While TDCIPP is quickly metabolized into BDCIPP in humans, the effects of continuous and cumulative exposure in our everyday environment have yet to be fully understood. A

recent study found that the concentration of TDCIPP that individuals were exposed to did not differ among those who removed the dust from their vehicles versus those that did not (Reddam et al., 2022). Overall, uncertainties about potential exposure routes as well as mechanisms underlying TDCIPP-induced effects on human reproduction and development underscore the need to further investigate this environmental contaminant.

**Section 1.5: Impact of TDCIPP on Early Development**

Using zebrafish as a model, prior studies within our lab found that initiation of TDCIPP exposure at 0.75 h post-fertilization (hpf) reliably disrupted DNA methylation from cleavage (2 hpf) through early gastrulation (6 hpf) as well as induced epiboly delay or arrest during gastrulation (Dasgupta et al., 2017, 2018, 2019; Kupsco et al., 2017; McGee et al., 2012). However, it's unclear whether TDCIPP-induced effects on cytosine methylation occur during later stages of embryonic development. Cytosine methylation is highly conserved across mammalian species in long stretches of cytosine-guanine pairs, or CpG islands. Approximately 2-5% of all cytosines are methylated in the mammalian genome, and methylated cytosines are found across the genome in a CpG, CHG, or CHH context (Fang et al., 2013). Therefore, investigating the potential risk of TDCIPP exposure to humans is important to increase our understanding of how certain environmental contaminants can alter the integrity of the epigenome and the mechanisms which regulate it. Furthermore, both the mode of action, conservation, and developmental plasticity of these alterations in relation to DNA methylation remain unclear. Overall, one of the objectives of this dissertation is to understand how TDCIPP alters cytosine methylation and if these alterations that are reliably reproduced in zebrafish are conserved within humans. Our central hypothesis is that TDCIPP-induced alterations to cytosine methylation are driven by a combination of pharmacokinetic and molecular alterations

during sensitive periods of development which may alter cell plasticity and cause alterations to cellular metabolism (i.e., ATP production).

Methylation is not only inherited through somatic cell divisions but plays a key role in epigenetic regulation (Becker and Workman, 2013). As described above, there is a direct link between DNA methylation, microRNA expression, and cellular metabolism. Within early zebrafish embryogenesis, exposure during cleavage is important in order to observe the delayed epiboly phenotype which is associated with TDCIPP (Dasgupta et al., 2018, 2017; Kupsco et al., 2017; McGee et al., 2012). Prior to 4 hpf, the zygotic genome almost entirely relies on maternal mRNA to carry out early developmental processes. However, exposure at 0.75 hpf leads to hypermethylation in a concentration-dependent manner after quantifying *in situ* levels of 5-mC in developing zebrafish embryos (2-10 hpf) (Avila-Barnard et al., 2022).

Little is known with regards to RNA methylation in developing organisms but even less is understood about how exogenous chemicals interact with or disrupt the translation and localization of mRNA. TDCIPP causes a consistent effect on DNA methylation which, at high concentrations, can lead to embryonic lethality of developing organisms (Chiu et al., 2022; Li et al., 2020). In addition, within zebrafish, parental exposure to TDCIPP can induce alterations to the F1 generation (Ding et al., 2020; Li et al., 2021). However, what remains to be understood is the mechanism by which TDCIPP exerts an effect on DNA methylation. Further research is also needed to understand if TDCIPP impacts global RNA methylation, its epigenetic modifiers, or lipid interactions within the yolk that regulate the RNA microenvironment.

**Section 1.6: Overview of Research Aims**

Although the effects of TDCIPP on DNA methylation and the epigenome in developing organisms have been previously studied, further research is needed regarding TDCIPP's specific mechanism of action and the impacts this mechanism has on epigenetic reprogramming and cellular metabolism. Within Chapter 2, we will utilize immunohistochemistry, high-content screening, and *in situ*-based protocols to develop a method that allows us to track 5-mC across multiple stages of development and dose concentrations within early embryogenesis of zebrafish embryos. Within Chapter 3, we will utilize bisulfite amplicon sequencing (BSAS), bioinformatics, *in vitro* assays, and *in situ*-based protocols to understand how TDCIPP exposure impacts cytosine methylation and 5-mC formation within developing zebrafish embryos. Within Chapter 4, we will rely on human embryonic kidney (HEK293) cells to determine whether TDCIPP affects cell viability, reactive oxygen species (ROS) production, global 5-mC methylation, cell membrane/mitochondrial staining, and intracellular ATP production by utilizing a combination of *in vitro*, *in situ*, and real-time cell analysis methods. While HEK293 cells are a transformed cell line and do not recapitulate normal biology, HEK293 is a widely used human cell line for assessing methylation patterning, aberrant epigenetic marks, and alterations to cellular metabolism in response to exposure to exogenous chemicals while, at the same time, providing a cost-effective model for investigating further understanding mechanisms of chemically-induced toxicity.

## Chapter 2: Rapid and Efficient Spatiotemporal Monitoring of Normal and Aberrant Cytosine Methylation within Intact Zebrafish Embryos

### Section 2.1 Abstract

Cytosine methylation is highly conserved across vertebrate species and, as a key driver of epigenetic programming and chromatin state, plays a critical role in early embryonic development. Enzymatic modifications drive active methylation and demethylation of cytosine into 5-methylcytosine (5-mC) and subsequent oxidation of 5-mC into 5-hydroxymethylcytosine, 5-formylcytosine, and 5-carboxylcytosine. Epigenetic reprogramming is a critical period during *in utero* development, and maternal exposure to chemicals has the potential to reprogram the epigenome within offspring. This can potentially cause adverse outcomes such as immediate phenotypic consequences, long-term effects on adult disease susceptibility, and transgenerational effects of inherited epigenetic marks. Although bisulfite-based sequencing enables investigators to interrogate cytosine methylation at base-pair resolution, sequencing-based approaches are cost-prohibitive and, as such, preclude the ability to monitor cytosine methylation across developmental stages, multiple concentrations per chemical, and replicate embryos per treatment. Due to the ease of automated *in vivo* imaging, genetic manipulations, rapid *ex utero* development time, and husbandry during embryogenesis, zebrafish embryos continue to be used as a physiologically intact model for uncovering xenobiotic-mediated pathways that contribute to adverse outcomes during early embryonic development. Therefore, using commercially available 5-mC-specific antibodies, we describe a cost-effective strategy for rapid and efficient spatiotemporal monitoring of cytosine methylation within an individual, intact zebrafish embryos by leveraging whole-mount immunohistochemistry, automated high-content imaging, and

efficient data processing using programming language prior to statistical analysis. To current knowledge, this method is the first to successfully detect and quantify 5-mC levels *in situ* within zebrafish embryos during early development. The method enables the detection of DNA methylation within the cell mass and also has the ability to detect cytosine methylation of yolk-localized maternal mRNAs during the maternal-to-zygotic transition. Overall, this method will be useful for the rapid identification of chemicals that have the potential to disrupt cytosine methylation *in situ* during epigenetic reprogramming.

**Section 2.2 Introduction**

Enzymatic modifications drive active methylation and demethylation of cytosine into 5-methylcytosine (5-mC) and subsequent oxidation of 5-mC into 5-hydroxymethylcytosine, 5-formylcytosine, and 5-carboxylcytosine (Huang et al., 2016; Zhang et al., 2016). Tris(1,3-dichloro-2-propyl) phosphate (TDCIPP) is a widely used flame retardant in the United States that has been previously demonstrated that alters the trajectory of cytosine methylation following early embryonic exposure from 0.75 h post-fertilization (hpf) through early gastrulation (6 hpf) (Avila-Barnard et al., 2022; Dasgupta et al., 2021, 2019; Kupsco et al., 2017; McGee et al., 2012; Vliet et al., 2019). Within vertebrates, 5-mC and its modified derivatives are critical for regulating early embryonic development (Geiman and Muegge, 2010). Fertilization of an embryo triggers demethylation of parental DNA, followed by maternal mRNA degradation, zygotic genome activation, and remethylation of the zygotic genome (Geiman and Muegge, 2010). Biologically relevant processes that utilize cytosine methylation include histone modification, recruitment of transcriptional machinery, RNA methylation, epigenetic reprogramming, and determination of chromatin structure (Rottach et al., 2009; Wossidlo et al., 2011). Cytosine methylation is also conserved among vertebrate species,

underscoring the importance of understanding and investigating how aberrant cytosine methylation may affect the trajectory of an organism's development (Rottach et al., 2009). Furthermore, *in utero* development is sensitive to maternal exposure and has the potential to cause adverse outcomes such as immediate phenotypic consequences, long-term effects on adult disease susceptibility, and transgenerational effects of inherited epigenetic marks (Baylin and Jones, 2011; Egger et al., 2004; Ooi et al., 2009).

Long stretches of cytosine-guanine pairs, or CpG islands, have been the primary foci of investigators that aim to characterize the dynamics of cytosine methylation across the genome (Greenberg and Bourc'his, 2019; Robertson, 2005, 2002). Bisulfite-based strategies such as whole-genome bisulfite sequencing, reduced representation bisulfite sequencing, and bisulfite amplicon sequencing represent the gold standard for interrogating cytosine methylation at base-pair resolution. However, sequencing-based approaches are cost-prohibitive and, as such, preclude the ability to monitor cytosine methylation across developmental stages, multiple concentrations per chemical, and replicate embryos per treatment. Furthermore, sequencing-based approaches also do not provide information about spatial localization, which is critical for understanding potentially affected cell types and areas within a developing embryo. Similarly, global DNA methylation assays such as methylation-dependent restriction analysis, 5-mC enzyme-linked immunoassays (ELISAs), and 5-methyl-2'-deoxycytidine (5-mC) liquid chromatography-mass spectrometry (LC-MS) rely on cell or tissue homogenates and, as such, preclude the ability to monitor the localization and magnitude of cytosine methylation over space and time within intact specimens (Egger et al., 2004; "Recent advances in the analysis of 5-methylcytosine and its oxidation products," 2014).

Due to the ease of automated *in vivo* imaging, genetic manipulations, rapid *ex utero* development time, and husbandry during embryogenesis, zebrafish embryos continue to be widely used as physiologically intact models for uncovering xenobiotic-mediated pathways that contribute to adverse outcomes during early embryonic development. Therefore, using commercially available antibodies specific to 5-mC, the protocol below describes a cost-effective strategy for rapid and efficient spatiotemporal monitoring of cytosine methylation within an individual, intact zebrafish embryos by leveraging whole-mount immunohistochemistry (IHC), automated high-content imaging, and efficient data processing using programming language prior to statistical analysis.

To our knowledge, this method is the first to monitor 5-mC within intact zebrafish embryos. The method enables the detection of DNA methylation within the cell mass and has the ability to detect cytosine methylation of yolk-localized maternal mRNAs during the maternal-to-zygotic transition. Overall, this method will be useful for the rapid identification of chemicals that have the potential to disrupt cytosine methylation *in situ* during epigenetic reprogramming.

**Section 2.3 Protocol**

Adult breeders were handled and treated in accordance with an Institutional Animal Care and Use Committee (IACUC)-approved animal use protocol (#20180063) at the University of California, Riverside.

**1. Zebrafish embryo collection and chemical exposure**

1.1. Add in-tank breeding traps to tanks containing adult male and female zebrafish that are sexually mature and reproductively viable. Add at least 3 traps per 6-L tank at least 12 h prior to collection at ~9:00 AM, which is the approximate time of fertilization and spawning of eggs within tanks.

1.2. Prepare a fresh exposure solution on the morning of collection. The exposure solution is prepared using a 5-mL pipette and adding 5.0 mL of particulate-free system water to a 60-mm glass Petri dish.

1.3. Then use a 10-µL glass microcapillary pipette to transfer 10 µL of vehicle (dimethyl sulfoxide, or DMSO) or chemical stock solution to system water in the glass dish.

1.4. Swirl the glass Petri dish to ensure the stock solution dissipates. Add another 5.0 mL of system water to the glass Petri dish and swirl the glass Petri dish to homogenize the exposure solution.

1.5. Repeat for each treatment group in replicates of four to yield 4 replicates per treatment.

1.6. After exposure solutions have been prepared, cap the glass dishes with glass lids to minimize evaporation.

1.7. While removing the breeding traps from each tank, carefully allow the water within each trap to drain out into the tank before removing it from each tank and making sure the trap stays right-side up.

1.8. Transfer the breeding traps to the lab sink and rinse them using a squirt bottle filled with reverse osmosis (RO) water into a fish net previously soaked in 10% bleach and rinsed with water. Rinse the embryos until all debris is cleared and only clean embryos remain.

1.9. Transfer the embryos from the fish net using an RO water-filled squirt bottle into a 100-mm plastic Petri dish. Randomly sort 50 live embryos at 0.75 h post-fertilization (hpf) and remove excess RO water.

1.10. Using a microspatula, place sorted embryos into the treatment solution. All embryos must be within vehicle or treatment solution no earlier than 9:45 AM. Swirl glass dishes to ensure embryos are evenly coated within the treatment solution.

1.11. After four replicate dishes (N = 50 per replicate) have been set up for each treatment group, place the glass lid on top of the exposure dishes and transfer all dishes into a temperature-controlled incubator set at 28 °C until 2 hpf, 4 hpf, 6 hpf, 8 hpf, or 10 hpf.

1.12. Prepare fresh 4% paraformaldehyde (PFA) at least 4 h prior to exposure termination and store at 4 °C.

1.12.1. Turn on the hotplate to 115 °C, make 20 mL of 1x phosphate-buffered saline (PBS) (2 mL of 10x PBS + 18 mL of RO water) in a 50-mL centrifuge tube, and weight out 800 mg of paraformaldehyde.

1.12.2. Within a chemical fume hood, transfer 1x PBS solution to a 250 mL Erlenmeyer flask, add 800 mg of paraformaldehyde, and then add 2 µL of 10 N NaOH. Place a thermometer inside the flask and place the flask on the hot plate and watch the temperature while stirring.

1.12.3. When the temperature reaches 62–65 °C, remove 4% PFA from the hot plate and allow it to cool to room temperature (RT). Store 4% PFA at 4 °C.

1.13. Once the exposure duration has ended, remove the embryos from the incubator and transfer all living embryos to a 1.5-mL microcentrifuge tube. Aspirate residual exposure solution using a 1-mL pipette and do not aspirate any embryos.

1.14. Add 500 µL of chilled 4% PFA to a 1.5 mL microcentrifuge tube and mix the embryos in 4% PFA by inversion several times. Allow the embryos to fix in 4% PFA overnight.

NOTE: It is not recommended to allow embryos to stay in PFA for longer than 12 h.

**2. Dechorionation of embryos**

2.1. On the following day, aspirate off 4% PFA, resuspend the embryos in 1x PBS, and gently pipette up and down for 30 s. If needed, stop the protocol at this step and store the embryos in 1x PBS at 4 °C for up to 48 h.

2.2. Using a plastic transfer pipette, carefully transfer fixed embryos to a RO water-filled glass dish and gently swirl for 30 s. Repeat this step one more time.

2.3. Use syringe needles under 5.0x magnification using a standard stereomicroscope to manually dechorionate all embryos. Do this by using the needle tip to puncture the chorion and gently peel it away from the yolk and cell mass(Dasgupta et al., 2021).

2.4. Once the embryos have been dechorionated, use a glass microcapillary pipette to transfer up to 25 intact embryos into one immunochemistry (IHC) basket and place the IHC basket into a 96-well plate. Use a 1-mL pipette to aspirate RO water from each well.

**3. Immunohistochemistry using 5-mC-specific antibody**

3.1. Resuspend the embryos in 500 µL of blocking buffer (1x PBST + 2% sheep serum + 2 mg/mL bovine serum albumin) per well and wrap the plate with parafilm and aluminum foil to protect them from the light. Incubate at 4 °C for 4 h on an orbital shaker (100 rpm).

3.2. Remove the parafilm wrap and aluminum and use a 1-mL pipette to aspirate the blocking buffer from each well and replace it with 500 µL of a 1:100 dilution of monoclonal mouse anti-5-mC antibody in the blocking buffer. Incubate all embryos with primary antibodies except for a subset of vehicle control embryos which will be incubated with the blocking buffer to account for background noise. Be careful not to disrupt the integrity of embryos nor aspirate embryos during this step.

3.3. Rewrap the plate in parafilm and aluminum foil and allow the plate to incubate at 4 °C overnight on an orbital shaker (100 rpm).

3.4. On the following day, remove the primary antibody solution from each well and replace it with 1x PBS + 0.1% Tween-20 (1x PBST). Wash each well 3 times with 1x PBST for 15 min per wash on an orbital shaker (100 rpm).

3.5. Replace 1x PBST with a 1:500 dilution of goat anti-mouse IgG antibody in blocking buffer and incubate all embryos with the secondary antibody. Let the plate incubate at 4 °C overnight on an orbital shaker (100 rpm).

3.6. On the following day, remove the secondary antibody and wash the residual solution 3 times with 1x PBST for 15 min per wash on an orbital shaker (100 rpm).

NOTE: The protocol can be stopped here for up to 48 h if the IHC baskets are stored in clean wells filled with 1x PBS.

3.7. Use a 1-mL pipette to aspirate 1x PBST from each well and place the IHC basket into a glass Petri dish filled with RO water. Under a standard stereomicroscope, randomly sort intact embryos into a 96-well plate, resulting in one embryo per well.

3.8. Using a 1-mL pipette, remove all RO water from individual wells and replace it with 200 µL of 1x PBS. Centrifuge plate for 3 min at 1 x g.

**4. Automated imaging of embryos within 96-well plates**

4.1. Image the embryos with a 2X objective under transmitted light and FITC using a high-content screening system (Table of Materials).

NOTE: A fluorescent image of each embryo was captured automatically using the above-mentioned magnification and a FITC filter (Lantz-McPeak et al., 2015).

4.1.1. Select Autofocus to ensure the focus of the camera was on the bottom of the plate and offset by the bottom thickness.

4.1.2. Select a FITC wavelength with an exposure duration of 100 ms and set the Autofocus to laser with a Z-offset. Observe and confirm proper image acquisition in several wells prior to commencing plate acquisition.

NOTE: The instrument automatically acquires images from all selected wells containing embryos. A 96-well plate required approximately 30 min for image acquisition and data storage. For the duration of the acquisition period, the internal temperature within the imaging system was maintained at RT.

4.2. Following image acquisition, carry out data analysis using the high-content screening system and a custom automated image analysis procedure. Select each embryo on the 96-well plate to be analyzed for total area and integrated intensity of fluorescence.

NOTE: The analysis included providing images that contained overlays of data points from the analysis.

4.3. Then tabulate the data points and export them from the high-content screening system by going under Measure and selecting Open Data Log to a spreadsheet. The plate acquisition and data analysis portions are depicted in Figure 2.1.

**5. Data analysis**

5.1 Upload the exported spreadsheet into a computer program where the deployer (dplyr) package is used to sort, summate data for each well, and filter by well number. The writexl package is then used to export the summated data into an Excel file.

5.1.1 5mC program code:

#Import Data set through read excel in upper right

```
#Load library dplyr
library(dplyr) #grouping by
Stage Label, summing total
area and total integrated
intensity average
OutputTDCIPP156105mC= TDCIPP15610 %>% group_by (StageLabel)

%>% summarise(

n = n(), total = sum(TotalArea), total2
= sum(IIA))
#load write excel and write into excel file and export to desktop
library(writexl)
write_xlsx(OutputTDCIPP156105mC, '~/Desktop/TDCIPP156105mc.xlsx')

#other replicate code

Output25mC= C5m2 %>% group_by (StageLabel) %>% summarise(

n = n(), total = sum(TotalArea), total2 =
sum(IIA))  write_xlsx(Output25mC,
'~/Desktop/5mc2.xlsx')
Output35mC= C5m3 %>% group_by (StageLabel) %>% summarise(

n = n(), total = sum(TotalArea), total2 =
sum(IIA))  write_xlsx(Output25mC,
'~/Desktop/5mc3.xlsx')
```

**Section 2.4 Representative Results**

The overall aim of this protocol is to determine whether a treatment affects the relative abundance of 5-mC by assessing total area and relative intensity of fluorescence within fixed and labeled zebrafish embryos. After completing the protocol, a fluorescence stereomicroscope can be used to first determine whether the whole-mount IHC was successful. When labeled embryos are observed under a FITC or GFP filter, a positive result is indicated by a positive FITC signal within the embryo whereas a negative result is indicated by the absence of fluorescence within control embryos. Using a high-content screening system, these results can also be confirmed during image acquisition using a FITC filter. In addition, during data analysis, the custom module will identify and quantify total area and integrated intensity of fluorescence. Representative images of successful results are shown in Figure 2.1, where acquired images were measured successfully by the custom module and individual data points (shown as blue overlay) were acquired for both total area and integrated intensity.

During data extraction, the threshold stringency within the custom module is an additional variable that needs to be optimized to maximize the signal-to-noise ratio and increase the probability of detecting a significant treatment-specific difference in 5-mC abundance. During optimization, this final threshold provided the largest separation between medians of control and treatment groups (e.g., the largest signal-to-noise ratio). Representative results at varying custom module thresholds that impact signal-to-noise ratios are presented within Figure 2.2.

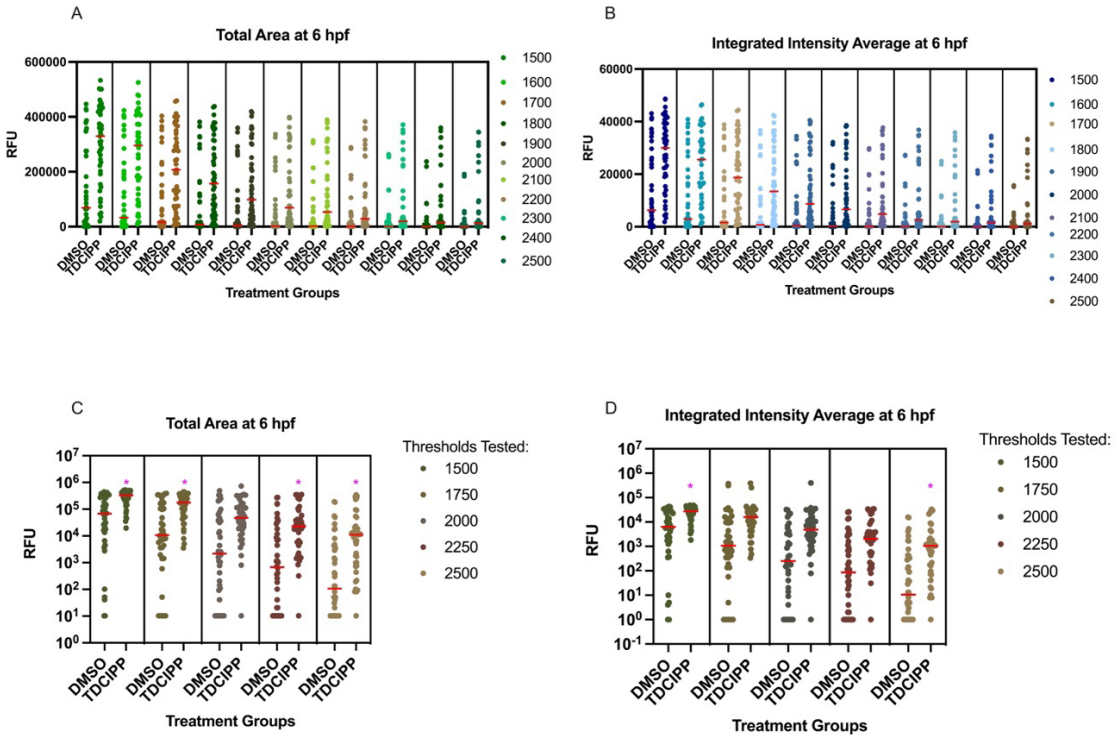


**Figure 2.1** Panels A-D show optimization of the custom module by assessing the median and distribution of 5-mC-specific total area and integrated intensity within zebrafish embryos at 6 hpf. A-B) Different thresholds tested are listed in the legend to the right (difference of 100 between each threshold) and are ordered by stringency, where 1500 and 2500 represent the least and most stringent threshold tested, respectively. C-D) Different thresholds tested are listed in the legend to the right (difference of 250 between each threshold) and ordered by stringency, where 1500 and 2500 represent the least and most stringent threshold tested, respectively. The (*) in C-D denotes thresholds that are significantly different from vehicle-treated embryos ($p<0.05$). For A-B, all thresholds tested were significant from the vehicle control. The x-axis denotes exposure to either vehicle (0.1% DMSO) or 0.78 μM TDCIPP (positive control). The y-axis denotes relative fluorescence. Panel A displays the total area of 5-mC detected within embryos as a function of treatment, whereas Panel B displays the integrated intensity of 5-mC within that same area. One embryo is represented by a single data point for a total N=96 for each treatment group. All exposures were performed in replicates of 4 dishes per treatment with 50 embryos per glass dish.

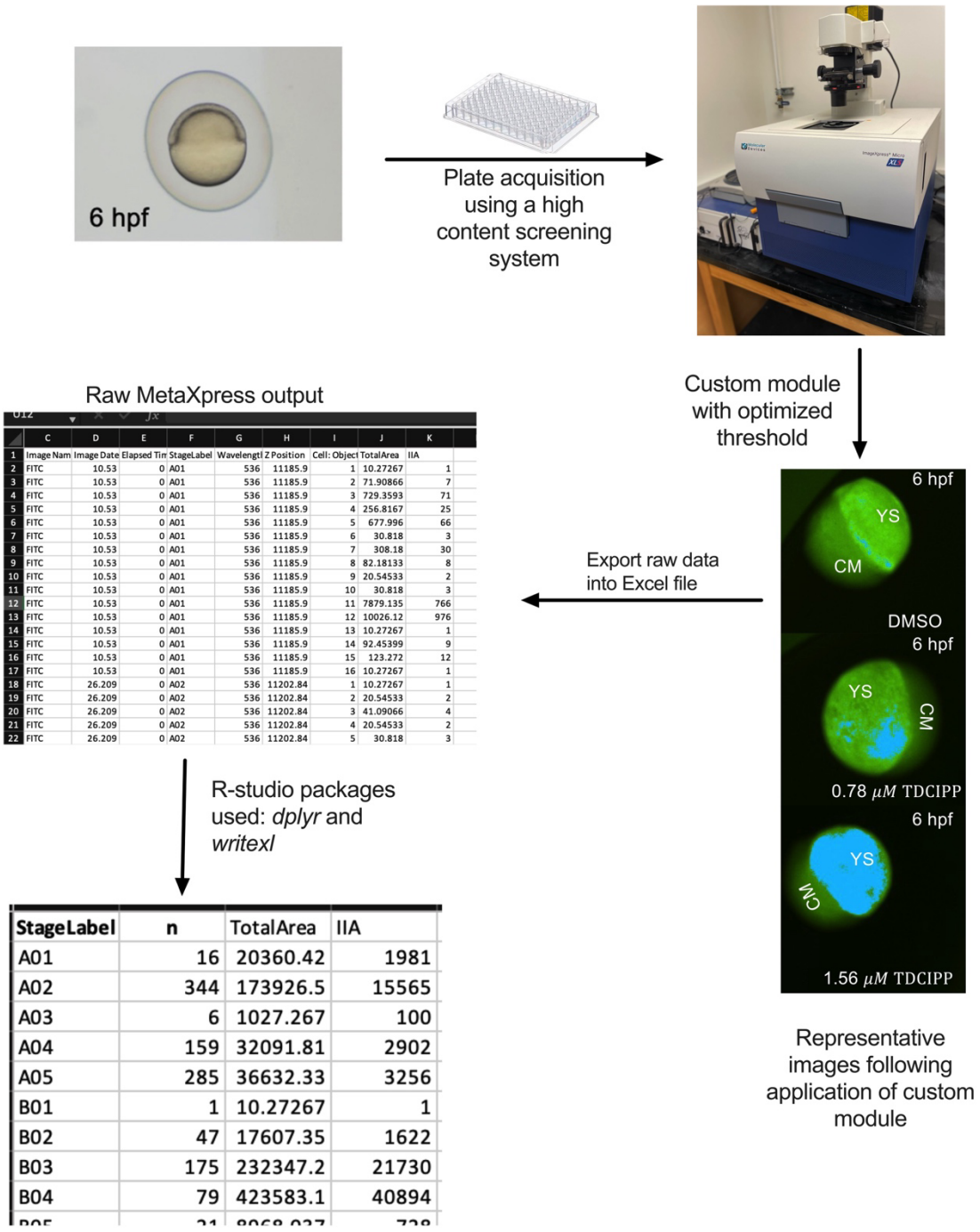


| Image Nam | Image Date | Elapsed Tim | StageLabel | Wavelengt | Z Position | Cell: Object | TotalArea | IIA |
|---|---|---|---|---|---|---|---|---|
| FITC | 10.53 | 0 | A01 | 536 | 11185.9 | 1 | 10.27267 | 1 |
| FITC | 10.53 | 0 | A01 | 536 | 11185.9 | 2 | 71.90866 | 7 |
| FITC | 10.53 | 0 | A01 | 536 | 11185.9 | 3 | 729.3593 | 71 |
| FITC | 10.53 | 0 | A01 | 536 | 11185.9 | 4 | 256.8167 | 25 |
| FITC | 10.53 | 0 | A01 | 536 | 11185.9 | 5 | 677.996 | 66 |
| FITC | 10.53 | 0 | A01 | 536 | 11185.9 | 6 | 30.818 | 3 |
| FITC | 10.53 | 0 | A01 | 536 | 11185.9 | 7 | 308.18 | 30 |
| FITC | 10.53 | 0 | A01 | 536 | 11185.9 | 8 | 82.18133 | 8 |
| FITC | 10.53 | 0 | A01 | 536 | 11185.9 | 9 | 20.54533 | 2 |
| FITC | 10.53 | 0 | A01 | 536 | 11185.9 | 10 | 30.818 | 3 |
| FITC | 10.53 | 0 | A01 | 536 | 11185.9 | 11 | 7879.135 | 766 |
| FITC | 10.53 | 0 | A01 | 536 | 11185.9 | 12 | 10026.12 | 976 |
| FITC | 10.53 | 0 | A01 | 536 | 11185.9 | 13 | 10.27267 | 1 |
| FITC | 10.53 | 0 | A01 | 536 | 11185.9 | 14 | 92.45399 | 9 |
| FITC | 10.53 | 0 | A01 | 536 | 11185.9 | 15 | 123.272 | 12 |
| FITC | 10.53 | 0 | A01 | 536 | 11185.9 | 16 | 10.27267 | 1 |
| FITC | 26.209 | 0 | A02 | 536 | 11202.84 | 1 | 10.27267 | 1 |
| FITC | 26.209 | 0 | A02 | 536 | 11202.84 | 2 | 20.54533 | 2 |
| FITC | 26.209 | 0 | A02 | 536 | 11202.84 | 3 | 41.09066 | 4 |
| FITC | 26.209 | 0 | A02 | 536 | 11202.84 | 4 | 20.54533 | 2 |
| FITC | 26.209 | 0 | A02 | 536 | 11202.84 | 5 | 30.818 | 3 |

| StageLabel | n | TotalArea | IIA |
|---|---|---|---|
| A01 | 16 | 20360.42 | 1981 |
| A02 | 344 | 173926.5 | 15565 |
| A03 | 6 | 1027.267 | 100 |
| A04 | 159 | 32091.81 | 2902 |
| A05 | 285 | 36632.33 | 3256 |
| B01 | 1 | 10.27267 | 1 |
| B02 | 47 | 17607.35 | 1622 |
| B03 | 175 | 232347.2 | 21730 |
| B04 | 79 | 423583.1 | 40894 |

**Figure 2.2** A flow diagram providing a graphical representation of the protocol for exposure and *in situ* detection of 5-methylcytosine for 6-hpf zebrafish embryos. The direction of the flow diagram is provided with black arrows. Exposures occurred in replicates of 4 replicate dishes per treatment and 50 embryos per replicate dish. cm = cell mass; ys = yolk sac.

**Section 2.5 Discussion**

During this protocol there are a few steps that are critical. First, when dechorionating embryos it is important to point the needle away from the tissue of the embryo/yolk sac/cell mass, as these portions of the developing embryo are very fragile and easy to puncture. Second, when transferring labeled embryos to individual wells, use a glass pipette to transfer embryos as they will adhere to a plastic pipette. Third, when performing whole-mount IHC, ensure that the plate is protected from light. Finally, after completing the whole-mount IHC protocol, allow the plate to incubate in 1X PBS at 4ºC overnight before imaging, as this will minimize autofluorescence that may interfere with imaging.

If there are embryos that have been severed during dechorionation or IHC, exclude these embryos from the remainder of the protocol. If no fluorescence is detected, this may be solved by incubating longer (for up to 16 hours). Since this is a 5-mC-specific antibody, both DNA or RNA may be labeled and having a general understanding of spatial localization is important. Some limitations in this method are that it is a non-targeted technique, meaning it will not provide the exact quantity of 5-mC but, rather, the relative abundance based on total area and integrated intensity of fluorescence. In addition, this protocol has only been tested on embryos prior to segmentation so, if testing later stages of development, some additional optimization may be needed. Furthermore, since the method is IHC-based, it may be susceptible to non-specific binding. Therefore, it is not certain that it is only staining 5-mC localized to DNA but may also stain 5-mC localized to RNA as well. Lastly, optimization of the data analysis threshold may be needed depending on the chemical and stringency of the conditions that are preferred.

Overall, this method is provides a quick and cost-efficient detection of 5-mC across multiple stages of development and chemical concentrations. Therefore, this method provides an alternative to cost-prohibitive bisulfite sequencing-based approaches. By offering this protocol, investigators can use this method to quickly screen chemicals and assess how the abundance of 5-mC may be affected during early embryonic development. In addition, this method may be utilized as a prescreening tool to identify the concentration range, period of development, and/or window of sensitivity in which the chemical of interest affects 5-mC abundance. Alternatively, this same method may be utilized for a different biomarker and antibody, albeit further optimization is needed. By utilizing this method, an investigator can quickly, efficiently, and cost-effectively screen and identify a chemical that alters the relative abundance of 5-mC within zebrafish embryos prior to investing in labor-intensive bisulfite sequencing-based approaches. However, this method is zebrafish-specific and further research is needed to determine whether 5-mC can be detected *in situ* within early embryos of other model organisms.

## Chapter 3: Tris(1,3-dichloro-2-propyl) phosphate disrupts the trajectory of cytosine methylation within developing zebrafish embryos

### Section 3.1 Abstract

Tris(1,3-dichloro-2-propyl) phosphate (TDCIPP) is an organophosphate ester-based flame retardant widely used within the United States. Within zebrafish, initiation of TDCIPP exposure at 0.75 h post-fertilization (hpf) reliably disrupts cytosine methylation from cleavage (2 hpf) through early-gastrulation (6 hpf). Therefore, the objective of this study was to determine whether TDCIPP-induced effects on cytosine methylation persist beyond 6 hpf. First, we exposed embryos to vehicle or TDCIPP from 0.75 hpf to 6, 24, or 48 hpf, and then conducted bisulfite amplicon sequencing of a target locus (*lmo7b*) using genomic DNA derived from whole embryos. Within both vehicle- and TDCIPP-treated embryos, CpG methylation was similar at 6 hpf and CHG/CHH methylation were similar at 24 and 48 hpf (relative to 6 hpf). However, relative to 6 hpf within the same treatment, CpG methylation was lower within vehicle-treated embryos at 48 hpf and TDCIPP-treated embryos at 24 and 48 hpf – an effect that was driven by acceleration of CpG hypomethylation. Similar to our previous findings with DNA methyltransferase, we found that, even at high μM concentrations, TDCIPP had no effect on zebrafish and human thymine DNA glycosylase activity (a key enzyme that decreases CpG methylation), suggesting that TDCIPP-induced effects on CpG methylation are not driven by direct interaction with thymine DNA glycosylase. Finally, using 5-methylcytosine (5-mC)-specific whole-mount immunochemistry and automated imaging, we found that exposure to TDCIPP increased 5-mC abundance within the yolk of blastula-stage embryos, suggesting that TDCIPP may impact cytosine methylation of maternally loaded mRNAs during the maternal-to-zygotic transition. Overall, our findings suggest that TDCIPP disrupts the

trajectory of cytosine methylation during zebrafish embryogenesis, effects which do not appear to be driven by direct interaction of TDCIPP with key enzymes that regulate cytosine methylation.

**Section 3.2 Introduction**

Tris(1,3-dichloro-2-propyl) phosphate (TDCIPP) is an organophosphate ester-based additive flame retardant and semi-volatile organic compound (SVOC) widely used within the United States (Dishaw et al., 2014; Doherty et al., 2019; Fu et al., 2013; Liu et al., 2016; McGee et al., 2012; Tran et al., 2021). As an SVOC, TDCIPP migrates from end-use products (e.g., polyurethane foam) into the air and partitions into environmental media such as indoor dust. For example, longer commutes are associated with increased human exposure to TDCIPP (Brandsma et al., 2014; Reddam et al., 2020), a finding that may be due to migration of TDCIPP from interior parts of vehicles such as car seats. In a cross-sectional European human biomonitoring study, TDCIPP and bis(1,3-dichloro-2-propyl) phosphate (BDCIPP, the primary metabolite of TDCIPP) were detected within 93% of hair follicle samples from mother-child pairs (Kucharska et al., 2015), suggesting that human exposure to TDCIPP is ubiquitous.

Previous studies using albino mice found that exposure to 10 μM TDCIPP decreased blastocyst formation and exposure to 100 μM TDCIPP was embryonic lethal, indicating that TDCIPP disrupted development of early mouse embryos in a dose-dependent manner (Yin et al., 2019). Within Chinese rare minnows, TDCIPP exposure induced apoptosis and altered multiple pathways related to DNA damage, effects that were due to TDCIPP-induced oxidative DNA lesions (Chen et al., 2019). Moreover, using zebrafish as a model, prior studies within our lab found that initiation of TDCIPP exposure at 0.75 h post fertilization (hpf) reliably disrupted DNA methylation from cleavage (2 hpf)

through early-gastrulation (6 hpf) as well as induced epiboly delay or arrest during gastrulation (Dasgupta et al., 2019, 2018, 2017; Kupsco et al., 2017; McGee et al., 2012). However, it's unclear whether TDCIPP-induced effects on cytosine methylation occur during later stages of embryonic development.

Epigenetic reprogramming occurs during early embryonic development (fertilization through blastocyst formation) and is highly conserved across multiple model organisms (Breton-Larrivée et al., 2019; Efimova et al., 2020; Jessop et al., 2018). Following fertilization, three processes occur during epigenetic reprogramming: 1) demethylation of paternal DNA; 2) degradation of maternally-loaded mRNA; and 3) remethylation of the zygotic genome (Potok et al., 2013; Tadros and Lipshitz, 2009). Regulation of cytosine methylation is critical during the maternal-to-zygotic transition (MZT) in order to activate the zygotic genome (Potok et al., 2013). During epigenetic reprograming, an embryo progresses through a series of methylation and demethylation steps that drive key processes of development such as cell fate, tissue formation, organogenesis, and neuronal development. Once epigenetic reprogramming is complete, zygotic DNA transcription commences and the zygote decreases reliance on maternal mRNA for cellular maintenance and function (Tadros and Lipshitz, 2009). Therefore, epigenetic reprogramming is critical for proper embryonic development, as key developmental landmarks (e.g., organogenesis) are tightly regulated and coordinated by the timing of genome-wide transcription.

Cytosine methylation is highly conserved across mammalian species in long stretches of cytosine-guanine pairs, or CpG islands. Approximately 2-5% of all cytosines are methylated in the mammalian genome, and methylated cytosines are found across the genome in a CpG, CHG, or CHH context (Fang et al., 2013). During epigenetic

reprogramming, active methylation and demethylation are driven by enzymatic modification of cytosine into 5-methylcytosine (5-mC) by DNA methyltransferase (DNMT) as well as oxidation of 5-mC into 5-hydroxymethylcytosine, 5-formylcytosine, and 5-carboxylcytosine by ten-eleven translocation (TET) enzymes. In addition, demethylase and thymine DNA glycosylase (TDG, coupled with base excision repair) are involved in decreasing 5-mC levels (Jessop et al., 2018). During early stages of development, regulation of cytosine methylation is necessary for the recruitment of transcriptional machinery and ultimately gene expression. Alterations in the normal trajectory of cytosine methylation may disrupt zygotic DNA transcription which, in turn, may adversely affect normal cell adherence, migration, viability, and division within developing embryos (Jones and Takai, 2001).

Using zebrafish as a model, the objective of this study was to determine whether TDCIPP-induced effects on DNA methylation persist beyond 6 hpf as well as whether TDCIPP directly affects zebrafish and human TDG activity. In order to accomplish this objective, we relied on 1) bisulfite amplicon sequencing to test whether TDCIPP-induced alterations in cytosine methylation within a previously identified locus (*lmo7b*) persisted later in embryonic development; 2) thymine DNA glycosylase (TDG) activity assays to determine whether TDCIPP directly affects zebrafish and human TDG activity; and 3) 5-mC-specific whole-mount immunochemistry and automated imaging to investigate whether TDCIPP affected the abundance of 5-mC *in situ* within intact embryos.

**Section 3.3 Materials and Methods**

*Animals*

Adult wild-type (5D strain) zebrafish were raised and maintained and bred on a recirculating system using previously described procedures (Mitchell et al., 2018). Adult

breeders were handled and treated in accordance with an Institutional Animal Care and Use Committee (IACUC)-approved animal use protocol (#20180063) at the University of California, Riverside.

*Chemicals*

TDCIPP (99% purity) was purchased from Chem Service, Inc. (West Chester, PA). Stock solutions of TDCIPP were prepared in high-performance liquid chromatography (HPLC)-grade dimethyl sulfoxide (DMSO) and stored within 2-mL amber glass vials with polytetrafluoroethylene-lined caps. Working solutions (1:1000 dilution of stock solutions) of vehicle (0.1% DMSO) and TDCIPP were prepared in particulate-free water from our recirculating system (pH and conductivity of ~7.2 and ~950 µS, respectively) immediately prior to each experiment.

*Bisulfite Amplicon Sequencing (BSAS)*

Based on our previous findings (Kupsco et al., 2017), we selected a concentration of TDCIPP (0.78 µM) that only induced a ~1.3-h epiboly delay at 6 h post-fertilization (hpf) in the absence of effects on embryo survival. To test whether TDCIPP-induced alterations in cytosine methylation within a previously identified locus (*lmo7b*) (Dasgupta et al., 2019; Kupsco et al., 2017) persisted later in embryonic development, embryos (50 per replicate dish) were treated with 10 mL of vehicle (0.1% DMSO) or 0.78 µM TDCIPP from 0.75 hpf to 6 hpf, 0.75 hpf to 24 hpf, or 0.75 hpf to 48 hpf in glass petri dishes (eight replicate dishes per treatment). Exposures were conducted under static conditions at 28ºC within a temperature-controlled incubator under a 14-h:10-h light:dark cycle. At 6, 24, and 48 hpf, 100 surviving embryos were pooled from two replicate dishes (4 replicate pools per group), snap-frozen in liquid nitrogen, and stored at -80ºC.

Genomic DNA (gDNA) was extracted, purified, and bisulfite-treated following previously described protocols (Kupsco et al., 2017). The region of interest (*lmo7b*) was PCR-amplified and amplicons were purified using previously described protocols (Kupsco et al., 2017). DNA quality was confirmed using an Agilent 2100 Bioanalyzer System (DNA 1000 and High Sensitivity DNA Kits for amplicons and libraries, respectively), and all amplicon and library concentrations were quantified using a Qubit 4.0 Fluorometer (Thermo Fisher Scientific, Waltham, MA, USA). Amplicons were pooled and libraries were prepared using a Nextera XT Library Prep Kit (Illumina, San Diego, CA, USA), and all libraries were paired-end sequenced on our Illumina MiniSeq Sequencing System using a 300-cycle High-Output Reagent Kit. Raw Illumina (fastq.gz) sequencing files (24 files) are available via NCBI's BioProject database under BioProject ID PRJNA780909 (>88.51% of reads were ≥Q30 across all runs). Using previously described protocols (Kupsco et al., 2017), downstream analysis of quality control and methylation differences were identified within Illumina's BaseSpace. MethylSeq was used to align reads and remove duplicate reads, and MethylKit was used for positions with ≥10X CpG coverage to identify significant methylation differences relative to time-matched vehicle controls; $q < 0.01$ was used to minimize false positives.

*Integration and Analysis of BSAS Data*

Including this study, we have utilized BSAS across three separate studies to investigate methylation of *lmo7b* within 2-, 4-, 6-, 24-, or 48-hpf zebrafish embryos following exposure to vehicle (0.1% DMSO), 0.78 μM TDCIPP, or 3.12 μM TDCIPP. Raw Illumina (fastq.gz) sequencing files for all three studies are available via NCBI's BioProject database under BioProject IDs PRJNA395080, PRJNA553577, and PRJNA780909. Cytosine report files containing methylation metrics and cytosine context (CpG, CHG, or

CHH) data at base-pair resolution were obtained from MethylSeq output files for the current study as well as our two prior studies (Dasgupta et al., 2019; Kupsco et al., 2017). For each treatment replicate and timepoint, the <Sample>.CX_report.txt.gz report was downloaded, and raw text files were extracted, indexed, and, depending on the size of the file, trimmed manually or via MATLAB to focus only on positions containing cytosines mapped to Chr1. Trimmed files were then imported into R where package deployer and writexl were used to 1) remove negative strand data, 2) calculate the total number of methylated and unmethylated cytosines (see below for equation), 3) aggregate data by cytosine context, 4) filter out positions where the summation of count methylated and unmethylated were equal to 0, and 5) export output data into Excel files. Data were then combined into a single Excel file and compiled relative to stage (hpf) to be further trimmed by creating a column where the summation between the count methylated and unmethylated could be used as a filter. Only positions with ≥10X coverage were used for statistical analysis.

$$Cs\ Methylated = \left( \frac{(Count\ Methylated)}{(Count\ Methylated + Count\ Unmethylated)} \right) * 100\%$$

$$Cs\ Unmethylated = \left( \frac{(Count\ Unmethylated)}{(Count\ Methylated + Count\ Unmethylated)} \right) * 100\%$$

*Thymine-DNA Glycosylase Assay*

We determined whether TDCIPP directly affects zebrafish and human TDG activity by 1) extracting nuclear proteins from untreated zebrafish embryos and HepG2 cells and 2) quantifying TDG activity *in vitro* in the presence or absence of TDCIPP. Immediately after spawning, newly fertilized zebrafish eggs were collected and placed into groups of approximately 100 per glass Petri dish within a light- and temperature-controlled incubator. Zebrafish embryos (100 per replicate) were collected at 24 hpf and stored at -80°C. HepG2

cells were purchased from American Type Culture Collection (Manassas, VA, USA) and grown within T75 culture flasks (Millipore Sigma, St. Louis, MO, USA) using previously described methods (Cheng et al., 2021). HepG2 cells were grown to 75% confluency then collected after 24 h, lysed, and stored in the lysate at -80°C. Nuclear proteins were extracted from whole zebrafish embryos and HepG2 cells using an EpiQuick Nuclear Extraction kit (Epigentek Group, Farmingdale, NY). Nuclear extracts were aliquoted and stored at -80°C following the manufacturer's instructions. Aliquots from each replicate were thawed on ice, pooled, and immediately analyzed using a BCA Protein Assay (Pierce Biotechnology, Rockford, IL, USA) to quantify protein concentrations. Absorbance was quantified using a Promega GloMax Multiplus Plate Reader/Luminometer, and total protein was quantified using a standard curve generated from bovine serum albumin (BSA).

TDG inhibition was quantified using an Epigenase Thymine DNA Glycosylase (TDG) Activity/Inhibition Assay Colorimetric Kit (Epigentek Group, Farmingdale, NY, USA). TDG activity within nuclear extracts (5 µg of protein per reaction) derived from 24-hpf zebrafish embryos and HepG2 cells was quantified in the presence of vehicle (0.1% DMSO) or TDCIPP (3.91, 7.81, 15.63, 31.25, and 62.5 µM). Four replicate reactions were conducted per treatment group. Absorbance was measured using a Promega GloMax Multiplus Plate Reader/Luminometer, and data were corrected for background and reported as relative fluorescence units. TDG activity was calculated using the following equation:

$$TDG\ Activity\ (OD/min/mg) = \left(\frac{sample\ OD - blank\ OD}{(Protein\ Amount\ (\mu g)\ x\ 90\ minutes)}\right) x\ 1000$$

*5-mC-specific Whole-mount Immunochemistry and Automated Imaging*

To investigate whether TDCIPP affected the abundance of 5-mC *in situ*, embryos were exposed to vehicle (0.1% DMSO) or TDCIPP (0.78 or 1.56 µM) from 0.75- to 10-hpf using procedures described above. Based on our previous findings (Kupsco et al., 2017), we selected 0.78 and 1.56 µM TDCIPP since these concentrations only induced a ~1.3- and ~1.7-h epiboly delay, respectively, at 6 hpf. At exposure termination, embryos were fixed in 4% paraformaldehyde (PFA) overnight at 4ºC. Fixed embryos were then manually dechorionated in a glass petri dish under a Leica MZ10 F stereomicroscope prior to storage in 1X phosphate-buffered saline (PBS) at 4ºC. Intact dechorionated embryos were then incubated with a 1:100 dilution of monoclonal mouse anti-5-mC antibody (Sigma-Aldrich, St. Louis, MO, USA) for 16 h at 4ºC, washed in 1X PBS + 0.1% Tween-20 (1X PBST) three times for 15 min, and then incubated with a 1:500 dilution of AlexaFluor 488-conjugated goat anti-mouse IgG antibody for 16 h at 4ºC (Thermo Fisher Scientific, Waltham, MA, USA).

Using a Leica MZ10 F stereomicroscope, intact embryos were identified and transferred to clear polystyrene 96-well plates (Thermo Fisher Scientific, Waltham, MA, USA) containing 250 µL 1X PBS per well, centrifuged for 3 min at 130 rpm, and then imaged (at 2X magnification) under transmitted light and FITC using our ImageXpress Micro XLS Widefield High-Content Screening System. Within MetaXpress 6.0.3.1658, each embryo was analyzed for total fluorescence area and integrated fluorescence intensity using custom automated image analysis procedures. After exporting data from MetaXpress into Excel files, R coding along with packages deployer and writexl were used to sort, summate data points for each well, filter by well number, and export summated data output from MetaXpress into an Excel file.

*Statistical Analyses*

A general linear model (GLM) analysis of variance (ANOVA) ($\alpha$=0.05) and Tukey-based multiple comparisons were performed using SPSS Statistics 24 for detecting significant within-treatment and/or within-stage differences in context-specific cytosine methylation data**,** TDG assay data, and 5-mC IHC data**.** For BSAS-derived data from this study, percent methylation differences were grouped by hierarchical clustering within Morpheus (Broad Institute, Cambridge, MA, USA) using Euclidean distance with a complete linkage method.

**Section 3.4 Results**

*TDCIPP-induced impacts on CpG methylation persist into later stages of development*

We relied on BSAS to quantify alterations in cytosine methylation within a previously identified locus (*lmo7b*) that was susceptible to TDCIPP exposure. Relative to embryos exposed to vehicle (0.1% DMSO) from 0.75 to 6 hpf, CpG methylation of *lmo7b* was significantly decreased following exposure to the vehicle (0.1% DMSO) from 0.75 to 48 hpf (but not 0.75 to 24 hpf) (Figure 3.1), whereas CHG and CHH methylation of *lmo7b* were not significantly different following exposure to the vehicle (0.1% DMSO) from 0.75 to 24 hpf nor 0.75 to 48 hpf (Figure 3.1). Relative to embryos exposed to 0.78 μM TDCIPP from 0.75 to 6 hpf, CpG methylation of *lmo7b* was significantly decreased following exposure to 0.78 μM TDCIPP from 0.75 to 24 hpf and 0.75 to 48 hpf (Figure 3.1), whereas CHG and CHH methylation of *lmo7b* was not significantly different following exposure to 0.78 μM TDCIPP from 0.75 to 24 hpf nor 0.75 to 48 hpf (Figure 3.1). Overall, these data suggest that 1) exposure to 0.78 μM TDCIPP may accelerate CpG hypomethylation of *lmo7b* by at least 24 h and 2) effects of TDCIPP on CpG methylation persist until at least 48 hpf.

Within-stage and within-treatment effects on CpG methylation were then assessed on four positions on *Imo7b* (Chr1), all of which were localized to a single amplicon that was sequenced using BSAS. Based on this analysis, we found that the magnitude of within-treatment effects (i.e., comparing 24 hpf or 48 hpf relative to 6 hpf within the same treatment) was higher than the magnitude of within-stage effects (i.e., comparing vehicle vs. TDCIPP within the same stage) (Figure 3.2), suggesting that, similar to overall CpG methylation (Figure 3.1), CpG methylation at the position-level is strongly stage-dependent within both vehicle- and TDCIPP-exposed embryos. Moreover, we found that positions 33664419 and 33664494 were more susceptible to TDCIPP-induced acceleration of CpG hypomethylation relative to positions 33664391 and 33664274 (Figure 3.2), suggesting that the effects of TDCIPP on CpG methylation within *Imo7b* may also be position-dependent (e.g., within regions that are CG-rich).

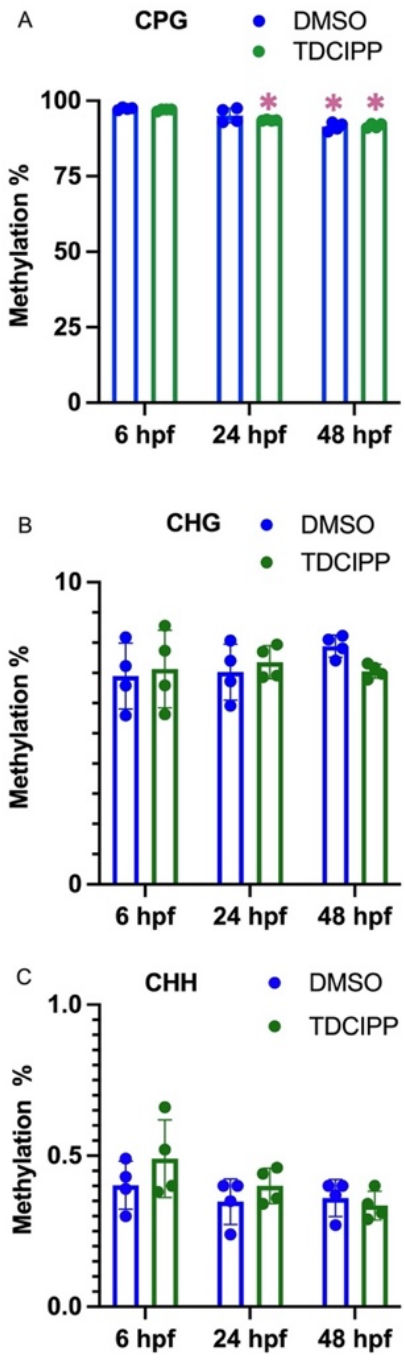


**Figure 3.1** Mean (± standard deviation) percent cytosine methylation of *Imo7b* in a CpG (A), CHG (B), or CHH (C) context following exposure of zebrafish embryos to vehicle (0.1% DMSO) or 0.78 µM TDCIPP from 0.75 hpf to 6 hpf, 0.75 hpf to 24 hpf, or 0.75 hpf to 48 hpf. Asterisk (*) denotes significant within-treatment difference ($p$<0.05) relative 6 hpf; N=4 independent replicates of genomic DNA per group.

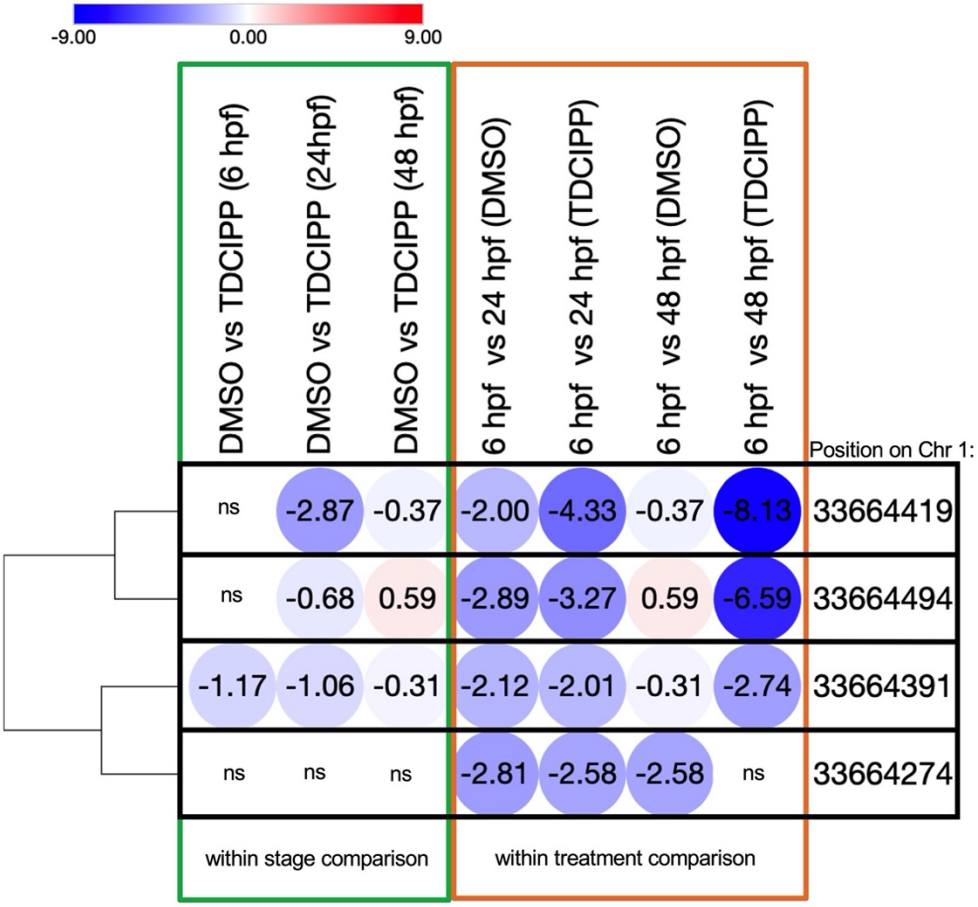


**Figure 3.2** Differences in percent CpG methylation on four *lmo7b* positions following exposure of zebrafish embryos to vehicle (0.1% DMSO) or 0.78 μM TDCIPP from 0.75 hpf to 6 hpf, 0.75 hpf to 24 hpf, or 0.75 hpf to 48 hpf. Data are presented as within-stage (relative to vehicle) and within-treatment (relative to 6 hpf) percent CpG methylation differences. Percent methylation differences were grouped by hierarchical clustering within Morpheus using Euclidean distance with a complete linkage method. N=4 independent replicates of genomic DNA per group; ns = not significant. Blue circles denote a significant percent methylation difference less than zero (hypomethylation), whereas red circles denote a significant percent methylation difference greater than zero (hypermethylation).

*TDCIPP disrupts the normal trajectory of CHH methylation within lmo7b*

Including this study, we have utilized BSAS across three separate studies to investigate methylation of *lmo7b* within 2-, 4-, 6-, 24-, or 48-hpf zebrafish embryos following exposure to vehicle (0.1% DMSO), 0.78 μM TDCIPP, or 3.12 μM TDCIPP.

However, in our prior studies, we did not analyze raw percent methylation data at base-pair resolution by cytosine context (CpG, CHG, or CHH). Therefore, we downloaded cytosine report files to integrate *lmo7b*-specific data from all three studies and identify potential cytosine context-specific effects as a function of stage and/or TDCIPP concentration. As expected, we found that, across all stages and treatments, percent CpG methylation (>95%) was substantially higher than percent CHG and CHH methylation (<10% and <1%, respectively) (Figure 3.3). There were more cytosines on a single amplicon of *lmo7b* within a CHH context (52 total) relative to positions within a CpG context (6 total) and CHG context (19 total). Therefore, we detected significant differences in CHH methylation at 4-, 6-, 24-, and 48-hpf (relative to 2 hpf) following initiation of exposure to vehicle (0.1% DMSO) at 0.75 hpf (Figure 3.3). However, this normal stage-dependent effect on CHH methylation was absent following exposure to 0.78 or 3.12 μM TDICPP, suggesting that, similar to CpG methylation, TDCIPP disrupts the normal trajectory of CHH methylation within developing zebrafish embryos (Figure 3.3).

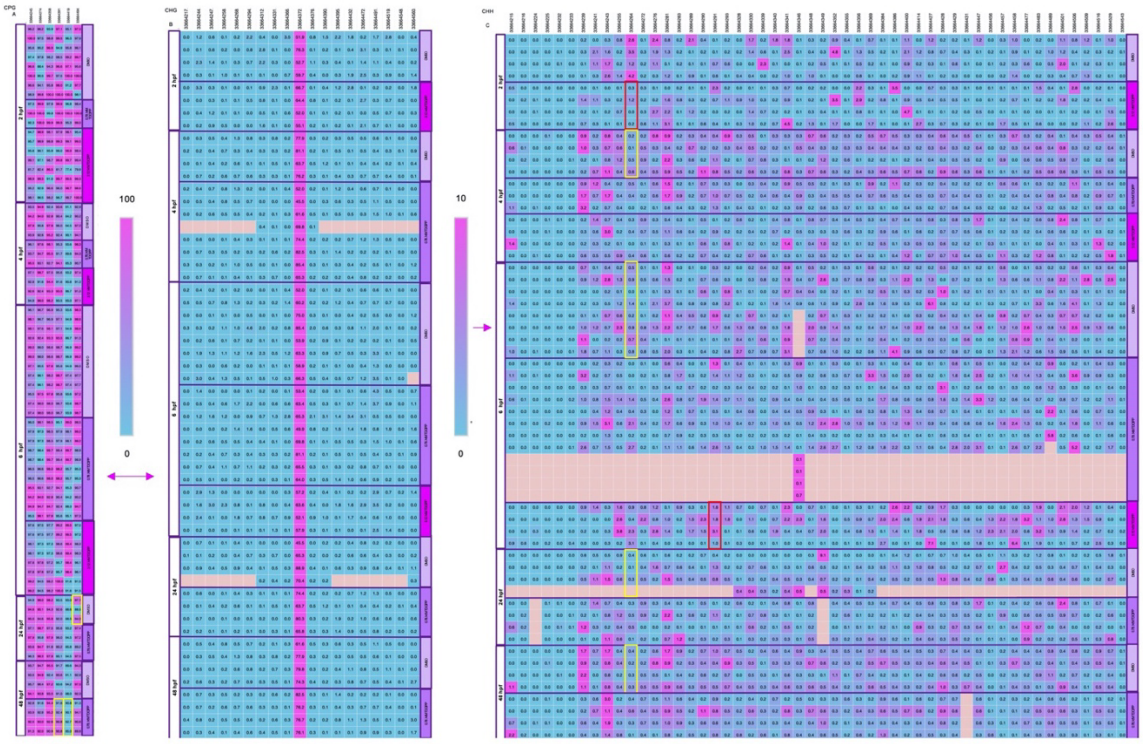

**Figure 3.3** Percent cytosine methylation of *Imo7b* at base-pair resolution in a CpG (A), CHG (B), or CHH (C) context within 2-, 4-, 6-, 24-, or 48-hpf zebrafish embryos following exposure to vehicle (0.1% DMSO), 0.78 μM TDCIPP, or 3.12 μM TDCIPP from 0.75-48 hpf. Squares denote percent cytosine methylation by position for each replicate. Blue denotes 0% cytosine methylation, whereas pink denotes 100% cytosine methylation. Significant within-stage or within-treatment positions ($p<0.05$) are outlined with a red or yellow box, respectively. N=4 independent replicates of genomic DNA per group.

*TDCIPP does not affect zebrafish nor human TDG activity in vitro*

TDCIPP concentrations ranging from 3.91-62.5 μM (the highest concentration tested) had no effect on zebrafish nor human TDG activity (Figure 3.4), suggesting that TDCIPP-induced effects on cytosine methylation are not driven by direct interaction with thymine DNA glycosylase.

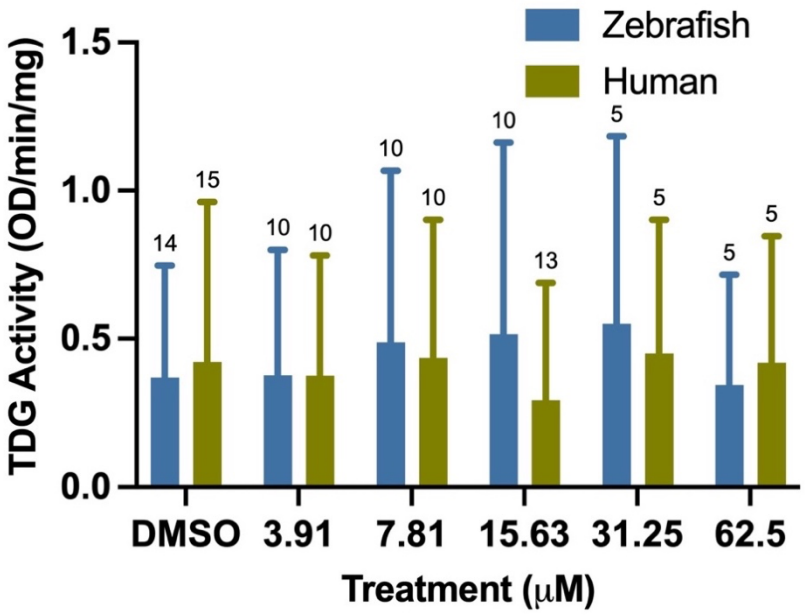


**Figure 3.4** Mean (± standard deviation) thymine DNA glycosylase (TDG) activity within nuclear extracts derived from 24-hpf zebrafish embryos and HepG2 cells following incubation in the presence of vehicle (0.1% DMSO) or TDCIPP (3.91, 7.81, 15,63, 31,25, and 62.5 μM). Numbers above bars denote number of replicate reactions conducted per treatment group.

*TDCIPP increases 5-mC abundance within the yolk of blastula-stage embryos*

We relied on 5-mC-specific whole-mount IHC and automated imaging to monitor TDCIPP-induced effects on cytosine methylation *in situ* as a function of stage and TDCIPP concentration. At 2 and 4 hpf**,** the vast majority of 5-mC was detected within the yolk of developing embryos (Figure 3.5), suggesting that the anti-5-mC antibody we used also labeled yolk-localized maternal mRNA containing methylated cytosines. However, at 6, 8 and 10 hpf, 5-mC was increasingly detected within portions of the cell mass, suggesting that cytosine methylation within the cell mass increases during gastrulation. Interestingly, using two different fluorescence-based measurements (total area or integrated intensity) as endpoints, we found that initiation of exposure at 0.75 hpf to 0.78 μM or 1.56 μM TDICPP resulted in a significant increase in yolk-localized cytosine methylation at 2 hpf

and/or 4 hpf relative to vehicle-exposed, phenotypically identical embryos at the same stage (Figure 3.5), suggesting that the downstream effects on TDCIPP on epiboly during gastrula (5.25-10 hpf) may be driven by disruption of yolk-localized cytosine methylation within the first 4 h of development.

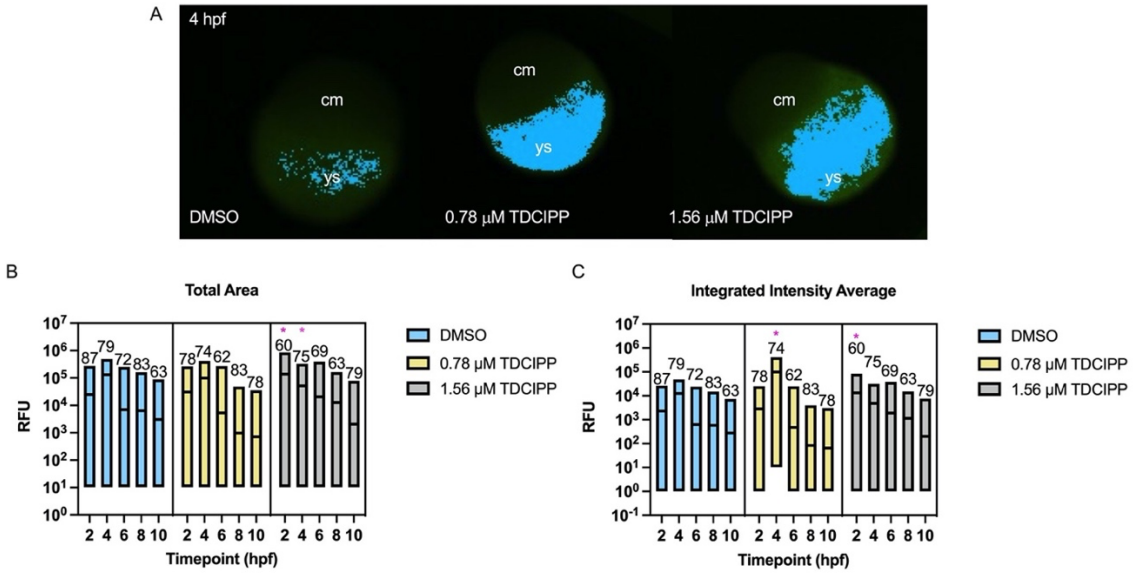


**Figure 3.5** TDCIPP-induced effects on cytosine methylation *in situ* as a function of developmental stage and TDCIPP concentration. Zebrafish embryos were exposed to vehicle (0.1% DMSO) or TDCIPP (0.78 or 1.56 μM) from 0.75- to 10-hpf and then processed for 5-mC-specific whole-mount immunochemistry. Intact embryos were imaged under transmitted light and FITC, and then analyzed using our ImageXpress Micro XLS Widefield High-Content Screening System. Representative images of 4-hpf embryos are shown in Panel A. Within MetaXpress 6.0.3.1658, each embryo was analyzed for total area (B) and total integrated intensity (C) of fluorescence using custom automated image analysis procedures. Asterisk (*) denotes significant within-stage difference ($p$<0.05) relative to vehicle controls. Numbers above bars denote number of intact embryos imaged per group. cm = cell mass; ys = yolk sac.

### Section 3.5 Discussion

This study builds upon our previous research demonstrating that TDCIPP impacts cytosine methylation within developing zebrafish embryos (Dasgupta et al., 2019; Kupsco et al., 2017; McGee et al., 2012; Volz et al., 2016). While we acknowledge that the nominal

concentrations of TDCIPP (0.78 and 1.56 μM) used within this study may be higher than concentrations detected within blood and/or placental tissues, our study suggests that TDCIPP – if elevated *in utero* – has the potential to impact the normal trajectory of cytosine methylation during early stages of embryonic development. Human exposure to TDCIPP continues to be ubiquitous around the world, and the concentration of BDCIPP – a primary metabolite of TDCIPP detected in urine – within humans has increased over the past 15 years (Hoffman et al., 2017a). As the dynamics of cytosine methylation are highly conserved among mammalian species and critical for regulating cell differentiation (Martin and Fry, 2018; Shen et al., 2007), our findings suggest that TDCIPP may impact cytosine methylation within mammalian embryos in addition to zebrafish embryos.

Interestingly, we found that TDCIPP-induced impacts on CpG methylation within *lmo7b* persisted into later stages of development, and the severity of this effect was dependent on the developmental stage, TDCIPP concentration, and chromosomal position. Although *lmo7b* was used as a readout for TDCIPP-induced effects on cytosine methylation in zebrafish embryos**,** we suspect that, similar to *lmo7b*, there may be genome-wide effects of TDCIPP on CpG methylation (Volz et al., 2016). Moreover, the magnitude of TDCIPP-induced effects on CpG methylation across the genome may be associated with downstream effects during blastulation and gastrulation (e.g., epiboly delays, etc.), as regulation of 5-mC is necessary for signaling processes that specify cell tissue fate across multiple species (Bartels et al., 2018; Jones, 2012). Indeed, similar to our findings in zebrafish, prior studies have reported that TDCIPP exposure disrupts early mouse embryonic development by inducing uneven blastomeres and abnormal blastocyst formation (Yin et al., 2019) – effects that may be a result of aberrant CpG methylation following fertilization.

Similar to CpG methylation, our analysis across a total of three BSAS studies (including this study) conducted within our lab revealed that TDCIPP also disrupts the normal trajectory of CHH methylation of *lmo7b*. To our knowledge, little is known about the role of CHH methylation in embryonic development, including within plants. In cotyledons, normal CHH methylation increases from 6% to 11% in earlier to later stages of development, respectively (An et al., 2017). In *Arabadopsis*, normal CHH methylation increases to 25% in normal mature embryos during development followed by a decrease in CHH methylation during germination (Gutzat et al., 2020). In zebrafish, benzo[a]pyrene (a known human carcinogen) induces changes in CHH methylation within the first few hours of development (Corrales et al., 2014), suggesting that other environmental chemicals may have an impact on CHH methylation during zebrafish embryogenesis. Overall, little is known about the physiological importance and impacts of alterations in CHH methylation, underscoring the importance of future investigations into how these alterations impact epigenetic reprogramming and developmental landmarks such as the MZT.

Our prior study demonstrated that TDCIPP does not affect DNMT activity *in vitro* at concentrations as high as 500 μM (the highest concentration tested) (Volz et al., 2016). Similarly, in this study we found that TDCIPP did not affect zebrafish nor human TDG activity *in vitro* at concentrations as high as 62.5 μM (the highest concentration tested). As a result, our studies to date suggest that the impacts of TDCIPP on cytosine methylation do not appear to be driven by direct interaction of TDCIPP with key enzymes (such as DNMT and TDG) that regulate cytosine methylation. However, additional research is needed to confirm whether TDCIPP directly affects the activity of TET and demethylase, as both enzymes are, like TDG, involved in decreasing 5-mC levels.

5-mC is a direct and stable biomarker for detecting alterations in epigenetic modifications (Efimova et al., 2020). Although 5-mC is one of the most important RNA modifications and TET proteins are responsible for 5-mC oxidation, little is known about the biological significance of methylated RNA beyond potential functions in control/regulation of gene transcription and protein translation (Zhang et al., 2016). To our knowledge, this is the first study to successfully detect and quantify 5-mC levels *in situ* within zebrafish embryos during early development. Surprisingly, we found that exposure to TDCIPP increased 5-mC abundance within the yolk of blastula-stage embryos, suggesting that, in addition to impacts on DNA methylation within the cell mass, TDCIPP may affect cytosine methylation of yolk-localized maternal mRNAs during the MZT. During early zebrafish development, the translation and subsequent degradation of maternal mRNAs are essential for zygotic genome activation (Tadros and Lipshitz, 2009) – a process that is tightly regulated by zygotically-derived miR-430 that deadenylates and targets several hundred maternal mRNAs for clearance (Giraldez et al., 2006). Moreover, 5-mC-modifed maternal mRNAs are more stable than non-5-mC-modifed maternal mRNAs during early zebrafish embryogenesis (Yang et al., 2019), suggesting that an abnormal increase in 5-mC-modifed maternal mRNAs may stall maternal mRNA decay and lead to a disruption in the timing of the MZT as well as developmental landmarks such as epiboly.

**Section 3.6 Conclusions**

In conclusion, our findings show that TDCIPP disrupts the normal trajectory of cytosine methylation within developing zebrafish embryos. Specifically, we found that 1) TDCIPP-induced impacts on CpG methylation persist into later stages of development; 2) TDCIPP disrupts the normal trajectory of CHH methylation within *lmo7b*; 3) TDCIPP does

not affect zebrafish nor human TDG activity *in vitro*; and 4) TDCIPP increases 5-mC abundance within the yolk of blastula-stage embryos. Overall, our findings suggest that TDCIPP disrupts cytosine methylation of zygotic DNA within the cell mass as well as maternal mRNA within the yolk – effects that appear to be independent of direct interaction of TDCIPP with enzymes that regulate cytosine methylation**.** Importantly, TDCIPP-induced disruption of cytosine methylation during epigenetic reprogramming has the potential to lead to downstream effects on embryonic development as well as adverse outcomes into adulthood such as cancer. Indeed, TDCIPP was added to California's Proposition 65 (Prop 65) list in 2011 based on its potential to cause cancer within humans.

Interestingly, TDCIPP-induced impacts on methylation do not appear to be driven by 1) direct interaction of TDCIPP with key enzymes (such as DNMT and TDG) that regulate cytosine methylation (Volz et al., 2016) nor 2) effects on methyl donor concentrations (Kupsco et al., 2017). Therefore, our findings to date point to an alternative mechanism underlying aberrant methylation such as TDCIPP-induced oxidative stress. TDCIPP is known to induce reactive oxygen species (ROS) production within human neuroblastoma cells (Li et al., 2017), and the role of oxidative stress in modifying the epigenome has been recognized as an important mechanism driving carcinogenesis (Wu and Ni, 2015). Therefore, additional research is needed to explore alternative mechanisms (such as oxidative stress) underlying aberrant methylation as well as understand the potential impacts of TDCIPP-induced effects on 5-mC-specific methylation and stability of maternally loaded mRNAs during early embryonic development within zebrafish and other human-relevant models. In addition, more research is needed to assess the potential association of TDCIPP exposure and altered DNA methylation status within human populations that experience chronic and ubiquitous exposure.

## Chapter 4: Tris (1,3-dichloro-2-propyl) phosphate disrupts cellular metabolism within human embryonic kidney (HEK293) cells

### Section 4.1 Abstract

Tris (1,3-dichloro-2-propyl) phosphate (TDCIPP) is a widely used, additive flame retardant that migrates from end-use products into environmental media (e.g., surface water, air, and dust), resulting in chronic exposure of human populations around the world. Prior epidemiological studies within the United States have found that human TDCIPP exposure is associated with a decrease in fecundity, a finding that may be driven by TDCIPP-induced implantation failure. However, little is known about whether TDCIPP disrupts the physiology of human embryonic cells at environmentally relevant concentrations. Therefore, the overall objective of this study was to determine whether TDCIPP alters cell viability, cytosine methylation, reactive oxygen species (ROS) levels, and cellular metabolism using human embryonic kidney (HEK293) cells as a model. Using CellTiter-Glo assays, we first found that, relative to vehicle controls, exposure to environmentally relevant concentrations of TDCIPP for 24 or 48 h resulted in a concentration-dependent increase in cell viability, a finding that was likely driven by an increase in the relative ATP abundance. In addition, using real-time live cell metabolic analysis, we found that TDCIPP exposure resulted in an increase in Oxygen Consumption Rate, Extracellular Acidification Rate, and Proton Efflux Rate during glycolysis. Second, we found that TDCIPP exposure up to 48 h did not affect global 5-methylcytosine (5-mC) methylation, cell membrane integrity, nor the abundance of mitochondria *in situ*. Using CellROX Green assays, we detected a significant, concentration-dependent decrease in ROS *in situ* (relative to vehicle-treated cells) after 48 h (but not 24 h) of TDCIPP exposure, suggesting that exposure to 0.1% DMSO alone may increase ROS generation within

HEK293 cells and TDCIPP may counteract the effects of 0.1% DMSO. Finally, using metabolomics focused on biomolecules involved in central carbon metabolism, we found that TDCIPP exposure significantly increased carnosine and impacted histidine metabolism pathways. Overall, our findings with TDCIPP point to a novel mechanism of action that may be relevant to human embryonic stem cells and/or other organohalogen flame retardants that are frequently detected within human biomonitoring studies.

**Section 4.2 Introduction**

All mammalian cells utilize cellular metabolism to generate biomolecules and metabolites which can be used to drive other cellular processes. There is a direct link between alterations in epigenetic marks (e.g., 5-methylcytosine) and the relative abundance of biomolecules that are produced from cellular metabolism. Activation of oncogenes, regulators, key signaling pathways, glucose transporters, key glycolytic enzymes or the loss of function of tumor suppressor genes can lead to adverse effects, such as glycolytic fluxes, inadequate ATP generation, and low formation of reactive oxygen species (ROS) – all of which promote malignant progression and survival of tumor cells (T. Oronsky et al., 2014; Vaupel and Multhoff, 2021; Zhu et al., 2020). Little is known about how exogenous chemicals influence the interaction among these intertwined processes. Originally postulated in 1923, the Warburg effect accelerates the conversion of glucose to lactate in malignant tumors even when there is no hypoxia (Vaupel and Multhoff, 2021). A high amount of ATP production promotes a cancer cell's high maintenance needs while low ROS formation negatively impacts cellular respiration and mitochondrial function.

Tris(1,3-dichloro-2-propyl) phosphate (TDCIPP) is an additive organophosphate flame retardant that is widely used within products such as textiles, plasticizers, and

polyurethane foam. As these products age, TDCIPP has the potential to migrate from its end-use product into environmental media such as air, dust, and surface water. Within the United States, TDCIPP has been detected in serum, urine, hair, breast milk, and placenta (Doherty et al., 2019; Ladd-Acosta, 2015; van der Veen and de Boer, 2012; Yang et al., 2019). Although TDCIPP rapidly metabolizes into mono- or diester metabolites that are excreted in urine, the high frequency of TDCIPP detection in urine is due to its ubiquitous exposure in our surrounding environment (Chupeau et al., 2020; Hoffman et al., 2017a). Moreover, humans are exposed to TDCIPP through multiple routes of exposure including inhalation, ingestion, and dermal absorption (Doherty et al., 2019). In 2011, TDCIPP was added to California's Proposition 65 (Prop 65) list based on its potential to cause cancer following ingestion (Dodson et al., 2012). Although the use of TDCIPP in furniture has declined within California, TDCIPP is still prevalent in our surrounding environment due to its high usage in a variety of consumer products including vehicles.

Prior epidemiological research that assessed oocyte fertilization in couples undergoing IVF indicted that detection of paternal BDCIPP (the primary TDCIPP metabolite) in urine at 0.43 μg/L was associated with a 8% decrease in fecundity (Carignan et al., 2018), a finding that may be driven by TDCIPP- or BDCIPP-induced implantation failure. Therefore, it is important to understand how cellular metabolism within sensitive windows of pre-implantation embryos might be perturbed by TDCIPP at environmentally relevant concentrations within human populations. However, as human embryonic stem cells are cost-prohibitive and require days to weeks to differentiate, we utilized human embryonic kidney (HEK293) cells as a model to begin investigating the potential impacts of TDCIPP on cellular metabolism. Therefore, the overall objective of this chapter is to address how TDCIPP exposure affects human embryonic kidney (HEK293) cells by

assessing cell viability, cellular metabolism (i.e., ATP production and central carbon metabolism), the abundance of mitochondria, cell membrane integrity, reactive oxygen species abundance, and glycolysis.

**Section 4.3 Materials and Methods**

*2.1 Chemicals*

TDCIPP (99% purity) was purchased from Chem Service, Inc. (West Chester, PA). Stock solutions of TDCIPP were prepared in high-performance liquid chromatography (HPLC)-grade dimethyl sulfoxide (DMSO) and stored within 2-mL amber glass vials with polytetrafluoroethylene-lined caps. Working solutions were prepared by spiking 1 μL of stock solutions into 999 μL of sterile cell culture media immediately prior to each exposure, resulting in 0.1% DMSO within all vehicle and treatment groups.

*2.2 HEK293 Cell Culture*

HEK293 cells were purchased from American Type Culture Collection (Manassas, VA, USA) and grown in Eagle's Minimum Essential Medium (ATCC, Manassas, VA, USA) supplemented with 10% fetal bovine serum (FBS) (ATCC, Manassas, VA, USA). Cells were maintained in a temperature- and $CO_2$-controlled incubator at 37°C and 5%, respectively. Cell culture media was changed every 48 h and cells were split at 70-90% confluency every four to five days (depending on confluency) using 0.25% Trypsin/0.53 EDTA (ATCC, Manassas, VA, USA).

*2.2.1 Cell Viability Assay*

HEK293 cells were counted using a hemocytometer and resuspended in 20 mL of sterile cell culture media at a concentration of ~$1x10^6$ and ~$5x10^5$ for 24 h and 48 h exposures, respectively. 200 μL of HEK293 cells were plated in sterile 96-well plates at a final concentration of ~$1x10^4$ and ~$5x10^3$ cells per well for 24 h and 48 h exposures,

respectively, and allowed to adhere overnight. Media was then removed from each well and replaced with 200 μL of media containing either vehicle (0.1% DMSO) or TDCIPP (0.015-31.25 μM) within 4 replicate wells per treatment. Cells were then incubated at 37°C and 5% $CO_2$ for 24 h or 48 h. In addition, blank wells (with cells, but without vehicle) and negative control wells (without cells) were also included to account for any DMSO-specific effects and/or background fluorescence. At the end of the exposure duration, the plate was allowed to equilibrate to room temperature. Treatment solutions were removed from all wells and replaced with 100 μL of sterile cell culture media (warmed to room temperature) and 100 μL of CellTiter-Glo reagent (Promega). The plate was mixed on an orbital shaker for 2 min to induce cell lysis and then allowed to incubate at room temperature for 10 min for the luminescent signal to stabilize. Luminescence was then measured using a GloMax-Multi + Detection Dual Injector System (Promega, Madison, WI, USA).

Interestingly, our CellTiter-Glo data revealed a concentration-dependent increase in cell viability within HEK293 cells after 24 h and 48 h of exposure. Therefore, this raised the question of whether TDCIPP interacted with key ATP-producing enzymes, as the CellTiter-Glo assay is based on ATP quantification as a readout for metabolically active cells. To address this question, HEK293 cells were plated and pre-treated for 12 h as previously described to either vehicle (0.1% DMSO), oligomycin (an ATP synthase inhibitor), or compound 3K (a pyruvate kinase M2, or PKM2, inhibitor) at the following concentrations: 0.05, 0.10, 0.50, or 1 μM. 1 μM was used as an upper limit, as previous studies found that 1 μM was sufficient to successfully disrupt mitochondrial or glycolytic activity without inducing cytotoxicity (Chinthala et al., 2016; Jastroch, 2012; Park et al., 2021). The exposure solution was aspirated from each well, replaced with 4% PFA for 5

min at room temperature, and washed three times for 5 min with 1X PBS. Cells were then counterstained with 1:4 solution of DAPI Fluoromount-G for 5 min at room temperature on an orbital shaker. Lastly, cells were washed three times for 5 min with 1X PBS at room temperature before finally being preserved in 250 μL of 1X PBS. To identify a maximum tolerated concentration (MTC) based on cytotoxicity, cells were counterstained with 1:4 solution of DAPI Fluoromount-G (Southern Biotechnology, GA) for 5 min at room temperature on an orbital shaker (100 rpm), rinsed with 1X PBS three times while gently shaking, and then imaged at 10X magnification under transmitted light and a DAPI using our ImageXpress Micro XLS Widefield High-Content Screening System. Within MetaXpress 6.0.3.1658, each well was analyzed for total fluorescence area intensity using custom automated image analysis procedures. After exporting data from MetaXpress into Excel files, R coding along with packages *deployer* and *writexl* were used to sort, and summate data points for each well, filter by well number, and export summated data output from MetaXpress into an Excel file. We then normalized luminescence data from CTG to DAPI total area to account for any well-to-well variability in the number of cell nuclei.

*2.2.2 Cell Viability Assay with Pre-Treatment*

We then pre-treated cells to vehicle (0.1% DMSO), the MTC of oligomycin, or the MTC of compound 3K for 12 h and then exposed cells to vehicle (0.1% DMSO), 0.015, 0.031, 0.061, 0.1225, 0.245, 0.49, 0.98, or 1.95 μM TDCIPP for either 24 h or 48 h. We also utilized untreated and negative control wells to account for any vehicle-specific effects. Each treatment group was conducted in replicates of eight. At the end of the exposure, we utilized four replicate wells for each treatment group and aspirated off the exposure solution. After aspirating off the exposure solution from each well, we then replaced it with 4% PFA for 5 min at room temperature. After 5 min, we aspirated 4% PFA

and then washed three times for 5 min with 1X PBS on an orbital shaker. Cells were then counterstained with a 1:4 solution of DAPI Fluoromount-G for 5 min. Lastly, cells were washed three times for 5 min with 1X PBS before being preserved in 250 μL of 1X PBS. For the remaining 4 replicates, we utilized a CellTiter-Glo (CTG) assay to determine cell viability and relative ATP abundance. Cells were imaged and analyzed as described above.

For DAPI, cells were imaged at 10X magnification under transmitted light and a DAPI filter using our ImageXpress Micro XLS Widefield High-Content Screening System. Within MetaXpress 6.0.3.1658, each well was analyzed for total fluorescence area using custom automated image analysis procedures. After exporting data from MetaXpress into Excel files, R coding along with packages *deployer* and *writexl* was used to sort, summate data points for each well, filter by well number, and export summated data output from MetaXpress into an Excel file. We then normalized CTG to DAPI to account for any variability in the number of cell nuclei. This helped us understand if pre-treatment with oligomycin or compound 3K mitigated TDCIPP-induced effects on cell viability or ATP abundance. In addition, this helped us understand if TDCIPP exposure indirectly interacted with key enzymes (ATP synthase and PKM2) that are involved in intracellular ATP production.

*2.3 5-methylcytosine (5-mC) Immunocytochemistry*

To quantify the abundance of 5-mC, cells were exposed to either vehicle (0.1% DMSO) or TDCIPP (0.015, 0.49, or 15.63 μM TDCIPP) as described above for either 24 h or 48 h. At exposure termination, cells were fixed using 50 μL of 4% PFA at room temperature for 5 min. Cells were then rinsed three times with 1X PBS and incubated in blocking buffer (1X PBST, 2 mg/mL bovine serum albumin, and 2% sheep serum) at room

temperature for 1 h on an orbital shaker rotating at 100 rpm. The blocking buffer was then replaced with 1:100 dilution of monoclonal mouse anti-5-mC antibody (Sigma-Aldrich, St. Louis, MO, USA) and incubated for 16 h at 4ºC on an orbital shaker rotating at 100 rpm. The primary antibody solution was removed and cells were then washed three times with 1X PBST for 5 min per wash. Cells were then incubated with a 1:500 dilution of AlexaFluor 488-conjugated goat anti-mouse IgG antibody for 16 h at 4ºC on an orbital shaker (100 rpm) (Thermo Fisher Scientific, Waltham, MA, USA). Cells were then counterstained with 1:4 solution of DAPI Fluoromount-G (Southern Biotechnology, GA) for 5 min at room temperature on an orbital shaker (100 rpm), rinsed with 1X PBS three times while gently shaking, and then imaged at 10X magnification under transmitted light, a DAPI filter, and a FITC filter using our ImageXpress Micro XLS Widefield High-Content Screening System. Within MetaXpress 6.0.3.1658, each well was analyzed for total fluorescence area and integrated fluorescence intensity using custom automated image analysis procedures. After exporting data from MetaXpress into Excel files, R coding along with packages *deployer* and *writexl* were used to sort, summate data points for each well, filter by well number, and export summated data output from MetaXpress into an Excel file.

*2.4 CellROX Green Assay*

We relied on CellROX Green Reagent (ThermoFisher, Carlsbad, CA) to identify whether TDCIPP increased the presence of reactive oxygen species. Cells were plated at a concentration of ~$1x10^4$ and ~$5x10^3$ cells per well for a 24 h and 48 h exposure, respectively. Cells were allowed to adhere for 24 h prior to aspirating cell culture media. Exposure solutions were prepared as described above, and cells were exposed to vehicle (0.1% DMSO) or 0.015, 0.061, 0.245, 0.49, 0.98, 3.91, or 15.63 μM TDCIPP (4 replicate wells per treatment group) for either 24 h or 48 h. Blank wells (with cells, but without

vehicle) and negative control wells (without cells) were included to account for any DMSO-specific effects and/or background fluorescence.

At exposure termination, treatment solutions were aspirated and each well was replaced with 200 μL CellROX Green Reagent diluted in cell culture media at a final concentration volume of 5 μM. Cells were then incubated for 30 min at 37°C. CellROX Green Reagent was removed and replaced with 150 μL of 4% PFA for 5 min at room temperature. PFA was removed and cells were then washed three times with 1X PBS for five minutes per wash at room temperature on an orbital shaker (100 rpm). Cells were then counterstained with a 1:4 solution of DAPI Fluoromount-G (Southern Biotechnology, GA) for 5 min at room temperature on an orbital shaker (100 rpm), rinsed with 1X PBS three times for 5 min each time while gently shaking. Cells were then imaged and analyzed as described above. We also normalized the data by dividing the total fluorescence area of ROS by DAPI-based cell count to account for well-to-well variability in cell counts.

*2.5 Cell Membrane Labeling*

We relied on AlexaFluor 488-conjugated WGA (Invitrogen) to identify whether TDCIPP perturbed cell membrane integrity by disrupting glycoprotein/glycolipid proteins within HEK293 cells. Cells were plated at a concentration of ~$1x10^4$ and ~$5x10^3$ cells per well for a 24 h and 48 h exposure, respectively. Cells were allowed to adhere for 12 h prior to aspirating cell culture media. We then pre-treated cells to vehicle (0.1% DMSO), the MTC of oligomycin, or the MTC of compound 3K for 12 h and exposed cells to vehicle (0.1% DMSO) or 0.061, 0.245, or 0.98 μM TDCIPP (4 replicate wells per treatment group) for either 24 h or 48 h. We utilize untreated and negative control wells to account for any vehicle-specific effects. At the end of the exposure, we utilized four replicate wells for each treatment group and aspirate off the exposure solution. We aspirated the exposure

solution and replaced it with 150 μL of 4% PFA for 5 min at room temperature. PFA was removed and the cells were then washed three times with 1X PBS for five minutes per wash at room temperature on an orbital shaker (100 rpm). We prepared a 1.0 mg/mL AlexaFluor 488-conjugated WGA stock solution in 1X PBS before diluting it into 1.0 mg/mL in Hank's Balanced Salt Solution (HBSS) for a final concentration of 5.0 μg/mL. We added 200 μL of diluted AlexaFluor 488-conjugated WGA to each well and allowed 10 min for incubation at room temperature. Cells were washed three times with 1X PBS before being counterstained with DAPI. Cells were then imaged and analyzed as described above.

*2.5 .2 MitoTracker Orange staining*

We relied on diluted MitoTracker Orange CM-$H_2$TMROS (ThermoFisher, Carlsbad, CA) to identify whether TDCIPP decreased the presence of active mitochondria. Using the methods described above, and cells were exposed to vehicle (0.1% DMSO) or 0.061, 0.245, 0.98, or 1.95 μM TDCIPP (4 replicate wells per treatment group) for either 24 h or 48 h. Blank wells (with cells but without vehicle) and negative control wells (without cells) were included to account for any DMSO-specific effects and/or background fluorescence. At the end of the exposure duration, we aspirated off the exposure solution replacing it with diluted MitoTracker Orange CM-$H_2$TMROS (ThermoFisher). Cells were then incubated for 40 min at 37°C. At the end of incubation, the MitoTracker Orange dye was aspirated off, cells were washed with cell media, and replaced with diluted CellROX Green to stain for ROS. Following incubation, CellRox Green solution was aspirated off and replaced with 4% PFA for 5 min at room temperature. Similar to our methods described above, cells were counterstained with DAPI, imaged, and analyzed. Data were normalized by dividing the total ROS fluorescence as well as the total mitochondria fluorescence by DAPI-based cell count to account for well-to-well variability in cell counts.

*2.6 Seahorse XFp Analyzer Assay*

*2.6.1 Real-Time ATP Production Assay*

HEK293 cells were plated in 80 μL at a confluency of ~4x$10^3$ cells per well in a Seahorse XFp cell culture miniplate and allowed to adhere overnight in a 37°C $CO^2$ incubator. We then exposed HEK293 cells to either vehicle (0.1% DMSO) or 0.015, 0.98, and 3.91 μM TDCIPP for 24 h using the methods described above (N=3 wells per treatment group). Per the Seahorse XFp Real-Time ATP Rate Kit User Guide, the sensor cartridge was hydrated one day prior to the assay at 37°C in a non-$CO_2$ incubator overnight using sterile molecular grade biology (MGB) water. On the day of the assay, MGB water was discarded from the utility plate and replaced with prewarmed XF Calibrant 50 min prior to loading the ports. Under sterile conditions, assay media was created by supplementing 10 mL of Seahorse XF DMEM Medium (pH= 7.4) with 10 mM of XF glucose, 1 mM of XF pyruvate, and 2 mM of XF glutamine and then warmed to 37°C in a non-$CO_2$ incubator. At exposure termination, cells were removed from a 37°C $CO^2$ incubator and examined under a microscope for confirmation of consistent plating and proper cell morphology. Cells were then washed with warmed seahorse media and transferred to a non-$CO_2$ incubator for incubation at 37°C for 45 min prior to the assay. As cells were incubating, fresh stock compound solutions of Oligomyocin (75 μM) and Rotenone + Anytimycin A (24 μM) were reconstituted and vortexed for ~1 min before being diluted to 1.5 μM and 0.5 μM, respectively. The diluted stock solutions were then added to their respective ports in the sensor cartridge and placed into the Seahorse XFp analyzer for calibration. After 45 min, the cells were washed with warmed assay media prior to being placed in the Seahorse XFp analyzer and the assay was started. Oxygen consumption rate (OCR), extracellular acidification rate (ECAR), and proton efflux rate

(PER) were recorded for each well. We then aspirated the Seahorse media from each well and replaced it with 200 μL of Hoechst 33342 dye diluted in Seahorse media for a final concentration of 0.002 μM per well. The cell plate was then placed in a non-$CO_2$ 37°C incubator for 5 min. Cells were then imaged on a Nikon Eclipse TI under a DAPI channel using a 10X objective and exported as a tiff for each replicate well. Each tiff was then imported into ImageJ to count the total number of detectable cells. OCR, ECAR, and PER rates were then imported into ImageJ to count the total number of detectable cells. OCR, ECAR, and PER rates were then normalized by their respective cell counts and initial readings for each time point.

*2.6.2 Glycolytic Rate Assay*

We investigated if TDCIPP impacted glycolysis within HEK293 cells by relying on an Agilent Seahorse XFp Glycolytic Rate Assay Kit (Agilent, Wilmington, DE). HEK293 cells were plated at a confluency of ~$4x10^3$ cells per well in a Seahorse XFp Microplate and then allowed to adhere overnight in a 37°C $CO^2$ incubator. We then used methods described above for the exposure of non-treated and blank wells to account for any vehicle-specific effects or background noise. We exposed cells to either vehicle (0.1% DMSO) or 0.061, 0.245, and 0.98 μM TDCIPP for 24 h using methods described above. As cells incubated, fresh stock compound solutions of Rotenone + Antimycin A (50 μM) and 2-deoxy-D-glucose (500 mM) were reconstituted and vortexed for ~1 min before being diluted to 0.5 μM and 50 mM, respectively, in warmed seahorse media. We then relied on a Glycolytic Rate Assay Kit in a Seahorse XFp Analyzer to measure the OCR, ECAR, and PER through real-time measurements of changes in glycolytic rates in vehicle- vs. TDCIPP-treated cells. Cells were then stained with Hoechst as well as imaged and analyzed as described above.

*2.7 Central Carbon Metabolism-Specific Metabolomics*

Cells were plated and exposed as described above. For analysis of biomolecules involved in central carbon metabolism, cells were exposed to either vehicle (01% DMSO), 0.061 μM TDCIPP, 0.245 μM TDCIPP, or 0.98 μM TDCIPP for 24 h (96 wells pooled per replicate; 4 replicates per treatment). At exposure termination, treatment solutions were removed and replaced with 50 μL of 1:2 dilution of Trysin-EDTA in cell culture media. Cells were then incubated for 3-5 min at 37°C before adding 100 μL of media to deactivate trypsin. Trypsinized cells (96 wells per replicate) were washed and then transferred into a 15-mL tube. Cells were centrifuged for 10 min at 1.2 rpm, and the supernatant was discarded and replaced with 200 μL of Hank's Balance Salt Solution (HBSS). The cell pellet was washed by gentle agitation and centrifuged for 10 min at 1.2 rpm, and cells were washed and centrifuged two more times.

On the third wash, 10 μL were removed from each sample to perform a cell count using a hemocytometer as well as a cell viability assay using a 1:1 dilution of Trypan Blue (ThermoFisher). Cells were then centrifuged for 20 min at 1.2 rpm. HBSS was removed and replaced with 50 μL of chilled 100% methanol. Cells were stored at -80°C overnight. On the following day, samples were sonicated for 10 min in an ice bath, vortexed, and sonicated for 5 min or until the cell pellet was completely disrupted. Samples were then centrifuged for 20 min at 4,000 rpm and 4°C in 15 mL falcon tube. The supernatant was then aspirated, transferred to an amber glass vial, and a nitrogen blower was used to evaporate the methanol. Samples were resuspended in 50 μL of methanol and then processed by UCR's Metabolomics Core using a Waters TQ-XS triple quadrupole mass spectrometer coupled to a Waters two-dimensional I-class UPLC.

Targeted metabolomics of polar, primary metabolites were performed at UCR's Metabolomics Core as previously described (Vliet et al., 2019). Briefly, the analysis was performed on a TQ-XS triple quadrupole mass spectrometer (Waters) coupled to an I-class UPLC system (Waters). Separations were carried out on a ZIC-pHILIC column (2.1 x 150 mm, 5 µM) (EMD Millipore). The mobile phases were (A) water with 15 mM ammonium bicarbonate adjusted to pH 9.6 with ammonium hydroxide and (B) acetonitrile. The flow rate was 200 µL/min and the column was held at 50° C. The injection volume was 2 µL. The gradient was as follows: 0 min, 90% B; 1.5 min, 90% B; 16 min, 20% B; 18 min, 20% B; 20 min, 90% B; 28 min, 90% B. The MS was operated in multiple reaction monitoring mode (MRM). Source and desolvation temperatures were 150° C and 600° C, respectively. Desolvation gas was set to 1100 L/hr and cone gas to 150 L/hr. Collision gas was set to 0.15 mL/min. All gases were nitrogen except the collision gas, which was argon. Capillary voltage was 1 kV in positive ion mode and 2 kV in negative ion mode. A quality control (QC) sample, generated by pooling equal aliquots of each sample, was analyzed periodically to monitor system stability and performance. Samples were analyzed in random order.

*Section 2.8 Statistical Analyses*

A general linear model (GLM) analysis of variance (ANOVA) ($\alpha$=0.05) and Tukey-based multiple comparisons were performed using SPSS Statistics 24 for detecting significant differences between TDCIPP-treated and vehicle groups for cell viability**,** CellROX-Green assay data, Seahorse ATP Rate, WGA data, Seahorse Glycolytic rate, and 5-mC IHC data. For the metabolomics data, we assessed all detectable metabolites that were statistically different in TDCIPP-treated groups relative to the vehicle control using a confidence interval between 90-80% confidence ($\alpha$=0.05, 0.1, and 0.2). For the

MitoTracker Orange assay data, all vehicle control and blank wells were compared against the negative control wells, and those that had no statistically significant difference were removed prior to analyzing data within SPSS.

**Section 4.4 Results**

*3.1 TDCIPP increases cell viability and relative abundance of ATP within HEK 293 cells*

We relied on CellTiter-Glo assays to quantify cell viability in HEK293 cells that were either continuously exposed to vehicle (0.1% DMSO) or TDCIPP for 24 h or 48 h. Overall, we found that, relative to vehicle controls, exposure to TDCIPP at environmentally relevant concentrations for 24 or 48 h resulted in a concentration-dependent increase in cell viability up to 0.245 μM (Figure 4.1). Since luminescence within the CellTiter-Glo assay is dependent on ATP production, we concluded that a TDCIPP-induced increase in cell viability was driven by an increase in the relative ATP abundance within HEK293 cells. However, we found that higher concentrations of TDCIPP did not induce an increase in cell viability relative to vehicle-treated cells (Figure 4.1). Interestingly, we found that this effect was strongest at 24 h and was not as pronounced after 48 h of exposure. In addition, we found that pre-treatment with ATP synthase and PKM2 inhibitors (up to 1 μM) did not affect the relative total number of cell nuclei in HEK293 cells (Figure 4.2). We found that exposure between 0.061-0.98 μM TDCIPP did not alter the total area of cell membrane or glycoprotein formation within HEK293 cells. Overall, our preliminary data suggest that 1) concentrations between 0.015-0.98 μM TDCIPP exposure increases cell viability of HEK293 cells at 24 h and 48 h; 2) ATP production is likely increased within TDCIPP-treated cells relative to vehicle-treated cells; and 3) pre-treatment with oligomycin or compound 3K does not mitigate TDCIPP-induced effects on cell viability or ATP abundance.

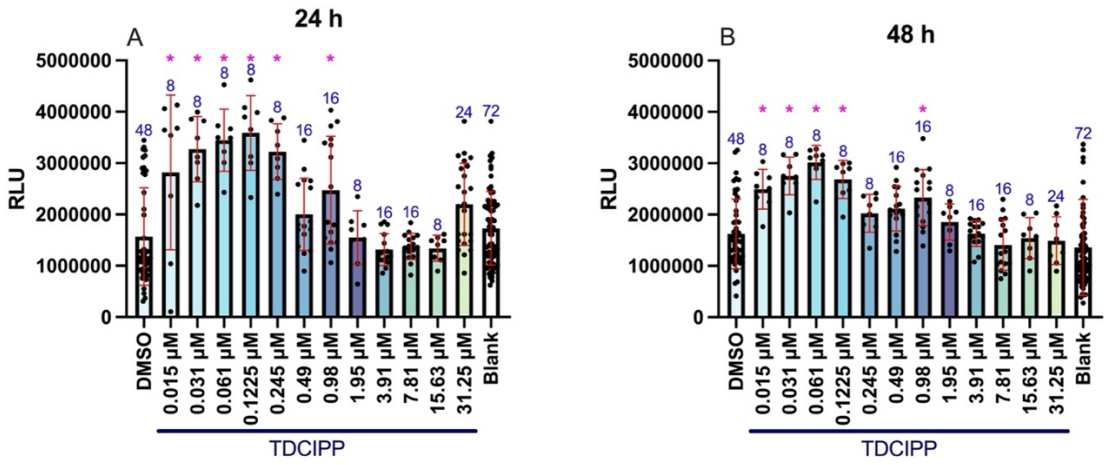


**Figure 4.1** Mean (± standard deviation) CellTiter-Glo luminescence of HEK293 cells exposed to either vehicle (0.1% DMSO) or 0.015-31.25 µM TDCIPP for 24 h (A) or 48 h (B). Blank = unexposed cells. Sample sizes (number of wells) are indicated above each treatment group. Asterisk (*) denotes a significant difference ($p<0.05$) relative to vehicle (0.1% DMSO).

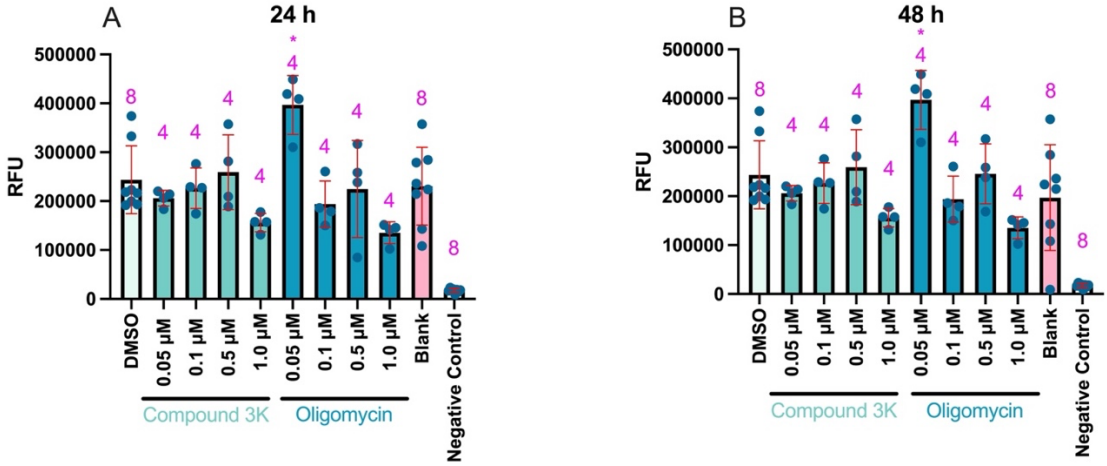


**Figure 4.2** Mean (± standard deviation) DAPI area of HEK293 cells pretreated with either vehicle (0.1% DMSO), oligomycin (0.05, 0.1, or 1.0 µM) or compound 3K (0.05, 0.1, or 1.0 µM) for 12 h. Cells were imaged under transmitted light and DAPI using our ImageXpress Micro XLS Widefield High-Content Screening System. Within MetaXpress 6.0.3.1658, each well was analyzed for total area of DAPI using custom automated image analysis procedures.

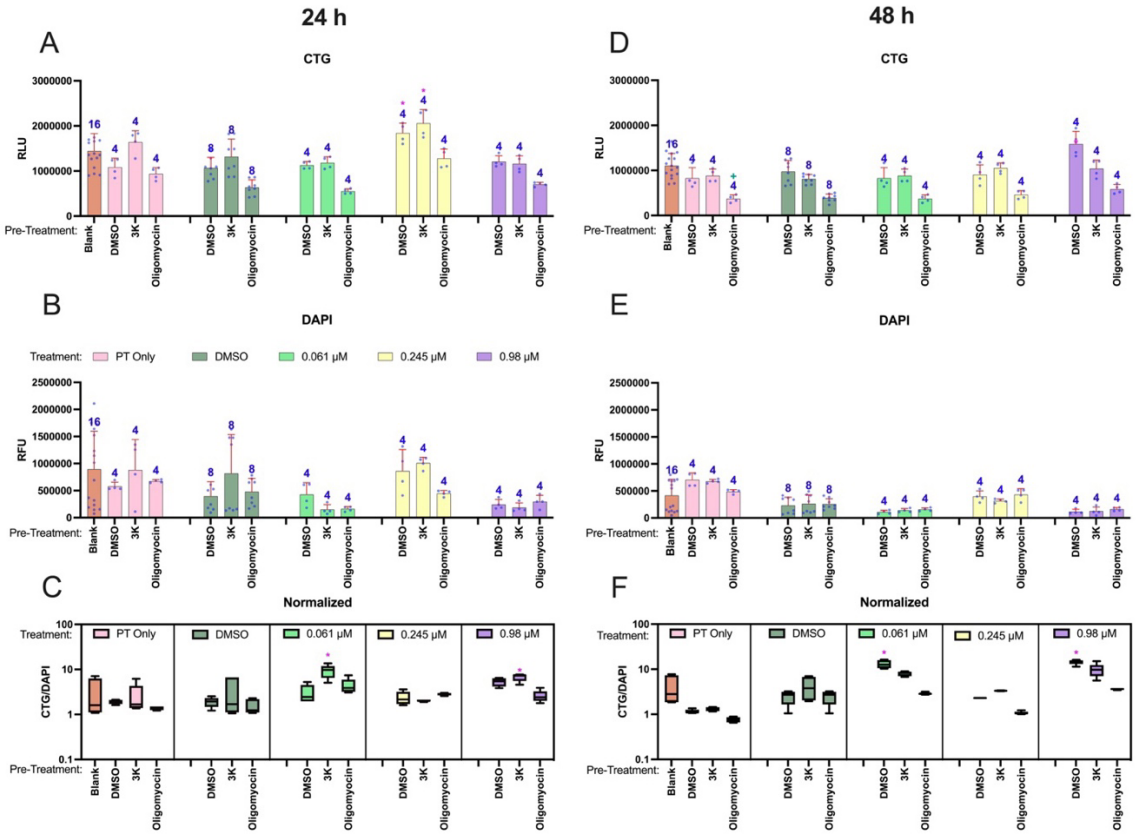


**Figure 4.3** Mean (± standard deviation) CellTiter-Glo luminescence of HEK293 cells exposed to either vehicle (0.1% DMSO) or 0.015-31.25 µM TDCIPP for 24 h (A) or 48 h (D). Mean (± standard deviation) DAPI area of HEK293 cells pretreated with either vehicle (0.1% DMSO), oligomycin (0.1225 µM) or compound 3K (0.1225 µM) for 12 h in 24 h (B) and 48 h €. Cells were imaged under transmitted light and DAPI using our ImageXpress Micro XLS Widefield High-Content Screening System. Within MetaXpress 6.0.3.1658, each well was analyzed for total area of DAPI using custom automated image analysis procedures. Panels C and F show mean (± standard deviation) CellTiter-Glo luminescence divided by DAPI stained area of HEK293 cells. Asterisk (*) denotes a significant difference ($p$<0.05) relative to vehicle controls. Blank = unexposed cells. Sample sizes (number of wells) are indicated above each treatment group. Asterisk (*) denotes a significant difference (p<0.05) relative to vehicle (0.1% DMSO).

*3.2 TDCIPP does not affect 5-mC abundance in situ within HEK293 cells*

We relied on 5-mC-specific immunocytochemistry to determine if TDCIPP exposure affected global cytosine methylation within HEK293 cells. We found that continuous exposure for either 24 h or 48 h TDCIPP up to 15.63 µM did not result in

statistically significant differences relative to vehicle-treated cells (Figure 4.4), suggesting that TDCIPP exposure up to 48 h does not affect the abundance of 5-mC *in situ* within HEK293 cells. Contrary to our findings within early zebrafish embryos, this may have been due to a lack of dynamic alterations in DNA methylation (e.g., epigenetic reprogramming) within HEK293 cells, resulting in the inability of TDCIPP to interfere with or alter methylation patterning. In addition, overall global 5-mC methylation is relatively low within HEK293 cells (Grosser et al., 2015). As such, future studies should focus on overexpressing enzymes that regulate DNA methylation to determine whether TDCIPP impacts active methylation/demethylation within HEK293 cells.

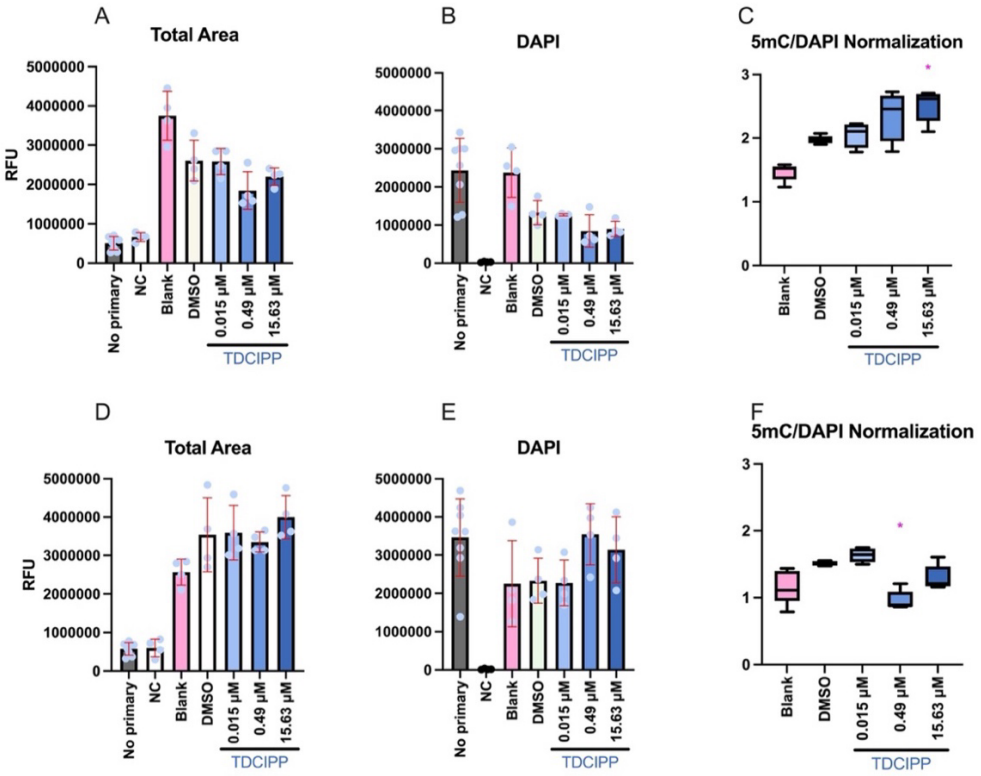


**Figure 4.4** Mean (± standard deviation) total area of 5-methylcytosine (5-mC) (A and D), DAPI (B and E), and 5-mc/DAPI (C and F) within HEK293 cells exposed to vehicle (0.1% DMSO), 0.015 µM TDCIPP, 0.49 µM TDCIPP, or 15.63 µM TDCIPP for 24 h (A-C) and 48 h (D-F). Asterisk (*) denotes a significant difference ($p<0.05$) relative to vehicle (0.1% DMSO).

*3.3 TDCIPP exposure results in a decrease in intracellular ROS*

We then relied on CellROX Green to detect and quantify ROS *in situ* within HEK293 cells. Based on these assays, we detected a concentration-dependent decrease in ROS relative to vehicle-treated cells after DAPI-based normalization. Interestingly, although 24 h of exposure resulted in no effect on ROS, we detected a statistically significant, concentration-dependent decrease in ROS (relative to vehicle-treated cells) after 48 h of exposure starting at 0.245 μM TDCIPP (Figure 4.5). ROS approached levels within untreated cells (blanks) by 3.91 μM TDCIPP (Figure 4.5), suggesting that 1) exposure to 0.1% DMSO alone may increase ROS generation within HEK293 cells and 2) TDCIPP may counteract the effects of 0.1% DMSO. Overall, these data indicate that 48 h of continuous TDCIPP exposure may decrease ROS from 0.245-15.63 μM relative to vehicle-treated cells.

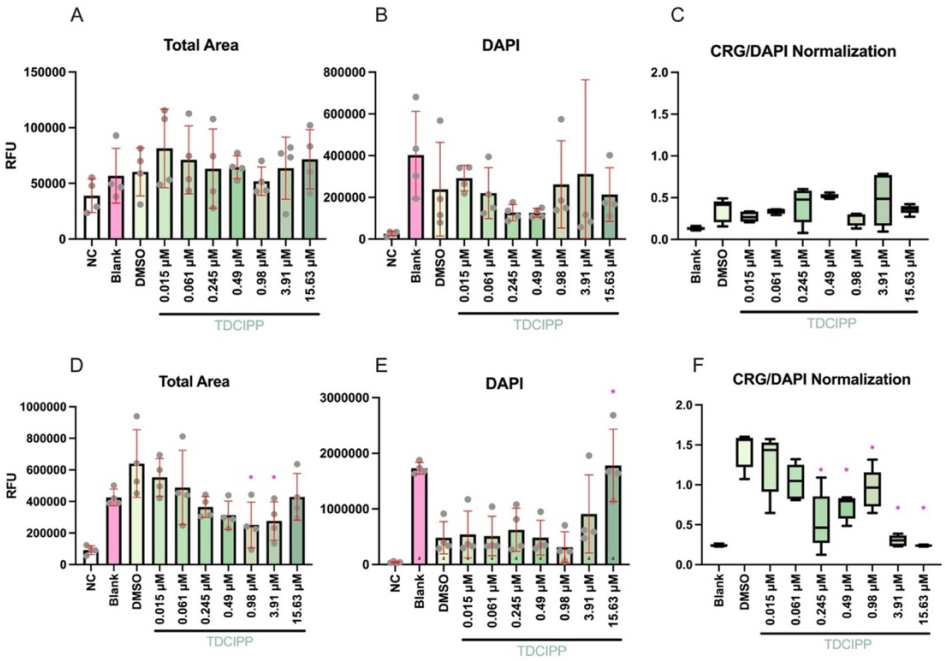


**Figure 4.5** Mean (± standard deviation) CellROX Green fluorescence of HEK293 cells exposed to either vehicle (0.1% DMSO) or 0.015-31.25 µM TDCIPP for 24 h (A-C) or 48 h (D-F). Blank = unexposed cells. Cells were imaged under transmitted light, DAPI, and FITC, and then analyzed using our ImageXpress Micro XLS Widefield High-Content Screening System**.** Within MetaXpress 6.0.3.1658, each well was analyzed for the total area of fluorescence for FITC (A and D) and DAPI (B and E) using custom automated image analysis procedures. Panels C and F show mean (± standard deviation) CellROX green fluorescence area divided by DAPI stained area of HEK293 cells. Asterisk (*) denotes a significant difference ($p$<0.05) relative to vehicle controls.

*3.4 TDCIPP does not affect cell membrane abundance in situ within HEK293 cells*

We relied on AlexaFluor 488-conjugated WGA to determine if TDCIPP exposure affected cell membrane integrity within HEK293 cells. We found that continuous exposure for either 24 h or 48 h TDCIPP (0.061, 0.245, and 0.98 µM) did not result in any statistically significant differences relative to vehicle-treated cells (Figure 4.6), suggesting that TDCIPP exposure up to 48 h does not affect cell membrane integrity *in situ* within HEK293 cells. In addition, we also found that pre-treatment with ATP-inhibiting enzyme compounds did not affect cell membrane integrity in the presence or absence of TDCIPP (Figure 4.6). This may be because TDCIPP is entering the cells either through simple diffusion or

utilizing a transport channel without altering the integrity of the cell membrane. Due to TDCIPP's hydrophobicity, TDCIPP may be partitioning into HEK293 cells without disrupting the composition or vesicular transport systems which maintain its integrity.

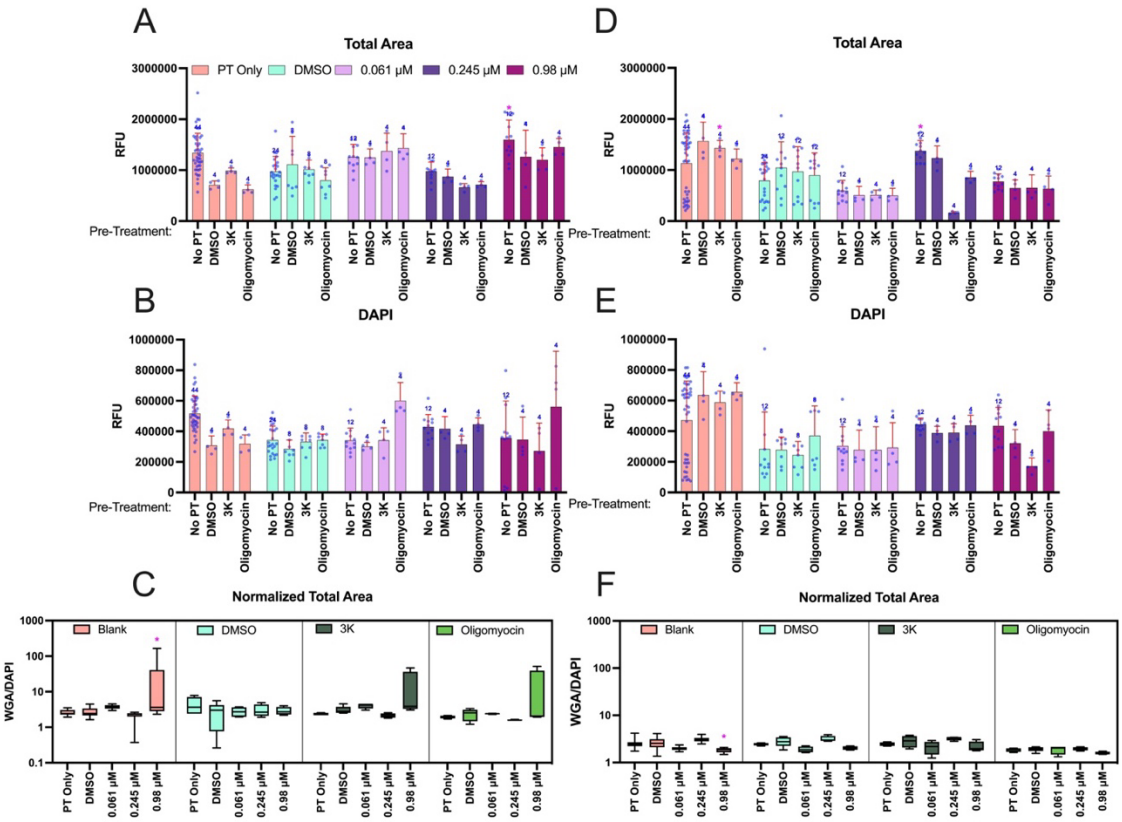


**Figure 4.6** Mean (± standard deviation) wheat germ agglutinin (WGA) of HEK293 cells exposed to either vehicle (0.1% DMSO) or 0.015-31.25 µM TDCIPP for 24 h (A-C) or 48 h (D-F). Blank = unexposed cells. Cells were imaged under transmitted light, DAPI, and FITC, and then analyzed using our ImageXpress Micro XLS Widefield High-Content Screening System. Within MetaXpress 6.0.3.1658, each well was analyzed for the total area of fluorescence for FITC (A and D) and DAPI (B and E) using custom automated image analysis procedures. Panels C and F show mean (± standard deviation) WGA fluorescence area divided by DAPI stained area of HEK293 cells. Asterisk (*) denotes a significant difference ($p$<0.05) relative to vehicle controls.

*3.5 TDCIPP does not affect the relative abundance of mitochondria within HEK293 cells*

Since relative ATP production and ROS levels were affected by TDCIPP, we relied on MitoTracker Orange CMTMRos to determine if TDCIPP affected the relative

abundance of mitochondria within HEK293 cells. We found that continuous exposure for either 24 h or 48 h to TDCIPP (0.061, 0.245, and 0.98 μM) did not result in statistically significant differences relative to vehicle-treated cells (Figure 4.7), suggesting that TDCIPP exposure up to 48 h does not affect the abundance of mitochondria *in situ* within HEK293 cells.

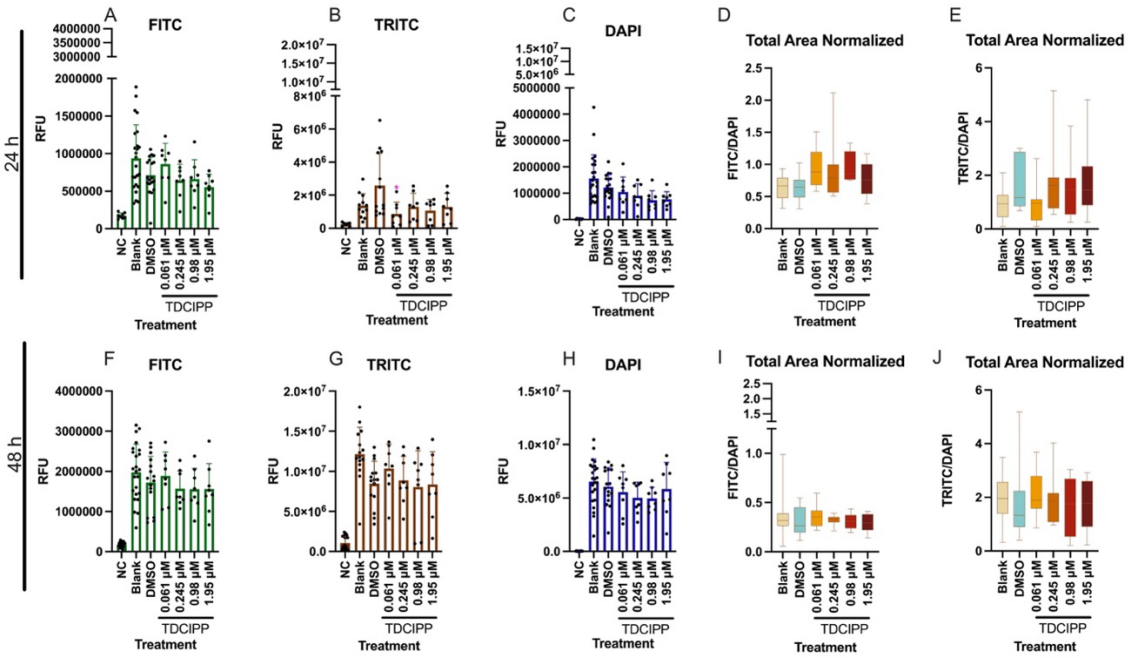


**Figure 4.7** Mean (± standard deviation) of MitoTracker Orange CMTMRos (B,G) and CellROX Green fluorescence (A,F) for HEK293 cells exposed to either vehicle (0.1% DMSO) or TDCIPP (0.061-1.95 μM) for 24 h (A-E) or 48 h (F-J). Blank = unexposed cells. Panels D, E, I and J show mean (± standard deviation) CellROX Green fluorescence/ MitoTracker Orange CMTMRos area divided by DAPI stained area of HEK293 cells. Asterisk (*) denotes a significant difference ($p$<0.05) relative to vehicle controls.

*3.6 TDCIPP exposure does not affect the rate of ATP production within HEK293 cells*

We relied on a Seahorse XFP ATP rate assay to determine if TDCIPP exposure affected the rate of ATP production within HEK293 cells. We found that continuous exposure for 24 h to TDCIPP (0.061, 0.245, and 0.98 μM) did not result in any statistically significant differences relative to vehicle-treated cells (Figure 4.8), suggesting that

TDCIPP exposure up to 24 h does not affect the rate of ATP production within live HEK293 cells.

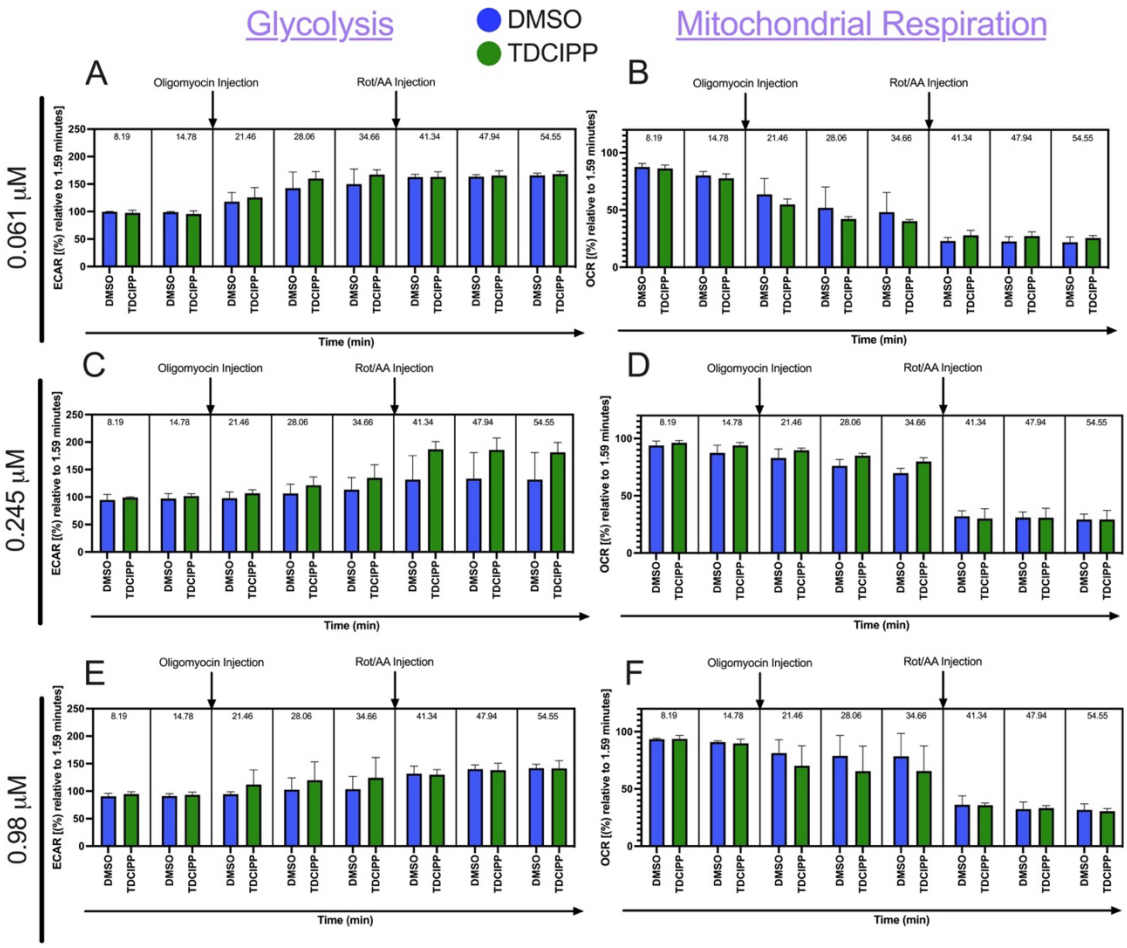


**Figure 4.8** Mean oxygen consumption rate (OCR) (A, C, E) and extracellular acidification rate (ECAR) (B,D,F) of HEK293 cells exposed to either vehicle (0.1% DMSO) or TDCIPP (0.061, 0.245, or 0.98 μM) for 24 h. Cells were measured using an Agilent Seahorse XFp ATP Rate assay and normalized by cell count as well as the initial base line reading. Asterisk (*) denotes a significant difference ($p$<0.05) relative to vehicle controls.

*3.7 TDCIPP exposure results in an increase in OCR, ECAR, and PER during glycolysis within HEK293 cells*

We relied on a Seahorse XFP glycolytic rate assay to determine if TDCIPP exposure affected the rate of glycolysis within HEK293 cells. We found that continuous exposure for 24 h to TDCIPP (0.061, 0.245, and 0.98 μM) resulted in an increase in

percent consumption rates of OCR, ECAR and PER relative to the initial first measurement (Figure 4.9), suggesting that TDCIPP exposure up to 24 h increases the rate of glycolysis within live HEK293 cells. Although there is not a clear concentration-response relationship between the concentration of TDCIPP and glycolytic rate of HEK 293 cells, we found that, similar to our CTG data, the level of significance relative to the vehicle control was lowest at 0.98 μM, medium at 0.061 μM, and highest in the 0.245 μM. Additionally, increases in glycolytic rate may indicate that cells have rewired metabolic activity which favors transforming cells into a tumorigenic state (Elia and Haigis, 2021).

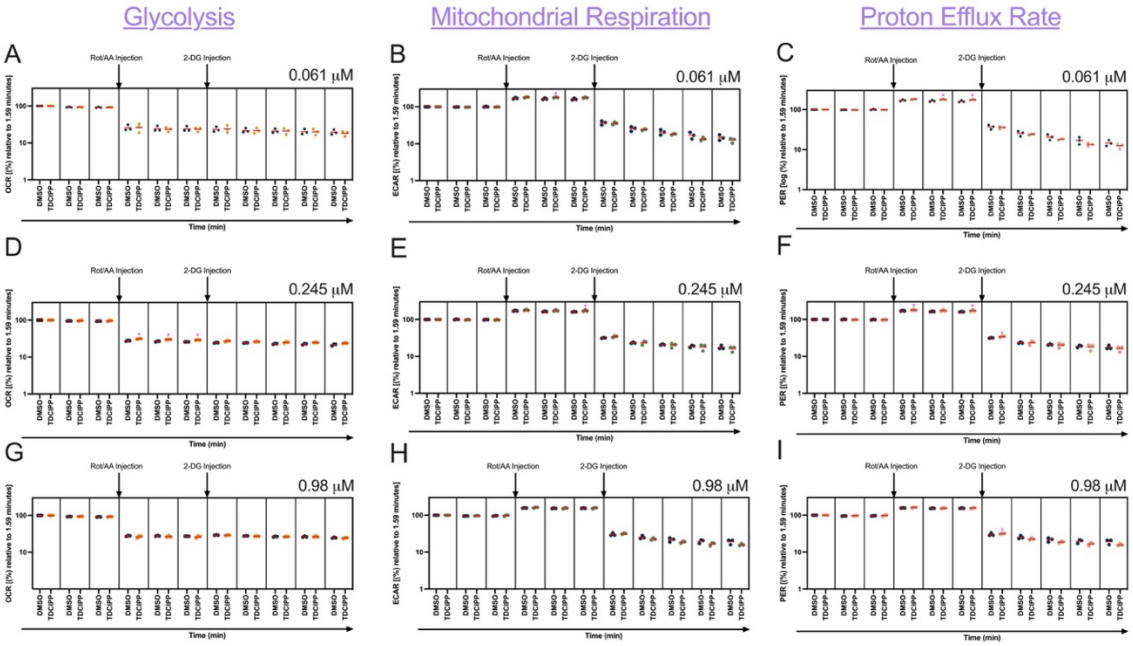


**Figure 4.9** Mean oxygen consumption rate (OCR) (A, D, G), extracellular acidification rate (ECAR) (B, E, H), and proton efflux rate (PER) (C, F, I) of HEK293 cells exposed to either vehicle (0.1% DMSO) or TDCIPP (0.061, 0.245, or 0.98 μM) for 24 h. Cells were analyzed using an Agilent Seahorse XFp Glycolytic Rate assay and normalized by cell count as well as the initial base line reading. Asterisk (*) denotes a significant difference ($p$<0.05) relative to vehicle controls.

*3.8 TDCIPP exposure significantly impacts histidine metabolism within HEK 293 cells*

We utilized targeted metabolomics to determine if TDCIPP exposure altered central carbon metabolism. We found that continuous exposure for 24 h to 0.245 μM TDCIPP resulted in alterations in the metabolic profile that was statistically significant at an $\alpha$=0.05, 0.1, or 0.2 relative to vehicle-treated cells (Figure 4.10). In addition, we found significant pathway impacts of TDCIPP on histidine metabolism, with an increase in intracellular carnosine levels following exposure to 0.245 μM TDCIPP (Figure 4.11). This suggests that TDCIPP exposure up to 24 h results in an increase in intracellular carnosine and impacts the histidine metabolism pathway within HEK293 cells, although this effect is strongly dependent on the TDCIPP concentration.

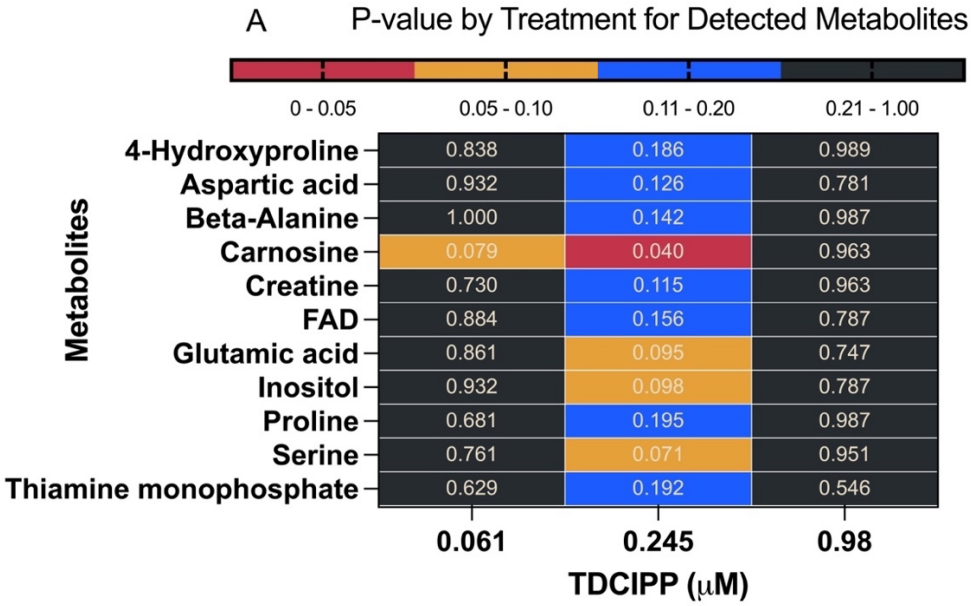


**Figure 4.10** GLM-generated p-values for HEK293 cells exposed to either 0.061, 0.245, or 0.98 μM TDCIPP for 24 h (A). p-values are relative to vehicle-treated cells. Red color denotes a significant difference ($p$<0.05) relative to vehicle controls.

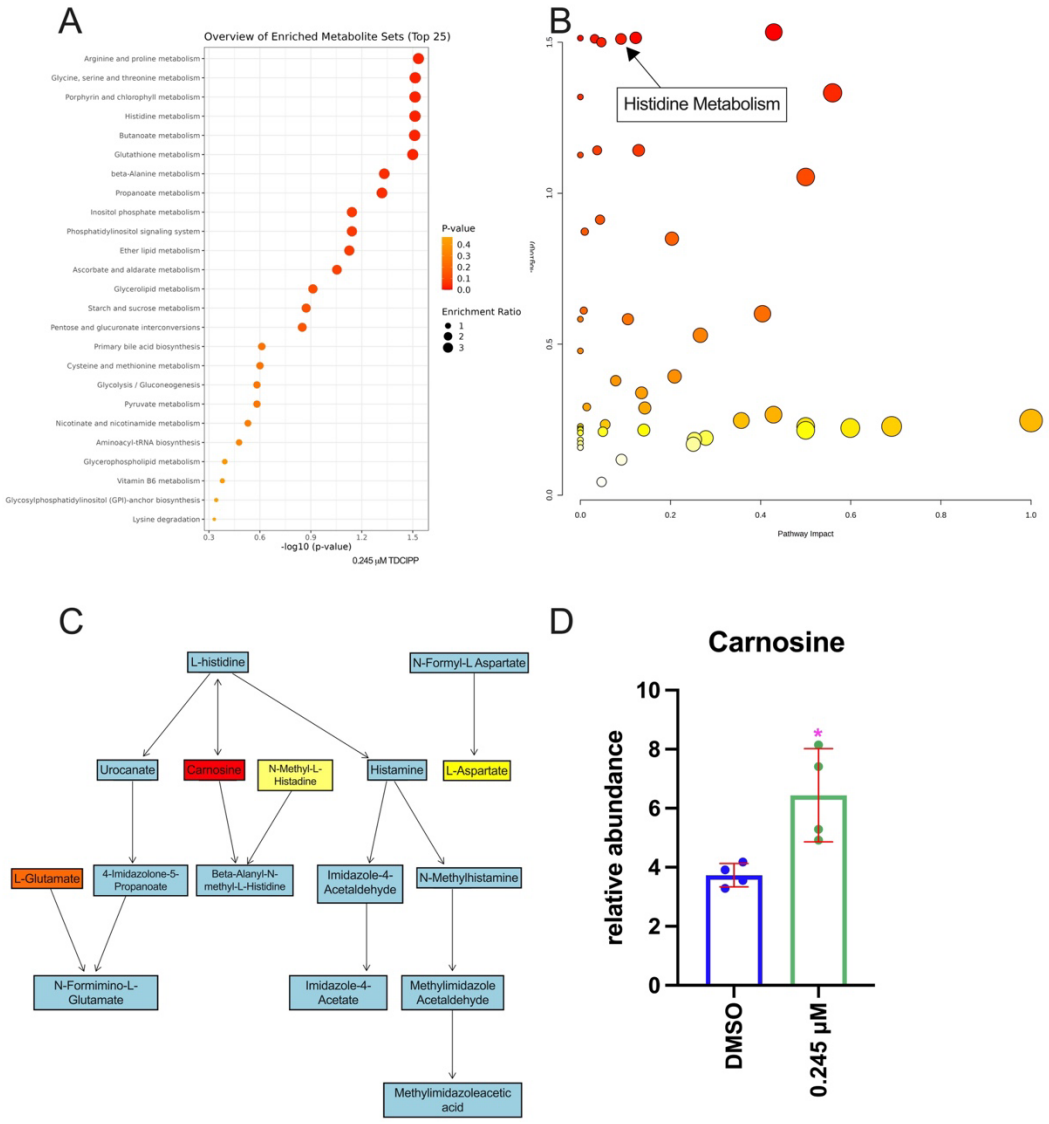


**Figure 4.11** Significantly enriched metabolites (A) and pathway analysis (B) from MetaboAnalyst output. Histidine pathway from Panel B along with significantly affected metabolites (C). Mean (± standard deviation) carnosine relative abundance of HEK293 cells exposed to either vehicle (0.1% DMSO) or 0.245 μM TDCIPP for 24 h (D). Asterisk (*) denotes a significant difference ($p$<0.05) relative to vehicle controls.

### Section 4.5 Discussion

Based on our results within HEK293 cells, our findings suggest that 1) TDCIPP increases relative ATP production in a concentration-dependent manner; 2) TDCIPP has

no effect on the 5-mC abundance, cell membrane integrity, or mitochondria abundance; 3) TDCIPP decreases ROS in a concentration-dependent manner; 4) TDCIPP exposure results in an increase in OCR, ECAR, and PER during glycolysis; and 5) TDCIPP exposure increases carnosine and impacts histidine metabolism.

We also found that TDCIPP impacts cellular metabolism by affecting the metabolic signature of these cells. This agrees with the literature which shows that cancer cells adapt to their environment by rewiring their metabolic profile in order to promote cell proliferation (Wong et al., 2013). Although we observed no differences in the number of cell nuclei, we did observe alterations in the metabolic profile of the cells. In addition, we also demonstrated that TDCIPP demonstrated enhanced aerobic glycolysis – another characteristic of the Warburg effect that is exhibited by tumorigenic cells such as HEK293 cells (Liberti and Locasale, 2016; Pellenz, 2023; T. Oronsky et al., 2014; Vaupel and Multhoff, 2021). Interestingly, we also found that TDCIPP-exposed cells decreased total detectable ROS. This may be due to TDCIPP's function as a flame retardant in scavenging ROS to quench a flame, but possibly also due to an increased abundance of carnosine. Carnosine is found in high levels in skeletal tissue and plays a role in antioxidant activity and scavenging carbonyls (Babizhayev et al., 2013; Barski et al., 2013; Peters et al., 2015).

Based on our findings to date, we can begin to propose an idea for how TDCIPP elicits toxicity within human embryonic kidney cells. Following partitioning into cells, TDCIPP may sequester ROS and create a reactive intermediate product which, in turn, disrupts ROS-mediated signaling pathways. In the mitochondria, ROS species are created as by-products of cellular metabolism but also play a role in oxidative reduction in the electron transport chain (Forrester et al., 2018; Lyakhovich, 2013; Thannickal and

Fanburg, 2000). Therefore, disruption of the balance of cellular ROS may, in turn, disrupt cellular homeostasis and metabolism. Certain diseases have been characterized by an increase in ROS, such as Fanconi Anemia or pulmonary fibrosis. However, little is known about disease etiology when cells are deficient in ROS. Furthermore, for this reason, future studies are needed to understand the underlying link between ROS function and disruption in cellular metabolism induced by OPFRs such as TDCIPP.

There are two primary limitations that may affect the interpretation of our results. First, it is unknown whether TDCIPP indirectly or directly interacts with key enzymes that regulate ATP production, and further research is needed to better understand the localization of increased ATP production within HEK293 cells. Second, we need to identify the source of increased ATP using a targeted method, such as GC-MS of isolated mitochondria, to ensure that there is a detectable increase in ATP and not simply an artifact of the CellTiter-Glo assay. Also, it is possible that we did not detect an effect of TDCIPP on 5-mC data since global DNA methylation assays are often less sensitive than sequencing-based methods. Finally, since HEK293 cells are transformed cells (albeit originally derived from normal kidneys of an aborted human fetus), tumorigenic cells do not accurately recapitulate normal biology and, as such, our findings may not be readily translated to normal human embryonic kidney cells that may have differences in Phase I and/or Phase II metabolism compared to HEK293 cells.

# Chapter 5: Summary and Conclusions

## 5.1 Summary

Tris(1,3-dochloro-2-propyl) phosphate (TDCIPP) is a ubiquitous additive flame retardant that we find in a variety of end-use products. However, due to the loose association between additive flame retardants and their end-use products, it has the capability as these products age or degrade to matriculate into environmental sinks such as indoor air and dust. Epidemiological studies have found that TDCIPP exposure can be traced and detected in human urine through its urinary metabolite BDCIPP. Increased levels of BDCIPP have been shown to be negatively correlated to decreased oocyte fertilization within IVF couples. In addition, previous research with our lab has found that TDCIPP exposure during embryonic development causes a variety of abnormalities such as disruption of dorsal/ventral patterning, alterations in methylation profiling during MZT transition, perturbations in cellular metabolism, and at certain concentrations embryonic lethality.

In Chapter 2, we developed a method that allowed us to track 5-mC (a common epigenetic biomarker) across multiple stages of development and utilizing multiple concentrations of TDCIPP. In Chapter 3, we found that TDCIPP-induced alterations to CpG methylation persist into the late stages of development while disrupting the normal trajectory of CHH cytosine methylation pattering and relative abundance of 5-mC within the yolk within developing zebrafish embryos. Finally, in Chapter 4 our findings demonstrate that exposure to environmentally relevant concentrations of TDCIPP leads to increased cell viability and relative abundance of ATP, decreased presence of intracellular ROS species, and alterations to cellular metabolism within human embryonic kidney (HEK 293) cells. Overall, these data provide insight into possible mechanistic

pathways that contribute to understanding the underlying molecular mechanism behind TDCIPP-induced toxicity and associated risk with embryonic exposure to TDCIPP in our environment.

### 5.2 Rapid and efficient spatiotemporal screening method

Due to the high conservation of cytosine methylation across mammalian species and, its dual function as a key in chromatin remodeling and epigenetic programming, we understand 5-mC plays a critical role in early embryonic development. Epigenetic reprogramming is a critical and time-sensitive period during in-utero development in which maternal exposure to chemicals has the potential to reprogram the epigenome within offspring causing developmental deviations from the normative trajectory. Potentially adverse outcomes that can result from this are immediate phenotypic consequences, long-term effects on adult disease susceptibility, and transgenerational effects of inherited epigenetic marks. Furthermore, more methods are needed to be able to understand how chemical exposure can alter 5-mC during embryonic development. Therefore, using commercially available 5-mC-specific antibodies, we created a cost-effective strategy for rapid and efficient spatiotemporal monitoring of cytosine methylation within individual, intact zebrafish embryos by utilizing whole-mount immunohistochemistry, automated high-content imaging, and efficient data processing using programming language prior to statistical analysis. The method enables the detection of not only DNA methylation within the cell mass but also could detect cytosine methylation of yolk-localized maternal mRNAs during the maternal-to-zygotic transition. Interestingly, the antibody is cross-reactive for RNA cytosine methylation (m5C) in addition to detecting DNA methylation (5-mC). To our knowledge, this method is the first to successfully detect and quantify 5-mC levels *in situ* within zebrafish embryos during early development.

Overall, this method is useful for the rapid screening of chemicals that have the potential to disrupt cytosine methylation *in situ* during epigenetic reprogramming while providing a quick and cost-efficient detection of 5-mC across multiple stages of development and chemical concentrations. Therefore, offering an alternative to cost-prohibitive and restrictive requirements of bisulfite sequencing-based approaches. By creating this protocol, investigators can utilize this method to quickly screen chemicals and assess how the abundance of 5-mC may be altered during early embryonic development. Alternatively, this method may be utilized as a prescreening tool to identify toxicologically important information such as concentration range, period of development, and/or window of sensitivity in which the chemical of interest affects 5-mC abundance.

Finally, this method may be utilized for a different biomarker and antibody, however, further optimization would be needed. By utilizing the method as is, an investigator can quickly, efficiently, and cost-effectively screen and identify a chemical that alters the relative abundance of 5-mC within zebrafish embryos prior to investing in labor-intensive bisulfite sequencing-based approaches. However, since the method is zebrafish-specific, further research is needed to determine whether 5-mC can be detected *in situ* within early embryos of other commonly utilized model organisms.

### 5.3 Tris(1,3-dichloro-2-propyl) phosphate disrupts the trajectory of cytosine methylation

In zebrafish, initiation of TDCIPP exposure at 0.75 h post-fertilization (hpf) reliably disrupts cytosine methylation from cleavage (2 hpf) through early-gastrulation (6 hpf). Disruption of cytosine methylation patterning in early embryonic stages can disrupt key developmental transitions such as epigenetic reprogramming and the maternal-to-zygotic transition. Within zebrafish, our lab found that TDCIPP exposure from cleavage through

gastrulation can result in a variety of developmental abnormalities, some of which are reversible and others are not. TDCIPP-induced effects of on an embryo within this time-sensitive window include disruption of dorsal/ventral patterning, epiboly delay, and epiboly arrest. While the toxicological information behind how TDCIPP exposure causes these perturbations is still not well understood and thus leaves a knowledge gap regarding its mechanism of action. This research aims to contribute to the knowledge gap by understanding more about TDCIPP effects on cytosine methylation and key enzymes which regulate its formation.

We first aimed to determine whether TDCIPP-induced effects we have seen on cytosine methylation persist beyond 6 hpf. We utilized bisulfite amplicon sequencing of a target locus (*lmo7b*) using genomic DNA derived from whole embryos. Relative to embryos exposed to vehicle (0.1% DMSO) from 0.75 to 6 hpf, CpG methylation of *lmo7b* was significantly decreased following exposure to the vehicle (0.1% DMSO) from 0.75 to 48 hpf (but not 0.75 to 24 hpf), whereas CHG and CHH methylation of *lmo7b* were not significantly different following exposure to the vehicle (0.1% DMSO) from 0.75 to 24 hpf nor 0.75 to 48 hpf. Overall, these data suggest that 1) exposure to 0.78 μM TDCIPP may accelerate CpG hypomethylation of *lmo7b* by at least 24 h and 2) effects of TDCIPP on CpG methylation persist until at least 48 hpf.

We further analyzed the BSAS data set for within-stage and within-treatment effects on CpG methylation by focusing on four positions on *lmo7b* (Chr1): 33664419, 33664494, 33664391, and 33664274. All of the positions were found to be localized to a single amplicon that was sequenced using BSAS. Based on this analysis, the magnitude of within-treatment effects (i.e., comparing 24 hpf or 48 hpf relative to 6 hpf within the same treatment) was higher than the magnitude of within-stage effects (i.e., comparing

vehicle vs. TDCIPP within the same stage. This finding suggests that, like overall CpG methylation, CpG methylation effects at the position level are strongly stage-dependent within both vehicle- and TDCIPP-exposed embryos. In addition, we found that for positions 33664419 and 33664494 were more susceptible to TDCIPP-induced acceleration of CpG hypomethylation relative to positions 33664391 and 33664274, suggesting that the effects of TDCIPP on CpG methylation within *lmo7b* may also be positionally dependent (e.g., within regions that are CG-rich).

In addition to this study, we pulled BSAS sequencing data from three separate studies to investigate methylation of *lmo7b* between timepoints 2-, 4-, 6-, 24-, or 48-hpf zebrafish embryos following exposure to either vehicle (0.1% DMSO), 0.78 μM TDCIPP, or 3.12 μM TDCIPP. We analyzed the raw percent methylation data at base-pair resolution by cytosine context (CpG, CHG, or CHH). We found that, across all stages and treatments, the percent CpG methylation (>95%) was substantially higher than the percent CHG and CHH methylation (<10% and <1%, respectively). There were more cytosines on a single amplicon of *lmo7b* within a CHH context (52 total) relative to positions within a CpG context (6 total) and CHG context (19 total). Moreover, we detected significant differences in CHH methylation at 4-, 6-, 24-, and 48-hpf (relative to 2 hpf) following initiation of exposure to vehicle (0.1% DMSO) at 0.75 hpf. However, this normal stage-dependent effect on CHH methylation was absent following exposure to 0.78 or 3.12 μM TDICPP, suggesting that, similar to CpG methylation, TDCIPP disrupts the normal trajectory of CHH methylation within developing zebrafish embryos.

Our previous findings with *in vitro* DNA methyltransferase (DNMT) we found that, even at high μM concentrations, TDCIPP had no effect on zebrafish DNMT activity. Similarly, when we utilized an *in vitro* assay to determine if TDCIPP had any effects on

human or zebrafish TDG activity. We tested TDCIPP concentrations ranging from 3.91-62.5 μM (the highest concentration tested) and found that there was no effect on zebrafish nor human TDG activity. Furthermore, this suggests that TDCIPP-induced effects on CpG methylation are not driven by direct interaction with TDG.

Finally, we utilized our developed protocol from Chapter 2, we relied on 5-mC-specific whole-mount IHC and automated imaging to monitor TDCIPP-induced effects on cytosine methylation *in situ* as a function of stage and TDCIPP concentration. We aimed to detect how TDCIPP exposure at 0.78 and 1.56 μM affects 5-mC across cleavage through blastula within zebrafish embryos. We found that exposure to TDCIPP increased 5-mC abundance within the yolk of blastula-stage embryos. The data revealed that at 2 and 4 hpf (during MZT transition), the vast majority of 5-mC was detected within the yolk of developing embryos. This further suggests that the anti-5-mC antibody we used also cross-labeled yolk-localized maternal methylated mRNA containing methyl-5-cytosine (m-5C).

At 6, 8, and 10 hpf, 5-mC was increasingly detected within portions of the cell mass, eluding that cytosine methylation within the cell mass increases during gastrulation. Interestingly, utilizing the quantitative total area or integrated intensity of fluorescence as endpoints, we found that initiation of exposure at 0.75 hpf to 0.78 μM or 1.56 μM TDICPP resulted in a significant increase in yolk-localized cytosine methylation at 2 hpf and/or 4 hpf relative to vehicle-exposed, phenotypically identical embryos at the same stage, suggesting that the downstream effects on TDCIPP on epiboly during gastrula (5.25-10 hpf) may be driven by disruption of yolk-localized cytosine methylation within the first 4 h of development. We understand now that TDCIPP may impact cytosine methylation of maternally loaded mRNAs during the maternal-to-zygotic transition. Overall, our findings

suggest that TDCIPP disrupts the trajectory of cytosine methylation during zebrafish embryogenesis, effects that do not appear to be driven by direct interaction of TDCIPP with key enzymes that regulate cytosine methylation.

**5.4 Tris (1,3-dichloro-2-propyl) phosphate disrupts cellular metabolism**

To address the knowledge gap about how TDCIPP disrupts the physiology of human embryonic cells at environmentally relevant concentrations we utilized a combination of pharmacological and toxicological approaches. The overall objective of this study was to determine whether TDCIPP alters cell viability, cytosine methylation, ROS levels, and cellular metabolism using human embryonic kidney (HEK293) cells as a model. To do this, we relied on metabolomics, real-time cell analysis, and functional pharmacologic approaches to begin uncovering the mechanism underlying TDCIPP-induced disruption of cellular metabolism. First, using CellTiter-Glo assays, we conducted a concentration-response curve for TDCIPP impacts on cell viability. We found that, relative to vehicle controls, exposure to TDCIPP at environmentally relevant concentrations for 24 or 48 h resulted in a concentration-dependent increase in cell viability up to 0.245 μM, a finding that was likely driven by an increase in the relative ATP abundance. To determine if we could reverse this effect, we added pre-treatments with compounds which inhibit ATP-producing enzymes. However, we found that pre-treatment with ATP synthase and PKM2 inhibitors (up to 1 μM) did not affect the relative total number of cell nuclei in HEK293 cells.

Utilizing 5-methylcytosine (5-mC)-specific immunocytochemistry, we found that TDCIPP exposure up to 48 h did not affect global cytosine methylation *in situ*. To understand how TDCIPP impacted ROS, we relied on using CellROX Green assays to quantify ROS *in situ* within HEK 293 cells. Although 24 h of exposure resulted in no effect

on ROS, we detected a statistically significant decrease in ROS (relative to vehicle-treated cells) after 48 h of exposure starting at 0.245 μM TDCIPP, suggesting that exposure to 0.1% DMSO alone may increase ROS generation within HEK293 cells and TDCIPP may counteract the effects of 0.1% DMSO.

To understand how TDCIPP impacts cell membrane integrity, we relied on WGA-specific cell membrane labeling. We continuously exposed HEK293 cells to TDCIPP (0.061, 0.245, and 0.98 μM) for either 24 h or 48 h TDCIPP exposure to determine if it affected cell surface glycoproteins. We found that TDCCIPP exposure did not result in any statistically significant differences relative to vehicle-treated cells. This suggests that TDCIPP exposure up to 48 h does not affect the cell membrane or glycoprotein formation *in situ* within HEK293 cells. In addition, we also found that incorporating our pre-treatment with compound 3K and Oligomycin (compounds which inhibit key ATP producing enzymes) did not affect the cell membrane abundance.

We relied on MitoTracker Orange CMTMRos dye to determine if TDCIPP exposure affected the relative abundance of mitochondria within HEK293 cells. We found that continuous exposure for either 24 h or 48 h TDCIPP (0.061, 0.245, and 0.98 μM) did not result in any statistically significant differences relative to vehicle-treated cells. This ultimately suggests that TDCIPP exposure up to 48 h does not compromise the abundance of mitochondria *in situ* within HEK293 cells.

We relied on a Seahorse XFP ATP rate assay to determine if TDCIPP exposure affected the rate of ATP production within HEK293 cells. We found that continuous exposure for 24 h to TDCIPP (0.061, 0.245, and 0.98 μM) did not result in any statistically significant differences relative to vehicle-treated cells. This suggests that 24h of exposure to TDCIPP does not impact the rate of ATP production within live HEK293 cells.

We relied on a Seahorse XFP glycolytic rate assay to determine if TDCIPP exposure alters the rate of glycolysis within HEK293 cells. We found that continuous exposure for 24 h to TDCIPP (0.061, 0.245, and 0.98 μM) resulted in statistically significant increases in percent consumption rates of OCR, ECAR, and PER relative to the initial first measurement when compared to the vehicle control (0.1% DMSO). This implied that 24 h of TDCIPP exposure resulted in an increased rate of glycolysis within live HEK293 cells. Though there is not a clear concentration-response relationship between the concentration of TDCIPP and glycolytic rate of HEK293 cells, we can see that, similar to our CTG data, the level of significance relative to the vehicle control was lowest at 0.98 μM, medium at 0.061 μM, and highest in the 0.245 μM.

Lastly, we utilized metabolomics to determine if TDCIPP exposure altered central carbon metabolism within HEK 293 cells. We found that 24 h of continuous exposure for to 0.245 μM TDCIPP resulted in alterations to the metabolic profile that was statistically significant at an $\alpha$=0.05, 0.1, or 0.2 relative to vehicle-treated cells. In addition, we found impacts on histidine metabolism for TDCIPP-exposed cells which caused significant pathway impacts. This was a result of a statistically significant increase in intracellular carnosine levels following exposure to 0.245 μM TDCIPP. Overall, we found that TDCIPP exposure up to 24 h results in an increase in intracellular carnosine and impacts the histidine metabolism pathway within HEK293 cells.

### 5.5. Further Directions and Consideration

TDCIPP is a known carcinogenic environmental toxicant in which we lack considerable data for regulatory decisions. Despite its ubiquitous use, the mechanism of action for TDCIPP has limited understanding and needs more accurate and efficient characterization of its toxicity. The combination of *in situ* and *in vitro* model assessment

utilized in this dissertation aims to fill some of those knowledge gaps and move us forward toward pointing towards a novel mechanism of action that may be relevant to human embryonic cells and/or other organohalogen flame retardants. The research conducted within Chapter 2 and 3 utilized zebrafish embryos, a commonly used vertebrate model to assess the effects of environmental contaminants on embryonic exposure during sensitive windows of development. Due to the conservation of these early embryonic stages across all vertebrate models, rapid *ex utero* development, fully sequenced genomes, as well as their similar epigenetic reprogramming periods, it is an exceptional model to utilize for toxicity testing. Commonly used pharmacological and sequencing methods were utilized in Chapter 3 to determine TDCIPP-induced impacts on cytosine methylation for early embryonic stages of zebrafish embryos. We then took our understanding from what we learned in Chapter 3 and began exploring alternative pathways for which TDCIPP could be affecting cellular metabolism in human embryonic cells. This allowed to begin to bridge the gap between *in vitro* and *in situ* characterization of toxicity and impacts on early embryonic development resulting from TDCIPP exposure. The research presented in this dissertation aimed to address 1) the global impacts of TDCIPP on *in situ* cytosine methylation (DNA or RNA) in spatial and temporal contexts within zebrafish embryos, 2) the impact of TDCIPP exposure on cytosine methylation and 5-mC formation within zebrafish embryos, and 3) how TDCIPP impacts cell viability and cellular metabolism within human embryonic cells.

Despite the novel approaches within this dissertation, there is still a relatively large overall data gap in the existing knowledge set. An example of this includes understanding the role m-5C RNA methylation plays in zebrafish embryonic development and where this falls in TDCIPP's adverse outcome pathway. We can predict that there is a relationship

between RNA methylation and DNA methylation as well as a timing or molecular switch which regulates it although we have yet to confirm this. Future work should include investigating and quantifying 5-hydroxymethyl cytosine, methyl-5-cytosine, and 5-methylcytosine within zebrafish embryos in order to understand how they may change as a result of TDCIPP exposure. By understanding how the timing, regulation, or availability of these key epigenetic biomarkers affect developmental timing and how organophosphate exposure can alter this, we can begin to address the underlying questions of chemical exposure in early embryonic development.

In addition, we see an overall stochastic effect of TDCIPP on cytosine methylation patterning which does not seem to be positionally specific but does seem to favor CpG or CHH methylation patterning, although the reason for why is also eluding. Future work should include following up with a BSAS experiment for a human embryonic stem cell model to assess the global cytosine methylation patterning as a result of TDCIPP exposure. From there, the data can be looked at for particular positions and genes that are up or down-regulated as a result of TDCIPP exposure for a low, medium, and high dose. In addition, it would be also interesting to see how TDCIPP exposure disrupts cell fate by understanding if TDCIPP exposure can revert or impair terminal differentiation from pluripotent progenitor cells to a determined germ layer (mesoderm, endoderm, ectoderm) and further differentiation (i.e., osteocyte, gliocytes, cardiocyte, or nephrocyte).

Lastly, we understand that TDCIPP perturbs normal cellular metabolism within HEK293 cells by altering the metabolic landscape but we do not understand how this is being done and if these alterations exist past 48 h of exposure. Future work should include investigating quantifying ATP via GC-MS/MS within the mitochondria of human embryonic cells to determine if the ATP abundance increases we observed are derived from the

mitochondria. In Chapter 4, we found that TDCIPP decreases total ROS within HEK293 cells. However, little is known about the diagnostic implications of low ROS and further research should be done to understand the disease etiology behind this. Future work should also include understanding the role TDCIPP plays in mitochondrial dysfunction and disruption of mitochondrial membrane integrity and if this is a result of why we see an increase in OCR, ECAR, and PER within HEK 293 cells. Future work should also include targeted proteomic profiling and untargeted protein quantification of human embryonic cells to understand how TDCIPP could impact protein production and abundance of key proteins. Looking further into this relationship between relationships and within them could potentially elucidate a mechanism of action for TDCIPP induced toxicity within early embryonic development.

The continuation of this work is essential to understanding a mechanism of action for how OPFRs perturb embryonic development as well as understanding how these disruptions in development can lead to adverse outcomes later in life. For example, future studies should also focus on understanding acute versus chronic exposure to TDCIPP for longer durations (i.e., 7, 14, 21 days) or transgenerational impacts on cytosine methylation patterning and development. Finally, using a variety of isomers for TDCIPP the structural analysis in composition and biotransformation of TDCIPP reactive intermediates and metabolites should be screened to determine whether there is a particular by-product that is being produced that could contributing to TDCIPP-induced toxicity.

## References

Agarwal, P., Morriseau, T.S., Kereliuk, S.M., Doucette, C.A., Wicklow, B.A., Dolinsky, V.W., 2018. Maternal obesity, diabetes during pregnancy and epigenetic mechanisms that influence the developmental origins of cardiometabolic disease in the offspring. Crit. Rev.

Clin. Lab. Sci. 55, 71–101. https://doi.org/10.1080/10408363.2017.1422109
An, Y.-Q.C., Goettel, W., Han, Q., Bartels, A., Liu, Z., Xiao, W., 2017. Dynamic Changes of Genome-Wide DNA Methylation during Soybean Seed Development. Sci. Rep. 7, 12263. https://doi.org/10.1038/s41598-017-12510-4

Aure, M.R., Fleischer, T., Bjørklund, S., Ankill, J., Castro-Mondragon, J.A., OSBREAC, Børresen-Dale, A.-L., Tost, J., Sahlberg, K.K., Mathelier, A., Tekpli, X., Kristensen, V.N., 2021. Crosstalk between microRNA expression and DNA methylation drives the hormone-dependent phenotype of breast cancer. Genome Med. 13, 72. https://doi.org/10.1186/s13073-021-00880-4

Avila-Barnard, S., Dasgupta, S., Cheng, V., Reddam, A., Wiegand, J.L., Volz, D.C., 2022. Tris(1,3-dichloro-2-propyl) phosphate disrupts the trajectory of cytosine methylation within developing zebrafish embryos. Environ. Res. 211, 113078. https://doi.org/10.1016/j.envres.2022.113078

Babizhayev, M.A., Lankin, V.Z., Savel'Yeva, E.L., Deyev, A.I., Yegorov, Y.E., 2013. Diabetes mellitus: novel insights, analysis and interpretation of pathophysiology and complications management with imidazole-containing peptidomimetic antioxidants. Recent Pat. Drug Deliv. Formul. 7, 216–256. https://doi.org/10.2174/18722113076661311171210 58

Barski, O.A., Xie, Z., Baba, S.P., Sithu, S.D., Agarwal, A., Cai, J., Bhatnagar, A., Srivastava, S., 2013. Dietary carnosine prevents early atherosclerotic lesion formation in apolipoprotein E-null mice. Arterioscler. Thromb. Vasc. Biol. 33, 1162–1170. https://doi.org/10.1161/ATVBAHA.112.300572

Bartels, A., Han, Q., Nair, P., Stacey, L., Gaynier, H., Mosley, M., Huang, Q.Q., Pearson, J.K., Hsieh, T.-F., An, Y.-Q.C., Xiao, W., 2018. Dynamic DNA Methylation in Plant Growth and Development. Int. J. Mol. Sci. 19. https://doi.org/10.3390/ijms19072144
Baylin, S.B., Jones, P.A., 2011. A decade of exploring the cancer epigenome - biological and translational implications. Nat. Rev. Cancer 11, 726–734. https://doi.org/10.1038/nrc3130

Becker, P.B., Workman, J.L., 2013. Nucleosome remodeling and epigenetics. Cold Spring Harb. Perspect. Biol. 5. https://doi.org/10.1101/cshperspect.a017905
Bird, A., 2002. DNA methylation patterns and epigenetic memory. Genes Dev. 16, 6–21. https://doi.org/10.1101/gad.947102

Brandsma, S.H., de Boer, J., van Velzen, M.J.M., Leonards, P.E.G., 2014. Organophosphorus flame retardants (PFRs) and plasticizers in house and car dust and

the influence of electronic equipment. Chemosphere 116, 3–9. https://doi.org/10.1016/j.chemosphere.2014.02.036

Breton-Larrivée, M., Elder, E., McGraw, S., 2019. DNA methylation, environmental exposures and early embryo development. Anim. Reprod. 16, 465–474. https://doi.org/10.21451/1984-3143-AR2019-0062

Cacabelos, R., 2019. Chapter 5 - Pathoepigenetics: The Role of Epigenetic Biomarkers in Disease Pathogenesis, in: Cacabelos, R. (Ed.), Pharmacoepigenetics. Academic Press, pp. 139–189. https://doi.org/10.1016/B978-0-12-813939-4.00005-X

Carignan, C.C., Mínguez-Alarcón, L., Williams, P.L., Meeker, J.D., Stapleton, H.M., Butt, C.M., Toth, T.L., Ford, J.B., Hauser, R., EARTH Study Team, 2018. Paternal urinary concentrations of organophosphate flame retardant metabolites, fertility measures, and pregnancy outcomes among couples undergoing in vitro fertilization. Environ. Int. 111, 232–238. https://doi.org/10.1016/j.envint.2017.12.005

Chen, R., Hou, R., Hong, X., Yan, S., Zha, J., 2019. Organophosphate flame retardants (OPFRs) induce genotoxicity in vivo: A survey on apoptosis, DNA methylation, DNA oxidative damage, liver metabolites, and transcriptomics. Environ. Int. 130, 104914. https://doi.org/10.1016/j.envint.2019.104914

Cheng, V., Reddam, A., Bhatia, A., Hur, M., Kirkwood, J.S., Volz, D.C., 2021. Utilizing systems biology to reveal cellular responses to peroxisome proliferator-activated receptor γ ligand exposure. Curr Res Toxicol 2, 169–178. https://doi.org/10.1016/j.crtox.2021.03.003

Chinthala, Y., Manjulatha, Sharma, P., Kvn, S.S., Jonnala, K., Arigari, N.K., Khan, F., Oh, S., 2016. Synthesis and cytotoxicity evaluation of novel andrographolide-1,2,3-triazole derivatives. J. Heterocycl. Chem. 53, 1902–1910. https://doi.org/10.1002/jhet.2505

Chiu, J.M.-Y., Lee, Y.-W., Su, K., 2022. Organophosphate-based flame retardant (tris(1,3-dichloro-2-propyl) phosphate) reduces fecundity and impairs embryonic development in marine invertebrates. Mar. Freshwater Res. 73, 1056–1063. https://doi.org/10.1071/MF22058

Chlorinated Tris [WWW Document], n.d. . Proposition 65 Warnings Website. URL https://www.p65warnings.ca.gov/fact-sheets/chlorinated-tris (accessed 8.4.22).

Chupeau, Z., Bonvallot, N., Mercier, F., Le Bot, B., Chevrier, C., Glorennec, P., 2020. Organophosphorus Flame Retardants: A Global Review of Indoor Contamination and Human Exposure in Europe and Epidemiological Evidence. Int. J. Environ. Res. Public Health 17. https://doi.org/10.3390/ijerph17186713

Colaneri, A., Wang, T., Pagadala, V., Kittur, J., Staffa, N.G., Jr, Peddada, S.D., Isganaitis, E., Patti, M.E., Birnbaumer, L., 2013. A minimal set of tissue-specific hypomethylated CpGs constitute epigenetic signatures of developmental programming. PLoS One 8, e72670. https://doi.org/10.1371/journal.pone.0072670

Corrales, J., Fang, X., Thornton, C., Mei, W., Barbazuk, W.B., Duke, M., Scheffler, B.E., Willett, K.L., 2014. Effects on specific promoter DNA methylation in zebrafish embryos and larvae following benzo[a]pyrene exposure. Comp. Biochem. Physiol. C. Toxicol. Pharmacol. 163, 37–46. https://doi.org/10.1016/j.cbpc.2014.02.005

Craig, J.A., Ceballos, D.M., Fruh, V., Petropoulos, Z.E., Allen, J.G., Calafat, A.M., Ospina, M., Stapleton, H.M., Hammel, S., Gray, R., Webster, T.F., 2019. Exposure of Nail Salon Workers to Phthalates, Di(2-ethylhexyl) Terephthalate, and Organophosphate Esters: A Pilot Study. Environ. Sci. Technol. 53, 14630–14637. https://doi.org/10.1021/acs.est.9b02474

Dasgupta, S., Cheng, V., Vliet, S.M.F., Mitchell, C.A., Volz, D.C., 2018. Tris(1,3-dichloro-2-propyl) Phosphate Exposure During the Early-Blastula Stage Alters the Normal Trajectory of Zebrafish Embryogenesis. Environ. Sci. Technol. 52, 10820–10828. https://doi.org/10.1021/acs.est.8b03730

Dasgupta, S., Cheng, V., Volz, D.C., 2021. Utilizing Zebrafish Embryos to Reveal Disruptions in Dorsoventral Patterning. Curr Protoc 1, e179. https://doi.org/10.1002/cpz1.179

Dasgupta, S., Vliet, S.M., Kupsco, A., Leet, J.K., Altomare, D., Volz, D.C., 2017. Tris(1,3-dichloro-2-propyl) phosphate disrupts dorsoventral patterning in zebrafish embryos. PeerJ 5, e4156. https://doi.org/10.7717/peerj.4156

Dasgupta, S., Vliet, S.M.F., Cheng, V., Mitchell, C.A., Kirkwood, J., Vollaro, A., Hur, M., Mehdizadeh, C., Volz, D.C., 2019. Complex Interplay Among Nuclear Receptor Ligands, Cytosine Methylation, and the Metabolome in Driving Tris(1,3-dichloro-2-propyl)phosphate-Induced Epiboly Defects in Zebrafish. Environ. Sci. Technol. 53, 10497–10505. https://doi.org/10.1021/acs.est.9b04127

Dean, W., Santos, F., Reik, W., 2003. Epigenetic reprogramming in early mammalian development and following somatic nuclear transfer. Semin. Cell Dev. Biol. 14, 93–100. https://doi.org/10.1016/s1084-9521(02)00141-6

Deichmann, U., 2016. Epigenetics: The origins and evolution of a fashionable topic. Dev. Biol. 416, 249–254. https://doi.org/10.1016/j.ydbio.2016.06.005

Ding, X., Sun, W., Dai, L., Liu, C., Sun, Q., Wang, J., Zhang, P., Li, K., Yu, L., 2020. Parental exposure to environmental concentrations of tris(1,3-dichloro-2-propyl)phosphate induces abnormal DNA methylation and behavioral changes in F1 zebrafish larvae. Environ. Pollut. 267, 115305. https://doi.org/10.1016/j.envpol.2020.115305

Dishaw, L.V., Hunter, D.L., Padnos, B., Padilla, S., Stapleton, H.M., 2014. Developmental exposure to organophosphate flame retardants elicits overt toxicity and alters behavior in early life stage zebrafish (Danio rerio). Toxicol. Sci. 142, 445–454. https://doi.org/10.1093/toxsci/kfu194

Dodson, R., Rodgers, K., Covaci, A., Van den Eede, N., Ionas, A., Dirtu, A., Perovich, L., Brody, J., Rudel, R., 2013. Health risks of flame retardants in California house dust. Environ. Health Perspect. 2013, 5292. https://doi.org/10.1289/isee.2013.o-3-15-02

Dodson, R.E., Perovich, L.J., Covaci, A., Van den Eede, N., Ionas, A.C., Dirtu, A.C., Brody, J.G., Rudel, R.A., 2012. After the PBDE phase-out: a broad suite of flame retardants in repeat house dust samples from California. Environ. Sci. Technol. 46, 13056–13066. https://doi.org/10.1021/es303879n

Doherty, B.T., Hammel, S.C., Daniels, J.L., Stapleton, H.M., Hoffman, K., 2019. Organophosphate Esters: Are These Flame Retardants and Plasticizers Affecting Children's Health? Curr Environ Health Rep 6, 201–213. https://doi.org/10.1007/s40572-019-00258-0

Efimova, O.A., Koltsova, A.S., Krapivin, M.I., Tikhonov, A.V., Pendina, A.A., 2020. Environmental Epigenetics and Genome Flexibility: Focus on 5-Hydroxymethylcytosine. Int. J. Mol. Sci. 21. https://doi.org/10.3390/ijms21093223

Egger, G., Liang, G., Aparicio, A., Jones, P.A., 2004. Epigenetics in human disease and prospects for epigenetic therapy. Nature 429, 457–463. https://doi.org/10.1038/nature02625

Elia, I., Haigis, M.C., 2021. Metabolites and the tumour microenvironment: from cellular mechanisms to systemic metabolism. Nat Metab 3, 21–32. https://doi.org/10.1038/s42255-020-00317-z

EpiSign Complete [WWW Document], n.d. URL https://www.ncbi.nlm.nih.gov/gtr/tests/592313/ (accessed 8.25.22).

Fabrizio, P., Garvis, S., Palladino, F., 2019. Histone Methylation and Memory of Environmental Stress. Cells 8. https://doi.org/10.3390/cells8040339

Fang, X., Corrales, J., Thornton, C., Scheffler, B.E., Willett, K.L., 2013. Global and gene specific DNA methylation changes during zebrafish development. Comp. Biochem. Physiol. B Biochem. Mol. Biol. 166, 99–108. https://doi.org/10.1016/j.cbpb.2013.07.007

Forrester, S.J., Kikuchi, D.S., Hernandes, M.S., Xu, Q., Griendling, K.K., 2018. Reactive oxygen species in metabolic and inflammatory signaling. Circ. Res. 122, 877–902. https://doi.org/10.1161/CIRCRESAHA.117.311401

Fu, J., Han, J., Zhou, B., Gong, Z., Santos, E.M., Huo, X., Zheng, W., Liu, H., Yu, H., Liu, C., 2013. Toxicogenomic responses of zebrafish embryos/larvae to tris(1,3-dichloro-2-propyl) phosphate (TDCPP) reveal possible molecular mechanisms of developmental toxicity. Environ. Sci. Technol. 47, 10574–10582. https://doi.org/10.1021/es401265q

Geiman, T.M., Muegge, K., 2010. DNA methylation in early development. Mol. Reprod. Dev. 77, 105–113. https://doi.org/10.1002/mrd.21118

Giraldez, A.J., Mishima, Y., Rihel, J., Grocock, R.J., Van Dongen, S., Inoue, K., Enright, A.J., Schier, A.F., 2006. Zebrafish MiR-430 promotes deadenylation and clearance of maternal mRNAs. Science 312, 75–79. https://doi.org/10.1126/science.1122689

Greenberg, M.V.C., Bourc'his, D., 2019. The diverse roles of DNA methylation in mammalian development and disease. Nat. Rev. Mol. Cell Biol. 20, 590–607. https://doi.org/10.1038/s41580-019-0159-6

Grosser, C., Wagner, N., Grothaus, K., Horsthemke, B., 2015. Altering TET dioxygenase levels within physiological range affects DNA methylation dynamics of HEK293 cells. Epigenetics 10, 819–833. https://doi.org/10.1080/15592294.2015.1073879

Gutzat, R., Rembart, K., Nussbaumer, T., Hofmann, F., Pisupati, R., Bradamante, G., Daubel, N., Gaidora, A., Lettner, N., Donà, M., Nordborg, M., Nodine, M., Mittelsten Scheid, O., 2020. Arabidopsis shoot stem cells display dynamic transcription and DNA methylation patterns. EMBO J. 39, e103667. https://doi.org/10.15252/embj.2019103667

Haghshenas, S., Levy, M.A., Kerkhof, J., Aref-Eshghi, E., McConkey, H., Balci, T., Siu, V.M., Skinner, C.D., Stevenson, R.E., Sadikovic, B., Schwartz, C., 2021. Detection of a DNA Methylation Signature for the Intellectual Developmental Disorder, X-Linked, Syndromic, Armfield Type. Int. J. Mol. Sci. 22. https://doi.org/10.3390/ijms22031111

Hoffman, K., Butt, C.M., Webster, T.F., Preston, E.V., Hammel, S.C., Makey, C., Lorenzo, A.M., Cooper, E.M., Carignan, C., Meeker, J.D., Hauser, R., Soubry, A., Murphy, S.K., Price, T.M., Hoyo, C., Mendelsohn, E., Congleton, J., Daniels, J.L., Stapleton, H.M., 2017a. Temporal Trends in Exposure to Organophosphate Flame Retardants in the United States. Environ Sci Technol Lett 4, 112–118. https://doi.org/10.1021/acs.estlett.6b00475

Hoffman, K., Gearhart-Serna, L., Lorber, M., Webster, T.F., Stapleton, H.M., 2017b. Estimated tris(1,3-dichloro-2-propyl) phosphate exposure levels for US infants suggest potential health risks. Environ Sci Technol Lett 4, 334–338. https://doi.org/10.1021/acs.estlett.7b00196

Huang, W., Lan, M.-D., Qi, C.-B., Zheng, S.-J., Wei, S.-Z., Yuan, B.-F., Feng, Y.-Q., 2016. Formation and determination of the oxidation products of 5-methylcytosine in RNA. Chem. Sci. 7, 5495–5502. https://doi.org/10.1039/c6sc01589a

Inbar-Feigenberg, M., Choufani, S., Butcher, D.T., Roifman, M., Weksberg, R., 2013. Basic concepts of epigenetics. Fertil. Steril. 99, 607–615. https://doi.org/10.1016/j.fertnstert.2013.01.117

Izzo, L.T., Affronti, H.C., Wellen, K.E., 2021. The Bidirectional Relationship Between Cancer Epigenetics and Metabolism. Annu Rev Cancer Biol 5, 235–257. https://doi.org/10.1146/annurev-cancerbio-070820-035832

Janke, R., Dodson, A.E., Rine, J., 2015. Metabolism and epigenetics. Annu. Rev. Cell Dev. Biol. 31, 473–496. https://doi.org/10.1146/annurev-cellbio-100814-125544

Jastroch, M., 2012. Expression of Uncoupling Proteins in a Mammalian Cell Culture System (HEK293) and Assessment of Their Protein Function, in: Palmeira, C.M., Moreno, A.J. (Eds.), Mitochondrial Bioenergetics: Methods and Protocols. Humana Press, Totowa, NJ, pp. 153–164. https://doi.org/10.1007/978-1-61779-382-0_10

Jessop, P., Ruzov, A., Gering, M., 2018. Developmental Functions of the Dynamic DNA Methylome and Hydroxymethylome in the Mouse and Zebrafish: Similarities and Differences. Front Cell Dev Biol 6, 27. https://doi.org/10.3389/fcell.2018.00027

Jones, P.A., 2012. Functions of DNA methylation: islands, start sites, gene bodies and beyond. Nat. Rev. Genet. 13, 484–492. https://doi.org/10.1038/nrg3230

Jones, P.A., Takai, D., 2001. The role of DNA methylation in mammalian epigenetics. Science 293, 1068–1070. https://doi.org/10.1126/science.1063852

Kucharska, A., Cequier, E., Thomsen, C., Becher, G., Covaci, A., Voorspoels, S., 2015. Assessment of human hair as an indicator of exposure to organophosphate flame retardants. Case study on a Norwegian mother-child cohort. Environ. Int. 83, 50–57. https://doi.org/10.1016/j.envint.2015.05.015

Kupsco, A., Dasgupta, S., Nguyen, C., Volz, D.C., 2017. Dynamic Alterations in DNA Methylation Precede Tris(1,3-dichloro-2-propyl)phosphate-Induced Delays in Zebrafish Epiboly. Environ Sci Technol Lett 4, 367–373. https://doi.org/10.1021/acs.estlett.7b00332

Ladd-Acosta, C., 2015. Epigenetic Signatures as Biomarkers of Exposure. Curr Environ Health Rep 2, 117–125. https://doi.org/10.1007/s40572-015-0051-2

Lantz-McPeak, S., Guo, X., Cuevas, E., Dumas, M., Newport, G.D., Ali, S.F., Paule, M.G., Kanungo, J., 2015. Developmental toxicity assay using high content screening of zebrafish embryos. J. Appl. Toxicol. 35, 261–272. https://doi.org/10.1002/jat.3029

Levy, M.A., McConkey, H., Kerkhof, J., Barat-Houari, M., Bargiacchi, S., Biamino, E., Bralo, M.P., Cappuccio, G., Ciolfi, A., Clarke, A., DuPont, B.R., Elting, M.W., Faivre, L., Fee, T., Fletcher, R.S., Cherik, F., Foroutan, A., Friez, M.J., Gervasini, C., Haghshenas, S., Hilton, B.A., Jenkins, Z., Kaur, S., Lewis, S., Louie, R.J., Maitz, S., Milani, D., Morgan, A.T., Oegema, R., Østergaard, E., Pallares, N.R., Piccione, M., Pizzi, S., Plomp, A.S., Poulton, C., Reilly, J., Relator, R., Rius, R., Robertson, S., Rooney, K., Rousseau, J., Santen, G.W.E., Santos-Simarro, F., Schijns, J., Squeo, G.M., St John, M., Thauvin-Robinet, C., Traficante, G., van der Sluijs, P.J., Vergano, S.A., Vos, N., Walden, K.K., Azmanov, D., Balci, T., Banka, S., Gecz, J., Henneman, P., Lee, J.A., Mannens, M.M.A.M., Roscioli, T., Siu, V., Amor, D.J., Baynam, G., Bend, E.G., Boycott, K., Brunetti-Pierri, N., Campeau, P.M., Christodoulou, J., Dyment, D., Esber, N., Fahrner, J.A., Fleming, M.D., Genevieve, D., Kerrnohan, K.D., McNeill, A., Menke, L.A., Merla, G., Prontera, P., Rockman-Greenberg, C., Schwartz, C., Skinner, S.A., Stevenson, R.E., Vitobello, A., Tartaglia, M., Alders, M., Tedder, M.L., Sadikovic, B., 2022a. Novel diagnostic DNA methylation episignatures expand and refine the epigenetic landscapes of Mendelian disorders. HGG Adv 3, 100075. https://doi.org/10.1016/j.xhgg.2021.100075

Levy, M.A., Relator, R., McConkey, H., Pranckeviciene, E., Kerkhof, J., Barat-Houari, M., Bargiacchi, S., Biamino, E., Palomares Bralo, M., Cappuccio, G., Ciolfi, A., Clarke, A., DuPont, B.R., Elting, M.W., Faivre, L., Fee, T., Ferilli, M., Fletcher, R.S., Cherick, F., Foroutan, A., Friez, M.J., Gervasini, C., Haghshenas, S., Hilton, B.A., Jenkins, Z., Kaur, S., Lewis, S., Louie, R.J., Maitz, S., Milani, D., Morgan, A.T., Oegema, R., Østergaard, E., Pallares, N.R., Piccione, M., Plomp, A.S., Poulton, C., Reilly, J., Rius, R., Robertson, S., Rooney, K., Rousseau, J., Santen, G.W.E., Santos-Simarro, F., Schijns, J., Squeo, G.M., John, M.S., Thauvin-Robinet, C., Traficante, G., van der Sluijs, P.J., Vergano, S.A., Vos, N., Walden, K.K., Azmanov, D., Balci, T.B., Banka, S., Gecz, J., Henneman, P., Lee, J.A., Mannens, M.M.A.M., Roscioli, T., Siu, V., Amor, D.J., Baynam, G., Bend, E.G., Boycott, K., Brunetti-Pierri, N., Campeau, P.M., Campion, D., Christodoulou, J., Dyment, D., Esber, N., Fahrner, J.A., Fleming, M.D., Genevieve, D., Heron, D., Husson, T., Kernohan, K.D., McNeill, A., Menke, L.A., Merla, G., Prontera, P., Rockman-Greenberg, C., Schwartz, C., Skinner, S.A., Stevenson, R.E., Vincent, M., Vitobello, A., Tartaglia, M., Alders, M., Tedder, M.L., Sadikovic, B., 2022b. Functional correlation of genome-wide DNA methylation profiles in genetic neurodevelopmental disorders. Hum. Mutat. https://doi.org/10.1002/humu.24446

Li, R., Yang, L., Han, J., Zou, Y., Wang, Y., Feng, C., Zhou, B., 2021. Early-life exposure to tris (1,3-dichloro-2-propyl) phosphate caused multigenerational neurodevelopmental toxicity in zebrafish via altering maternal thyroid hormones transfer and epigenetic modifications. Environ. Pollut. 285, 117471. https://doi.org/10.1016/j.envpol.2021.117471

Li, R., Zhou, P., Guo, Y., Lee, J.-S., Zhou, B., 2017. Tris (1,3-dichloro-2-propyl) phosphate-induced apoptotic signaling pathways in SH-SY5Y neuroblastoma cells. Neurotoxicology 58, 1–10. https://doi.org/10.1016/j.neuro.2016.10.018

Li, Y., Huang, K., Jiang, J., Xiao, Y., An, L., Zhang, S., Kang, Q., Chen, R., Jia, Y., Zhang, X., Liu, C., Hu, J., 2020. Mass mortality of fish embryos in a lake ecosystem attributable to a flame retardant. Authorea Preprints. https://doi.org/10.22541/au.159069383.30337964

Liberti, M.V., Locasale, J.W., 2016. The Warburg effect: How does it benefit cancer cells? Trends Biochem. Sci. 41, 211–218. https://doi.org/10.1016/j.tibs.2015.12.001

Liu, C., Su, G., Giesy, J.P., Letcher, R.J., Li, G., Agrawal, I., Li, J., Yu, L., Wang, J., Gong, Z., 2016. Acute Exposure to Tris(1,3-dichloro-2-propyl) Phosphate (TDCIPP) Causes Hepatic Inflammation and Leads to Hepatotoxicity in Zebrafish. Sci. Rep. 6, 19045. https://doi.org/10.1038/srep19045

Lyakhovich, A., 2013. Damaged mitochondria and overproduction of ROS in Fanconi anemia cells. Rare Dis. 1, e24048. https://doi.org/10.4161/rdis.24048

Ma, Y., Stubbings, W.A., Cline-Cole, R., Harrad, S., 2021. Human exposure to halogenated and organophosphate flame retardants through informal e-waste handling activities - A critical review. Environ. Pollut. 268, 115727. https://doi.org/10.1016/j.envpol.2020.115727

Martin, E.M., Fry, R.C., 2018. Environmental Influences on the Epigenome: Exposure-Associated DNA Methylation in Human Populations. Annu. Rev. Public Health 39, 309–333. https://doi.org/10.1146/annurev-publhealth-040617-014629

Martínez-Iglesias, O., Naidoo, V., Cacabelos, N., Cacabelos, R., 2021. Epigenetic Biomarkers as Diagnostic Tools for Neurodegenerative Disorders. Int. J. Mol. Sci. 23. https://doi.org/10.3390/ijms23010013

McGee, S.P., Cooper, E.M., Stapleton, H.M., Volz, D.C., 2012. Early zebrafish embryogenesis is susceptible to developmental TDCPP exposure. Environ. Health Perspect. 120, 1585–1591. https://doi.org/10.1289/ehp.1205316

Mitchell, C.A., Dasgupta, S., Zhang, S., Stapleton, H.M., Volz, D.C., 2018. Disruption of Nuclear Receptor Signaling Alters Triphenyl Phosphate-Induced Cardiotoxicity in Zebrafish Embryos. Toxicol. Sci. 163, 307–318. https://doi.org/10.1093/toxsci/kfy037

Nguyen, L.V., Diamond, M.L., Venier, M., Stubbings, W.A., Romanak, K., Bajard, L., Melymuk, L., Jantunen, L.M., Arrandale, V.H., 2019. Exposure of Canadian electronic waste dismantlers to flame retardants. Environ. Int. 129, 95–104. https://doi.org/10.1016/j.envint.2019.04.056

Nwanaji-Enwerem, J.C., Colicino, E., 2020. DNA Methylation-Based Biomarkers of Environmental Exposures for Human Population Studies. Curr Environ Health Rep 7, 121–128. https://doi.org/10.1007/s40572-020-00269-2

Ooi, S.K.T., O'Donnell, A.H., Bestor, T.H., 2009. Mammalian cytosine methylation at a glance. J. Cell Sci. 122, 2787–2791. https://doi.org/10.1242/jcs.015123

Park, J.H., Kundu, A., Lee, Su Hyun, Jiang, C., Lee, Song Hee, Kim, Y.S., Kyung, S.Y., Park, S.H., Kim, H.S., 2021. Specific Pyruvate Kinase M2 Inhibitor, Compound 3K, Induces Autophagic Cell Death through Disruption of the Glycolysis Pathway in Ovarian Cancer Cells. Int. J. Biol. Sci. 17, 1895–1908. https://doi.org/10.7150/ijbs.59855

Pellenz, S., 2023. Warburg Effect [WWW Document]. URL https://www.antibodies-online.com/warburg-effect-pathway-146/?utm_source=cco&utm_medium=email&utm_content=warburg-effect-resource&utm_campaign=warburg-effect (accessed 3.27.23).

Peters, V., Klessens, C.Q.F., Baelde, H.J., Singler, B., Veraar, K.A.M., Zutinic, A., Drozak, J., Zschocke, J., Schmitt, C.P., de Heer, E., 2015. Intrinsic carnosine metabolism in the human kidney. Amino Acids 47, 2541–2550. https://doi.org/10.1007/s00726-015-2045-7

Piletič, K., Kunej, T., 2016. MicroRNA epigenetic signatures in human disease. Arch. Toxicol. 90, 2405–2419. https://doi.org/10.1007/s00204-016-1815-7

Potok, M.E., Nix, D.A., Parnell, T.J., Cairns, B.R., 2013. Reprogramming the maternal zebrafish genome after fertilization to match the paternal methylation pattern. Cell 153, 759–772. https://doi.org/10.1016/j.cell.2013.04.030

Recent advances in the analysis of 5-methylcytosine and its oxidation products, 2014. . Trends Analyt. Chem. 54, 24–35. https://doi.org/10.1016/j.trac.2013.11.002

Reddam, A., Herkert, N., Stapleton, H.M., Volz, D.C., 2022. Partial dust removal in vehicles does not mitigate human exposure to organophosphate esters. Environ. Res. 205, 112525. https://doi.org/10.1016/j.envres.2021.112525

Reddam, A., Tait, G., Herkert, N., Hammel, S.C., Stapleton, H.M., Volz, D.C., 2020. Longer commutes are associated with increased human exposure to tris(1,3-dichloro-2-propyl) phosphate. Environ. Int. 136, 105499. https://doi.org/10.1016/j.envint.2020.105499

Robertson, K.D., 2005. DNA methylation and human disease. Nat. Rev. Genet. 6, 597–610. https://doi.org/10.1038/nrg1655

Robertson, K.D., 2002. DNA methylation and chromatin - unraveling the tangled web. Oncogene 21, 5361–5379. https://doi.org/10.1038/sj.onc.1205609

Rooney, K., Sadikovic, B., 2022. DNA Methylation Episignatures in Neurodevelopmental Disorders Associated with Large Structural Copy Number Variants: Clinical Implications. Int. J. Mol. Sci. 23. https://doi.org/10.3390/ijms23147862

Rottach, A., Leonhardt, H., Spada, F., 2009. DNA methylation-mediated epigenetic control. J. Cell. Biochem. 108, 43–51. https://doi.org/10.1002/jcb.22253

Sadikovic, B., Levy, M.A., Kerkhof, J., Aref-Eshghi, E., Schenkel, L., Stuart, A., McConkey, H., Henneman, P., Venema, A., Schwartz, C.E., Stevenson, R.E., Skinner, S.A., DuPont, B.R., Fletcher, R.S., Balci, T.B., Siu, V.M., Granadillo, J.L., Masters, J., Kadour, M., Friez, M.J., van Haelst, M.M., Mannens, M.M.A.M., Louie, R.J., Lee, J.A., Tedder, M.L., Alders, M., 2021. Clinical epigenomics: genome-wide DNA methylation analysis for the diagnosis of Mendelian disorders. Genet. Med. 23, 1065–1074. https://doi.org/10.1038/s41436-020-01096-4

Sassone-Corsi, P., 2013. Physiology. When metabolism and epigenetics converge. Science. https://doi.org/10.1126/science.1233423

Shen, L., Kondo, Y., Guo, Y., Zhang, J., Zhang, L., Ahmed, S., Shu, J., Chen, X., Waterland, R.A., Issa, J.-P.J., 2007. Genome-wide profiling of DNA methylation reveals a class of normally methylated CpG island promoters. PLoS Genet. 3, 2023–2036. https://doi.org/10.1371/journal.pgen.0030181

Shi, W., Haaf, T., 2002. Aberrant methylation patterns at the two-cell stage as an indicator of early developmental failure. Mol. Reprod. Dev. 63, 329–334. https://doi.org/10.1002/mrd.90016

Stapleton, H.M., Klosterhaus, S., Eagle, S., Fuh, J., Meeker, J.D., Blum, A., Webster, T.F., 2009. Detection of organophosphate flame retardants in furniture foam and U.S. house dust. Environ. Sci. Technol. 43, 7490–7495. https://doi.org/10.1021/es9014019

T. Oronsky, B., Oronsky, N., R. Fanger, G., W. Parker, C., Z. Caroen, S., Lybeck, M., J. Scicinski, J., 2014. Follow the ATP: Tumor Energy Production: A Perspective. Anti-Cancer Agents in Medicinal Chemistry- Anti-Cancer Agents) 14, 1187–1198.

Tadros, W., Lipshitz, H.D., 2009. The maternal-to-zygotic transition: a play in two acts. Development 136, 3033–3042. https://doi.org/10.1242/dev.033183

Tedder, M.L., DuPont, B.R., Lee, J.A., Louie, R.J., Kerkhof, J., Sadikovic, B., Friez, M.J., 2022. 30. The application of DNA methylation episignatures to resolve variants of uncertain clinical significance. Cancer Genet. 264, 10. https://doi.org/10.1016/j.cancergen.2022.05.033

Thakur, C., Chen, F., 2019. Connections between metabolism and epigenetics in cancers. Semin. Cancer Biol. 57, 52–58. https://doi.org/10.1016/j.semcancer.2019.06.006

Thannickal, V.J., Fanburg, B.L., 2000. Reactive oxygen species in cell signaling. Am. J. Physiol. Lung Cell. Mol. Physiol. 279, L1005-28. https://doi.org/10.1152/ajplung.2000.279.6.L1005

Tost, J., 2020. 10 years of Epigenomics: a journey with the epigenetic community through exciting times. Epigenomics 12, 81–85. https://doi.org/10.2217/epi-2019-0375

Tran, C.M., Lee, H., Lee, B., Ra, J.-S., Kim, K.-T., 2021. Effects of the chorion on the developmental toxicity of organophosphate esters in zebrafish embryos. J. Hazard. Mater. 401, 123389. https://doi.org/10.1016/j.jhazmat.2020.123389

van der Veen, I., de Boer, J., 2012. Phosphorus flame retardants: properties, production, environmental occurrence, toxicity and analysis. Chemosphere 88, 1119–1153. https://doi.org/10.1016/j.chemosphere.2012.03.067

Vaupel, P., Multhoff, G., 2021. Revisiting the Warburg effect: historical dogma versus current understanding. J. Physiol. 599, 1745–1757. https://doi.org/10.1113/JP278810
Vliet, S.M.F., Dasgupta, S., Sparks, N.R.L., Kirkwood, J.S., Vollaro, A., Hur, M., Zur Nieden, N.I., Volz, D.C., 2019. Maternal-to-zygotic transition as a potential target for niclosamide during early embryogenesis. Toxicol. Appl. Pharmacol. 380, 114699. https://doi.org/10.1016/j.taap.2019.114699

Volz, D.C., Leet, J.K., Chen, A., Stapleton, H.M., Katiyar, N., Kaundal, R., Yu, Y., Wang, Y., 2016. Tris(1,3-dichloro-2-propyl)phosphate Induces Genome-Wide Hypomethylation within Early Zebrafish Embryos. Environ. Sci. Technol. 50, 10255–10263. https://doi.org/10.1021/acs.est.6b03656

Wang, S., Wu, W., Claret, F.X., 2017. Mutual regulation of microRNAs and DNA methylation in human cancers. Epigenetics 12, 187–197. https://doi.org/10.1080/15592294.2016.1273308

Wong, N., De Melo, J., Tang, D., 2013. PKM2, a Central Point of Regulation in Cancer Metabolism. Int. J. Cell Biol. 2013, 242513. https://doi.org/10.1155/2013/242513

World Health Organization, International Programme on Chemical Safety, 1998. Flame retardants : tris(chloropropyl) phosphate and tris(2-chloroethyl) phosphate. World Health Organization.

Wossidlo, M., Nakamura, T., Lepikhov, K., Marques, C.J., Zakhartchenko, V., Boiani, M., Arand, J., Nakano, T., Reik, W., Walter, J., 2011. 5-Hydroxymethylcytosine in the mammalian zygote is linked with epigenetic reprogramming. Nat. Commun. 2, 241. https://doi.org/10.1038/ncomms1240

Wu, Q., Ni, X., 2015. ROS-mediated DNA methylation pattern alterations in carcinogenesis. Curr. Drug Targets 16, 13–19. https://doi.org/10.2174/1389450116666150113121054

Yang, J., Zhao, Y., Li, M., Du, M., Li, X., Li, Y., 2019. A Review of a Class of Emerging Contaminants: The Classification, Distribution, Intensity of Consumption, Synthesis Routes, Environmental Effects and Expectation of Pollution Abatement to Organophosphate Flame Retardants (OPFRs). Int. J. Mol. Sci. 20. https://doi.org/10.3390/ijms20122874

Yin, S.-Y., Chen, L., Wu, D.-Y., Wang, T., Huo, L.-J., Zhao, S., Zhou, J., Zhang, X., Miao, Y.-L., 2019. Tris(1,3-dichloro-2-propyl) phosphate disturbs mouse embryonic development by inducing apoptosis and abnormal DNA methylation. Environ. Mol. Mutagen. 60, 807–815. https://doi.org/10.1002/em.22322

Zhang, H.-Y., Xiong, J., Qi, B.-L., Feng, Y.-Q., Yuan, B.-F., 2016. The existence of 5-hydroxymethylcytosine and 5-formylcytosine in both DNA and RNA in mammals. Chem. Commun. 52, 737–740. https://doi.org/10.1039/c5cc07354e

Zhu, X., Xuan, Z., Chen, J., Li, Z., Zheng, S., Song, P., 2020. How DNA methylation affects the Warburg effect. Int. J. Biol. Sci. 16, 2029–2041. https://doi.org/10.7150/ijbs.45420